# A Geomagnetic Secular Variation Study by Separation of A Field Variation into Its Spectral Components

糸田, 千鶴

(Degree)
博士（理学）

(Date of Degree)
1992-03-31

(Date of Publication)
2008-07-23

(Resource Type)
doctoral thesis

(Report Number)
甲1126

(JaLCDOI)
https://doi.org/10.11501/3062300

(URL)
https://hdl.handle.net/20.500.14094/D1001126

博 士 論 文

# A Geomagnetic Secular Variation Study by Separation of A Field Variation into Its Spectral Components

(変動成分分離による地磁気永年変化の研究)

平成4年3月

神戸大学大学院自然科学研究科

糸田千鶴

DOCTRAL THESIS

# A Geomagnetic Secular Variation Study by Separation of A Field Variation into Its Spectral Components

**Chizu ITOTA**

Division of Environmental Science,
The Graduate School of Science and Technology,
Kobe University,
Nada, Kobe 657, Japan

March, 1992

## Abstract

A new method was introduced to analyze paleosecular variations of the earth's magnetic field direction. The method consists of four steps. First, a time series of a pair of declination and inclination is transformed to those of axial dipole field reference frame. Second, characteristic periodicities are deduced by spectral analysis. Third, the secular variation (SV) components of the periodicities are separated through bandpass filters. Last, motions of field vectors are investigated by polar projections and curvature analysis for each secular variation component. Validity of this method was first examined on a sedimentary secular variation record from central to southwest Japan for the last 11500 years. After succeeded in isolation of some intrinsic features of the geomagnetic secular variation, the same analysis was performed on the SV records from U.K., North America, and Australia. Two SV components of different frequency bands were isolated for each SV record, and analyzed.

Predominance of westward drifting components in the geomagnetic field variation during the last 10000 years was shown by a SV component in the low frequency band from Japan and the SV components in both high and low frequency bands from the other three sites. The durations dominated by motions of clockwise sense were longer than those of counter-clockwise sense. Almost all looping features were observed in the intervals of clockwise sense. Especially, in the interval from 4200 - 1700 years B.P., continuous clockwise rotations of field vector were commonly seen in the SVs of low frequency component from Japan and in those of high frequency components from the other three sites. From the correlation functions calculated for the low frequency SVs of the three sites in the Northern Hemisphere, the drifting velocity was estimated 0.16°/year - 0.13°/year. The correlation function of up-down components in the low frequency SVs between Australia and Japan, which are located at equatorial symmetric positions, showed that there was no time-lag of SV

features. This does not deny the result obtained from the three SV records in the Northern Hemisphere that westward drifting is a dominant feature.

The change of field oscillation direction in a polar projection shows that one standing field persists for 3000 - 4000 years long. The duration for break of smooth clockwise looping in the low frequency SV in Japan is 3500 years, which suggests that a standing field actively fluctuates for 3500 years long. The time length of 3000 - 4000 years may be a characteristic of activity for standing fields during the last 10000 years.

## Acknowledgements

The author would like to record her heartily gratitude to Professor K.Yaskawa, who has given her attractive guidance to the Geomagnetism and priceless advices during the study. Dr. M. Hyodo is gratefully acknowledged for his generous instruction through the investigation. He has always given invaluable suggestions and made precious discussion. Drs. N. Isezaki and S. Yamaguchi are appreciated having given the author an important introduction to the filtering analyses. The author is thankful to Drs. H. Inokuchi and H. Morinaga for their helpful comments and useful advices. Special thanks are due to Dr. Y. Otofuji for his great encouragement.

**A Geomagnetic Secular Variation Study by Separation of A Field Variation into Its Spectral Components**

## CONTENTS

# A Geomagnetic Secular Variation Study by Separation of A Field Variation into Its Spectral Components

## 1. A Method and Its Application to A Record from Japan

## 1-1. INTRODUCTION

Past geomagnetic fields reconstructed from remanent magnetization of lacustrine or rapidly deposited marine sediments extend our knowledge about natures of the geomagnetism. Such sediments usually provide continuous records of the geomagnetic secular variation (SV) for times more than several thousands of years. They enable to investigate the geomagnetic nature over a time range longer than those of historical SV records, which are only four hundred years.

A number of records of paleomagnetic secular variation (PSV) have been recently obtained from Holocene sediments. They show very complex changes of field vectors with various types and sizes of loops, cusps, and oscillating features when projected on to a certain plane. The complex changes may be caused by decay and/or growth of a geocentric dipole field, regional non-dipole fields (Yukutake and Tachinaka, 1968a), and westward drifting non-dipole fields. Runcorn (1959) and Skiles (1970) suggested that a westward (or eastward) drifting non-dipole source produces the clockwise (or counter-clockwise) rotation of geomagnetic field direction at a site of the earth's surface when viewed toward its north-seeking end. Single standing non-dipole source which changes its own intensity will make oscillations of field vectors. Thus, some simple behaviors of the geomagnetic field can be expected, but they have never been observed. It may be because the geomagnetic field consists of different types of variations, resulting in very complex motions of field vector. Many types of complex secular variation are possible with combination of different sources, e.g. in Creer and Tucholka (1983b).

Two major ways are currently used to describe characteristics of PSV data. One is to deduce periodicities from its time series. The other is to describe the sense of rotation of geomagnetic direction.

Spectral analysis provides a powerful tool to search for buried periodic features. Fourier and maximum entropy method (MEM) analyses have been usually employed for data of PSV's during the last 10000 years (Turner and Thompson, 1981; Barton

and McElhinny, 1982; Creer and Tucholka, 1983a, b; Lund and Banerjee, 1985). Spectral analyses so far have identified two general bands of spectral peaks; the period ranges of 7000 - 12000 years per cycle and 500 - 3500 years per cycle (Lund and Olsen, 1987). Barton (1983) suggested the latter band was further separated into two, 600 - 1000 years per cycle and 2000 - 3000 years per cycle.

Sense of rotation of the geomagnetic vector is conveniently displayed by Bauer plots (Bauer, 1896) or VGP plots and the curvature of its path (Creer et al., 1986). Plots of curvature of the VGP paths as a function of time usually show complex patterns (Creer and Tucholka, 1983a, b; Smith and Creer, 1986; Creer et al., 1986). Clockwise and counter-clockwise rotations are alternated in short durations. There is no coherency among the plots for PSV's from different sites (Creer and Tucholka, 1983a, b). It means that the local field variation would play no negligible part in a secular variation.

By the previous analyses, it is apparent that secular variations of the past geomagnetic field consist of several components of motion provably originated from different source fields. The SV components should be separated to clarify the characteristic features of sources. Spherical harmonic analysis is valuable to separate and describe the SV components of observed fields. However the areas where PSV data have been observed are limited to only several sites on the globe, distributed mainly on the Northern Hemisphere, so that spherical harmonic analysis is invalid. Some other ways are required for PSV data.

We introduce a new method to describe the nature of paleosecular variation. The method is characterized by the analysis of filtered time-series data, which is based on the idea that every field components has its own periodicity. This method is illustrated, applied to a paleosecular variation record from central to southwest Japan (Hyodo et al., 1992, in preparation). The record has been constructed from magnetization of several wide-diameter (20 cm) cores of marine and lacustrine sediments. It is the data at 50 years intervals covering the duration from 11500 years B.P. to 400 years B.P..

## 1-2. DATA

### 1-2-1. Sampling

Seven cores of sediments have been sampled from two lakes and four sites in the Inland Sea in the central to southwest Japan; Lake Kizaki (KZ1 and KZ3; 36.6°N, 137.8°E), Lake Yogo (YG1; 35.5°N, 136.2°E), Osaka Bay (OS2; 34.6°N, 135.3°E and OS3; 34.4°N, 135.1°E), Harima-Nada (HR1; 34.5°N, 134.7°E) and Mizushima-Nada (MZ1; 34.4°N, 133.6°E) (Fig. 1-2-1; Horie et al, 1980; Hyodo and Yaskawa, 1980, 1986a, 1986b; Hyodo et al., 1985; Hyodo et al, 1992, in preparation). The sediment cores were 20 cm in diameter and split into halves. Four or five specimens were taken from each depth layer of every 5 cm intervals.

### 1-2-2. Paleomagnetic Results

Paleomagnetic measurements were made with a cryogenic magnetometer of SCT. Declination, inclination and intensity of natural remanent magnetization (NRM) were measured. Stability of remanence was examined by progressive AF-demagnetization on pilot specimens selected from every 1-m segment. The specimens of KZ1, KZ3, YG1, OS2 and MZ1 have very stable remanence with no directional shift after demagnetization. Thus, effect of secondary viscous magnetization in the NRM's of the five cores are negligibly small. Magnetizations of OS3 and HR1 were multi-component. The magnetization directions systematically shift every step of demagnetization (Hyodo et al., 1985 ; Hyodo & Yaskawa, 1986a). Post-depositional remanent magnetization (PDRM) process can cause multi-component of remanence and explain the systematic shifting of remanence direction after demagnetization according to the model proposed by Hyodo & Yaskawa (1986a). The averaged declination and inclination were calculated in each depth level for every cores.

## 1-2-3. Chronology

Age control was performed by twelve absolute ages, tephrochronology, and pollen analyses. Shell pieces were used for dating marine sediments. Wood fractions were used for dating of the Lake Kizaki sediments, and analyses of total organic fractions were made for the sediments of Lake Yogo.

Dating by tephrochronology was made on two thin layers of tephra in the sediments of Lake Yogo by Arai (1981 : private communication). According to the analyses of maximum grain size, free crystal, mineral composition, type and color of volcanic glass and refractive index, the two tephras were identified as "Akahoya" and "Oki". Their conventional radiocarbon ages are 6300 years b.p. (Maeda et al., 1982) and 9300 years b.p. (Arai et al., 1981), respectively.

Pollen-chronology reinforced the depth versus age relationship in the core of OS2. *Lepidobalanus* and *cyclobalanopsis* are the two major elements of pollen around Osaka Bay during Holocene times. The content of *lepidobalanus* which is abundant about 10000 years b.p. gradually decreases with time while *cyclobalanopsis* suddenly starts to increase after 7000 years B.P. and exceeds the content of *lepidobalanus* by 6000 years b.p. (Maeda, 1976 ; Furutani, 1979). It has been revealed that the percentage of *lepidobalanus* and *cyclobalanopsis* at the base of OS2 are 7.5 and 27.0 %, respectively (Tojo, 1976). The equilibrium depth of the two pollens would be deeper beyond the base of OS2 and therefore the age of the base would be younger than 6000 years b.p..

The conventional radiocarbon ages are calibrated according to the data by dendrochronology (Klein, 1982) for ages after 8000 years b.p. and the data by varve chronology (Shove, 1983) for ages before 8000 years b.p.. For the past 2000 years, especially, Stuiver's (1982) high precision calibration data by dendrochronology were used.

## 1-2-4. Stacking of Directional Vectors

A composite secular variation was constructed using horizon-average remanence direction of all the cores. Prominent features of the secular variation records of declination and inclination were correlated to those of the master core, YG1, by visual matching. Fifteen to nineteen tie-points were decided for each core matching maxima and minima of declination and inclination fluctuations. Radiocarbon dates in individual cores were subsequently transferred to the equivalent depths of YG1 determined by a linear interpolation between tie-points. The tie-points of prominent magnetic features were then dated by linear interpolations between age data points. Consequently time scales of other cores were constructed with dates of the tie-points. Then, declination and inclination of horizon mean magnetization of each cores were transferred to a time scale of the Christian Era.

The low amplitude of declination and inclination changes of OS3 and HR1 should be due to the filtering effect due to post depositional remanent magnetization process. The original secular variations were deduced from the filtered records by the deconvolution method (Hyodo, 1984; Hyodo et al, 1992). The remanence direction data of OS3 and HR1 were deconvoluted over the whole lengths. For the cores KZ1 and KZ3, the directions partly deconvoluted with $Z_{1/2} = 20$ cm were used in the time range of 3500 - 5500 years B.P. and the original data in the ranges before 5500 years B.P. and after 3500 years B.P.. For the cores OS2, YG1 and MZ1, there were no need to deconvolute.

Reference frames of each core were adjusted using Denham's (1981) "paleomagnetic pattern matching" technique. This is to make stacking with more consistent SV data to avoid smoothing-out of fine SV features. A data set of unit-vector time series is rotated so as to get good agreement with the other data set. The frame rotation was made by finding iteratively the pole and angle of rotation examining cross-correlation of unit-vector time series. The rotational adjustment was made as to match with the Japanese archaeomagnetic data (Hirooka, 1971 and 1983). Fig.1-2-2 shows a stacked secular variation averaged every 50 years windows. For windows where no data available, directional data were linear interpolated.

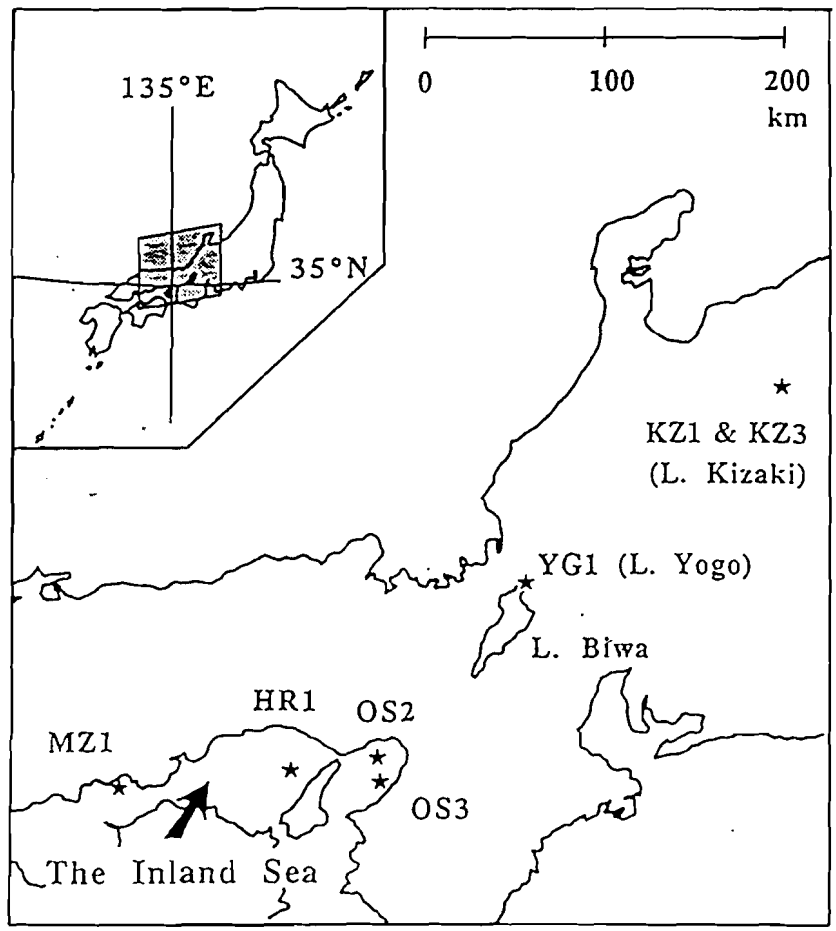


Fig. 1-2-1. Location of sampling sites of Lake Kizaki (core names = KZ1 and KZ3), Lake Yogo (YG1), Osaka Bay (OS2 and OS3), Harima-nada (HR1) and Mizushima-Nada (MZ1). Stars show the locations of cores.

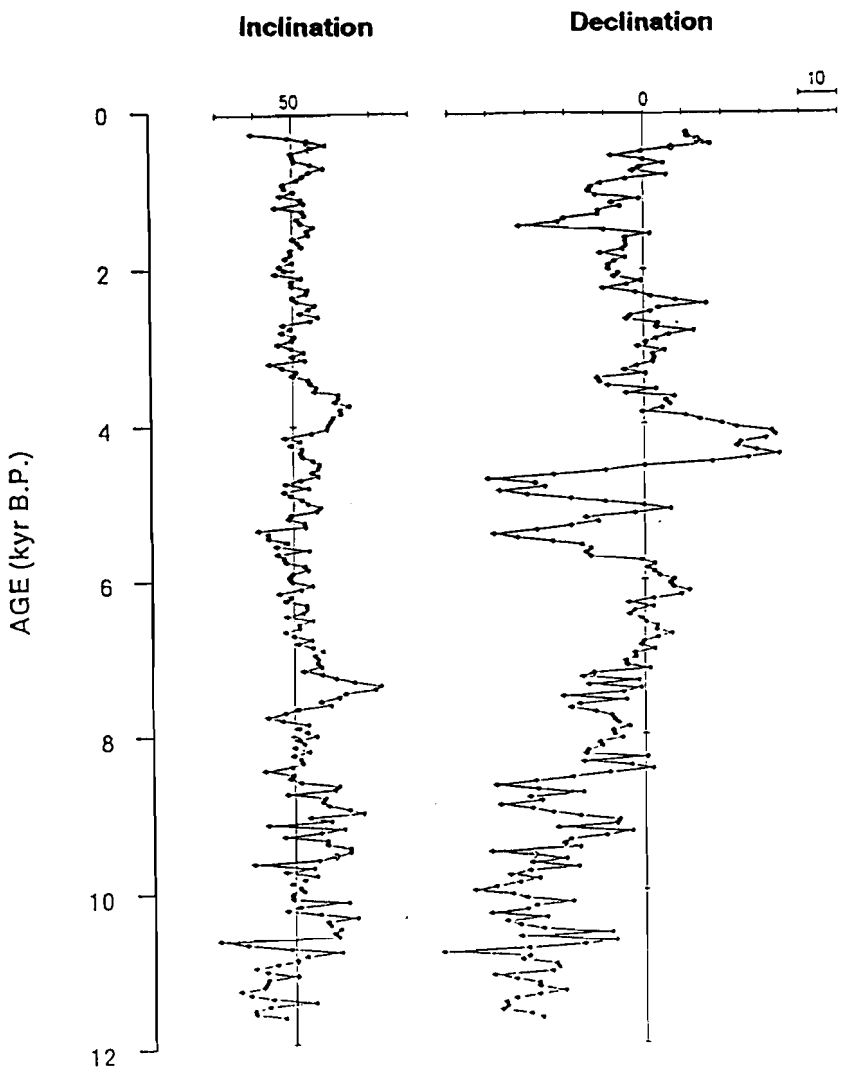


Fig. 1-2-2. A composite secular variation constructed by stacking seven cores from central to southwest Japan. Solid circles show declinations and inclinations of magnetization directions averaged every 50 years windows. Open circles are linear interpolated data.

## 1-3. METHODS AND RESULTS

### 1-3-1. Geocentric Axial Dipole Field Reference Frame

A time series of unit field vectors expressed by a pair of declination and inclination was transformed into that in a new reference frame defined as in Fig. 1-3-1. X-axis coincides with direction of the axial dipole field (ADF) at the site. Y-axis is in a horizontal plane and perpendicular to the X-axis, east direction being positive. Z-axis is perpendicular to both the X- and Y-axes, having positive direction under a rule of right handed system. In the Northern Hemisphere, a positive Z-component shows a downward direction. A unit field vector is expressed by two components in this reference frame. One is east-west (E-W) component defined by the angle between the X-axis and the field vector projected on to the XY-plane. The other is up-down (U-D) component expressed by the angle of the vector from the XY-plane.

The transformation from an ordinary pair of declination and inclination to a pair of E-W and U-D components is performed as follows. The inclination ($\Phi$) of the geocentric axial dipole field direction (X) at a site is defined as

$$\Phi = \tan^{-1}(2 \cdot \tan\theta) \qquad (1)$$

where $\theta$ is a site latitude. A pair of declination (D) and inclination (I) can be expressed with orthogonal three components (X', Y', Z'):

$$\begin{aligned} X' &= \cos D \cdot \cos I \\ Y' &= \sin D \cdot \cos I \\ Z' &= \sin I \end{aligned} \qquad (2)$$

The X'- and Y'- axes are in horizontal plane and the Z'- axis coincides to a vertical

axis. A set of three components of the axial dipole reference frame (X, Y, Z) are calculated from the angle $\Phi$ and these three components,

$$\begin{aligned} X &= X' \cos \Phi + Z' \sin \Phi \\ Y &= Y' \\ Z &= -X' \sin \Phi + Z' \cos \Phi \end{aligned} \qquad (3)$$

A pair of E-W and U-D components can be defined as follows;

$$\text{E-W} = \tan^{-1} (X / Y)$$
$$\text{U-D} = \tan^{-1} [(X^2 + Y^2)^{1/2} / Z]$$

A data set of secular variation from central to southwest Japan (Fig. 1-2-2) was transformed into these two components (Fig. 1-3-2). The data points were obtained after filtering out components with frequencies higher than 5.0 cycles per kyr (period = 200 years).

It is difficult to visualize behavior of motion of a field vector in separate time-dependency plots of E-W and U-D components. A polar projection centered about a norm is often used to map the motion of such vectors. Fig. 1-3-3 shows the polar projections of HCJPN. The direction of ADF was selected as a norm. Secular variation of field directions can be seen as an orbit of end points of unit vectors projected on to the YZ-plane, which is here viewed along the X-axis from negative to positive.

## 1-3-2. Spectral analyses

The start point of this study is that complex features of PSV are due to the mixing of variations who have own characteristic times. Spectral analysis provides a powerful tool to define the mixing periodic features.

Maximum entropy method (MEM) analysis (Burg, 1967) has been commonly used for spectral estimates in PSV studies. There are one problem remaining in this method. The optimum selection of the order of prediction error filter ($m$) is undefined. In the MEM analysis, a wrong choice of the order results in a wrong spectrum form. However such a wrong choice can be avoided by the Akaike's final prediction error (FPE) criterion (Akaike, 1969a, b, and 1970) as discussed by Ulrych and Bishop (1975). They examined its suitability for various types of time series, and concluded that this criterion works very well. At the following, MEM of Burg's algorithm and the Akaike's FPE criterion are introduced briefly.

*Theory*

1) Autoregressive Model

The value of the variable at time $t$, $X(t)$, is derived linearly from a purely random Gaussian process according to the previous $m$ values of the variable:

$$X(t) = a_1X(t\text{-}1) + a_2X(t\text{-}2) + .... + a_mX(t\text{-}m) + B(t) \qquad (1)$$

where $m$ is known as the order of the autoregressive (AR) process, $a_1$, $a_2$, ...., $a_m$ are constants, $B(t)$ is called the innovation of the process, and the mean of both AR process and $B(t)$ are zero.

Using $\gamma_i$ ( $= -a_i$), the equation (1) is rewritten as

$$X(t) + \gamma_1X(t\text{-}1) + \gamma_2X(t\text{-}2) + .... + \gamma_mX(t\text{-}m) = B(t) \qquad (2)$$

The equation (2) is a recursive prediction equation of $X(t)$ so the set of coefficients (1, $\gamma_1$, $\gamma_2$, ...., $\gamma_m$) is called the prediction error filter. Since the variable $B(t)$, the prediction error, is the convolution of this filter with vector $X(t)$. Let us multiply throughout in equation (2) by $X(t\text{-}m)$ for every $t$, and take expected values, then from $E[X(t\text{-}m)\cdot B(t)] = 0$:

$$C(k) + \gamma_1 C(k\text{-}1) + \gamma_1 C(k\text{-}1) + \cdots\cdots + \gamma_m C(k\text{-}m) = 0 \quad k > 0 \quad (3)$$

is introduced (Yule - Walker equation). Where $C(k)$ is an autocorrelation coefficient of lag $k$; $C(k)= E[X(i)\cdot X(i\text{-}k)]$.

2) Maximum Entropy Method

Burg (1967) proposed a method of spectral estimation of a stationary random uniformly sampled process. The spectrum is found as the result from maximizing the entropy of the process. The method was named maximum entropy method (MEM) illustrated as follows.

An entropy ($H$) of a stationary Gaussian process can be related with its spectral density $S(f)$ as,

$$H = \frac{1}{4 f_N} \int_{-f_N}^{f_N} \log S(f)\, df \qquad (4)$$

where $f_N$ is the Nyquist frequency.

The relationship between the spectral density and the autocorrelation coefficient can be written by the Wiener - Khintchine equation.

$$\int_{-f_N}^{f_N} S(f)\, Z_k\, df = C(k) \qquad (-\infty \le k \le \infty) \qquad (5)$$

Equation (5) can be written as

$$\int_{-f_N}^{f_N} [S(f)\, Z_k - \frac{1}{2f_N}\, C(k)]\, df = 0 \qquad (-\infty \le k \le \infty) \qquad (6)$$

Therefore

$$S(f) = \frac{1}{2f_N} \sum_{-\infty}^{\infty} C(k)\, Z^{-k} \qquad (7)$$

where

$$Z = \exp(i2\pi f \Delta t) \qquad (8)$$

Rewriting (4) using (7) gives

$$H = \frac{1}{4f_N} \int_{-f_N}^{f_N} \sum_{-\infty}^{\infty} C(k)\, Z^{-k}\, df \qquad (9)$$

Of course we only know a definitive number of autocorrelation function $C(k)$. Let us assume that the first $m$ autocorrelation coefficient $C(0)$, $C(1)$, ... $C(m\text{-}1)$ are exactly known. The next unknown autocorrelation coefficient $C(m)$ is chosen in such a manner that the entropy of the process is maximized at the step. An entropy of a discrete stationary Gaussian process $X(t)$, $t = 1, 2, \ldots m$, is expressed as

$$H = \frac{1}{2} \log [\det C_m] \qquad (10)$$

which is equivalent to (4), where $C_m$ is the semipositive definite Toeplitz autocorrelation matrix of the process $X(t)$,

$$C_m = \begin{bmatrix} C(o) & C(1) & \cdots & C(m) \\ C(1) & C(2) & \cdots & C(m\text{-}1) \\ \cdot & \cdot & & \cdot \\ \cdot & \cdot & & \cdot \\ C(m) & C(m\text{-}1) & \cdots & C(1) \end{bmatrix}$$

Thus the coefficient $C(m)$ is determined by maximizing [det $C_m$] with respect to $C(m)$. The solution is easily shown to be

$$\det \begin{bmatrix} C(1) & C(0) & \cdots & C(m\text{-}1) \\ C(2) & C(2) & \cdots & C(m\text{-}2) \\ \cdot & \cdot & & \cdot \\ \cdot & \cdot & & \cdot \\ C(m) & C(m\text{-}1) & \cdots & C(1) \end{bmatrix} = 0 \qquad (11)$$

It is also expressed by the spectral density $S(f)$ as

$$\int_{-f_N}^{f_N} \frac{Z^{-k}}{S(f)}\, df = 0 \qquad (12)$$

Equation (12) means that $1/S(f)$ can be written by the $2m+1$ coefficients, that is

$$\frac{1}{S(f)} = \sum_{k=0}^{m} b_k Z^k \qquad (13)$$

Equation (13) is also expressed as

$$\frac{1}{S(f)} = \frac{2 f_N}{P_m} \left( \sum_{k=0}^{m} \gamma_k Z^k \right) \left( \sum_{k=0}^{m} \gamma_k^* Z^{-k} \right) \qquad (14)$$

From (14) and (7),

$$\left[\sum_{k=0}^{m} C(k)\,Z^{-k}\right]\left[\sum_{k=0}^{m} \gamma_k Z^{k}\right] = \frac{P_m}{\sum_{k=0}^{m} \gamma_k^{*} Z^{-k}} \tag{15}$$

From (15), $m$+1 equations are obtained as

$$\begin{aligned}
&C(0) + \gamma_1 C(1) + \gamma_2 C(2) + \cdots + \gamma_m C(m) = P_m \\
&C(1) + \gamma_1 C(2) + \gamma_2 C(3) + \cdots + \gamma_m C(m\text{-}1) = 0 \qquad (16) \\
&\quad\cdot \qquad\cdot \qquad\qquad\cdot \qquad\qquad\qquad\cdot \qquad\cdot \\
&\quad\cdot \qquad\cdot \qquad\qquad\cdot \qquad\qquad\qquad\cdot \qquad\cdot \\
&C(m) + \gamma_1 C(m\text{-}2) + \gamma_2 C(m\text{-}3) + \cdots + \gamma_m C(1) = 0
\end{aligned}$$

The equations except the first one are equal to (3). Thus, the series of 1, $\gamma_1$, $\gamma_2$, ..., $\gamma_m$, is the prediction error filter of this time series; $X(1)$, $X(2)$, ... $X(N)$. $P_m$ is the output power of this filter. There are $m$+2 unknown parameters in $m$+1 equations of (16). Here we introduce a criterion that $P_m$ must be the minimum value of averaging results of forward filtering and backward filtering of the signals ($X(1)$, $X(2)$, ... $X(N)$).

When we get unknown parameters, $\gamma_1$, $\gamma_2$, ..., $\gamma_m$, $P_m$, then the MEM spectral density is calculated as,

$$S(f) = \frac{P_m}{2 f_N} \frac{1}{\left|\sum_{k=0}^{m} \gamma_\kappa Z k\right|^2}$$

$$= \frac{P_m}{2 f_N} \frac{1}{\left|1 + \sum_{k=1}^{m} \gamma_\kappa Z k\right|^2} \tag{17}$$

which is obtained from equation (16).

3) Burg's Estimation of Parameters

Burg (1967) suggested a method of estimating the prediction error filter coefficients that requires no prior estimations of the autocorrelation coefficients. In his formulation, the coefficients $\gamma_{m,k}$ ($k$ = 1 to $m$), $P_m$, and also $C(m)$ are calculated from those of step $m$-1 by recurrence formulae.

When we have known the coefficients of order $m$-1, $\gamma_{m-1,k}$ ($k$ = 1 to $m$-1), $P_{m-1}$, $C(m-1)$, those of order $m$ are determined from next procedures.

(i) $\gamma_{m,k}$

The recurrence formula of $\gamma_{m,k}$ is

$$\gamma_{m,k} = \gamma_{m-1,k} + \gamma_{m,m} \cdot \gamma_{m-1,m-k} \qquad (18)$$

where

$$\gamma_{m,k} = 1 \qquad k > 0$$
$$= 0 \qquad k > i$$

Therefore, if we know the value of $\gamma_{m,m}$, we can obtain all the coefficients of filter of order $m$. Burg's criterion, "minimizing the averaged value of $P_m$ resulted from forward filtering and backward filtering of the signals", is written as:

$$P_m = \frac{1}{2\,(N - m)} \cdot \sum_{i=1}^{N-m} \left[ \left( X_i + \sum_{k=1}^{m} \gamma_{m,k} \cdot X_{i+k} \right)^2 + \left( X_{i+m} + \sum_{k=1}^{m} \gamma_{m,k} \cdot X_{i+m-k} \right)^2 \right]$$

$$\longrightarrow \text{Min.} \qquad (19)$$

is rewritten with (18)

$$P_m = \frac{1}{2\,(N-m)} \sum_{i=1}^{N-m} [\,(\,b_{m,i} + \gamma_{m,m} \cdot b'_{m,i}\,)^2 + (b'_{m,i} + \gamma_{m,m} \cdot b_{m,i}\,)^2]$$

$$\longrightarrow \text{Min.}$$

That is

$$\frac{\partial P_m}{\partial \gamma_{m,m}} = 0$$

Then $\gamma_{m,m}$ can be written as

$$\gamma_{m,m} = \frac{-2 \sum_{i=1}^{N-m} b_{m,i} \cdot b'_{m,i}}{\sum_{i=1}^{N-m} (b_{m,i}^{\,2} + b'_{m,i}{}^{2})} \qquad (20)$$

where

$$b_{m,i} = b_{m-1,i} + \gamma_{m-1,m-1} \cdot b'_{m-1,i}$$

$$b'_{m,i} = b'_{m-1,i+1} + \gamma_{m-1,m-1} \cdot b_{m-1,i+1}$$

$$b_{0,i} = b'_{0,i} = X_i \;;\; b_{1,i} = X_i \,,\, b'_{1,i} = X_{i+1}$$

Here

$$\frac{\partial^2 P_m}{\partial \gamma_{m,m}^2} = \frac{1}{N-m} \sum_{i=1}^{N-m} (b_{m,i} + \gamma_{m,m} \cdot b'_{m,i}) > 0$$

therefore $P_m$ is a minimum value. When we get $\gamma_{m,m}$ from (20), we can also estimate all the $\gamma_{m,k}$ by equation (18).

(ii) $\boldsymbol{P_m}$

The recurrence formula of $P_m$ is,

$$\begin{bmatrix} P_{m-1} \\ 0 \\ \cdot \\ \cdot \\ 0 \\ \Delta_{m-1} \end{bmatrix} + \gamma_{m,m} \begin{bmatrix} \Delta_{m-1} \\ 0 \\ \cdot \\ \cdot \\ 0 \\ P_{m-1} \end{bmatrix} = \begin{bmatrix} P_m \\ 0 \\ \cdot \\ \cdot \\ 0 \\ 0 \end{bmatrix} \qquad (21)$$

where

$$P_{m-1} = C(0) + \gamma_{m-1,1} \cdot C(1) + \ldots\ldots + \gamma_{m-1,m-1} \cdot C(m-1)$$
$$\Delta_{m-1} = C(m) + \gamma_{m-1,1} \cdot C(m-1) + \ldots\ldots + \gamma_{m-1,m-1} \cdot C(1)$$

The bottom of these equations of (21) is

$$0 = \Delta_{m-1} + \gamma_{m,m} \cdot P_{m-1}$$

Then is

$$\gamma_{m,m} = -\frac{\Delta_{m-1}}{P_{m-1}} \qquad (22)$$

From the first of the equations of (21),

$$P_m = P_{m-1} + \gamma_{m,m} \cdot \Delta_{m-1} \tag{23}$$

Substituting (22) for (23),

$$P_m = P_{m-1} ( 1 - \gamma_{m,m}^2) \tag{24}$$

is obtained. Thus we can calculate $P_m$ from $\gamma_{m,m}$.

(iii) $C(m)$

From the last of the equations (16),

$$C(m) = - [ \gamma_1 C(m-2) + \gamma_2 C(m-3) + \quad \cdots + \quad \gamma_m C(1) ] \tag{25}$$

Equation (25) means that the new autocorrelation coefficient $C(m)$ can be calculated from filters coefficients $\gamma_{m,k}$ and $C(k)$ ($k = 0$ to $m$-1). $C(m)$ is not directory calculated from signals $X(t)$.

We have calculated all the unknown parameters of order $m$; $\gamma_{m,k}$ ($k = 1$ to $m$), $C(m)$, and $P_m$. The parameters of order $m$+1 can be calculated similarly. Then we can obtain the MEM spectral density of preferred order of the prediction error filter from equation (17).

4) Akaike's Final Prediction Error

We present here a brief outline of the Akaike's final prediction error (FPE) scheme (Akaike, 1969a, b, 1970, Ulrych and Bishop, 1975). An estimate of the FPE of order $m$ is calculated by a following definition,

$$(\mathrm{FPE})_m = \frac{N + (m+1)}{N - (m+1)} \cdot S_m^2 \qquad (26)$$

where

$$S_m^2 = \frac{1}{N-m} \sum_{i=m+1}^{N} [X(i) + \gamma_{m,1}X(i\text{-}1) + \gamma_{m,2}X(i\text{-}2) + .. + \gamma_{m,m}X(i\text{-}m)] \qquad (27)$$

From the equation (2), the equation (27) can be rewritten as

$$S_m^2 = \frac{1}{N-m} \sum_{i=m+1}^{N} [B(i)^2] \qquad (28)$$

That is, $S_m^2$ is a mean square of the prediction error. The first factor of right side of equation (26) increases as the order $m$ is increased. The FPE tends to be large when unnecessarily large value of $m$ is adopted. When $m$ is less than most optimum order for prediction, then $S_m^2$ tends to be large, and thus the FPE tends to be significantly large. Thus by seeking the minimum of the FPE, we shall be able to arrive at an autoregressive model of the most optimum order. So the MEM spectral density should be calculated at the order. Even if the FPE fails to show a clearly defined minimum, it is better empirically that the $m < 3N^{1/2}$.

Other commonly used criteria for selecting order $m$ are Ulrych and Clayton's criterion: $m = N / 3$ or $N / 2$ (Ulrych and Clayton, 1976), and Berryman's criterion: $m = 2N\,(\ln 2N)\text{-}1$. Barton and McElhinny (1982) concluded that the Akaike's FPE criteria, when calculated using Burg's estimates of the autocorrelation coefficients, is useful for estimating $m$. On the contrary, other two criteria were shown to tend to overestimate the order.

*Application and Results*

Spectral analysis was carried out using the maximum entropy method (MEM; Burg, 1967) on the time series of E-W and U-D components, and on the total vector series every which was represented by a complex number of $(Y+iZ)$, where $i=(-1)^{1/2}$ (Denham, 1975). Lengths of prediction error filter ($m$) used in our MEM analyses were chosen satisfying the Akaike's FPE criterion and an empirical formula of $m < 3N^{1/2}$, where $N$ is the number of data.

Table 1-3-1 shows the results of spectral analyses. We picked up the spectral peaks whose powers are larger than 10% of the power of the largest peak. The spectral peaks of periods longer than the data length (= 11000 years) were omitted because of their less reliability. Further, the spectral peaks of period < 500 years were removed because the high frequency signals have small amplitudes so that they easily undergo the influence of errors.

To test the stability of the obtained spectra throughout the length of the time series, periods of spectral peaks were recalculated within a sliding window of 5000 years every 500 years. The results are summarized in Fig. 1-3-4, where each point shows a period of the spectral peak within a sliding window.

Stable spectral peaks are obtained at about 2000 and 800 years per cycle for the E-W component almost consistent with the results of whole data analysis. For the U-D component, a quite different result was obtained. Only the spectra of period of 1400 years is stably calculated and those of 3700 and 716 years per cycle in Table 1-3-1 are not. The periodicity of about 700 years per cycle appears in the U-D component only before 3500 year B.P.. Clockwise rotation of a field vector on the YZ-plane has two stable periodicities, 1600 and 750 years per cycle. The periodicity of about 700 years per cycle is rather stable for counter-clockwise rotation while those of longer than 900 years per cycle obtained in the whole data analysis are unstable.

The periods of spectral peaks from the three data sets seem to be concentrated in the bands of about 600 - 800 and 1200 - 3500 years per cycle, which are shown by the thin- and bold-striped areas in Fig. 1-3-4, respectively. These two bands are consistent with a previous work (Barton, 1983), and they are considered to be due to

non-dipole fields (Lund and Olsen, 1987). Especially, the longer band (1200 - 3500 years per cycle) is concordant to the time for the non-dipole field to rotate 360 degrees by the westward drifting rates estimated from the historical field variation (Bullard et al., 1950; Whitman, 1958; Yukutake, 1962, 1968, 1987; Yukutake and Tachinaka, 1968a, b; Matsushima and Honkura, 1988).

## 1-3-3. Separation of Quasi Periodic Motions

The two bands of periodicity obtained above may suggest that there are at least two different sources for secular variation. The complex motion of a field vector shown in Fig. 1-3-3 would be reflected by the combined effect of these periodic ones. Then the two periodic components were isolated from the original PSV data using Chebyshev bandpass filters, to investigate the nature of periodic motions simplified.

*Theory*

1) Recursive Filter

A digital filter whose input ($x_t$) and output ($y_t$) satisfy a formula,

$$y_t = a_0 x_t + a_1 x_{t-1} + a_2 x_{t-2} + \cdots\cdots - b_1 y_{t-1} - b_2 y_{t-2} - \cdots\cdots$$

can be expressed after z-transformation,

$$H(z) = \frac{a_0 + a_1 z + a_2 z^2 + \cdots}{b_0 + b_1 z + b_2 z^2 + \cdots} \qquad (1)$$

Such filters, whose z-transformation is expressed by a proportion of polynomials variable $z$, are named recursive filters.

A transfer function of a most simple recursive filter is

$$H(z) = \frac{a_0 + a_1 z + a_2 z^2}{b_0 + b_1 z + b_2 z^2} \tag{2}$$

and its output data are calculated by

$$y_t = a_0 x_t + a_1 x_{t-1} + a_2 x_{t-2} - b_1 y_{t-1} - b_2 y_{t-2}.$$

where, $x_t$, $y_t = 0$ when $t \leq 0$. A general formula of such filter is

$$H(z) = G_0 \prod_{j=1}^{M} H_j(z)$$

$$H_j(z) = \frac{1 + a_{1,j} z + a_{2,j} z2}{1 + b_{1,j} z + b_{2,j} z^2} \tag{3}$$

This mean that a filter $H(z)$ is a cascade of filters $H_j(z)$.

A frequency response of a filter $H_j(z)$ is obtained by substituting

$$z = \exp(-i\omega)$$

into transfer function (3), that is,

$$H_j(z) = \frac{a_{1,j} + (a_{2,j} + 1) \cos \omega - i\,(a_{2,j} - 1) \sin \omega}{b_{1,j} + (b_{2,j} + 1) \cos \omega - \mathrm{i}\,(b_{2,j} - 1) \sin \omega} \tag{4}$$

2. Chebyshev Filter (Type 1)

The type 1 Chebyshev filter is one of recursive filters characterized by its equiripple passband, whose frequency response $C(\sigma)$ is defined by

$$|C_n(\sigma)|^2 = \frac{1}{\{1 + [\varepsilon T_n(\sigma)]\}^2} \tag{5}$$

where $n$ and $\varepsilon$ are positive integers, $\sigma$ is a nondimensional angular frequency, and $T_n(\sigma)$ is the Chebyshev polynomial of order $n$, that is

$$T_n(\sigma) = \cos(n \cos^{-1}\sigma) \tag{6}$$

At $|\sigma| \leq 1$, $\cos^{-1}\sigma$ is real and then

$$|T_n(\sigma)| \leq 1$$

Thus we have

$$\frac{1}{(1 + \varepsilon^2)} \leq |C_n(\sigma)|^2 \leq 1 \qquad |\sigma| \leq 1 \tag{7}$$

On the other hand $T_n(\sigma)$ is a polynomial of order $n$,

$$T_n(\sigma) = 2^{n-1}\,\sigma^n + 2^{n-2}\,\sigma^{n-1} + \cdots\cdots$$

As $|\sigma|$ increases to infinity, $T_n(\sigma)$ is expected to rapidly grow. Thus $|C_n(\sigma)|^2$ is diminished with order

$$|C_n(\sigma)|^2 \sim (2^{n-1}\,\varepsilon\,\sigma^n)^{-2} \qquad |\sigma| \geq 1 \tag{8}$$

and so, with relatively small $\varepsilon$ and relatively large $n$, $|C_n(\sigma)|$ has a nature of lowpass filter, who "pass" the signals with frequency $\sigma$, $|\sigma| \leq 1$.

In order to obtain a digital expression of the frequency response $C_n(\sigma)$ from equation (5), we must find its poles. The poles are given by the zeros of the denominator of (5) that is, by

$$1 + [\varepsilon T_n(\sigma)]^2 = 0$$

$$T_n(\sigma) = \pm i / \varepsilon \tag{9}$$

Since $T_n(\sigma)$ is defined as equation (6), this becomes

$$\cos n \cos^{-1}\sigma = \pm i / \varepsilon$$

$$n \cos^{-1}\sigma = \cos^{-1}(\pm i / \varepsilon) \tag{10}$$

Let

$$\sigma = \cos(\phi + i\psi) \tag{11}$$

and let

$$\pm i / \varepsilon = \cos(\alpha + i\beta),$$

$$= \cos\alpha \cos i\beta - \sin\alpha \sin i\beta$$

$$= \cos\alpha \cosh\beta - i \sin\alpha \sinh\beta \tag{12}$$

Real and imaginary parts of the equation (12) give two equations

$$\cos\alpha \cosh\beta = 0$$

$$\sin\alpha \sinh\beta = \pm i / \varepsilon$$

From the first of these two equations, since $\cosh\beta \neq 0$ ( real $\beta$ ),

$$\cos\alpha = 0$$

and therefore

$$\alpha = \pi / 2 + k\pi$$

The second equation becomes

$$\sin(\pi / 2 + k\pi)\, \sinh\beta = \pm 1 / \varepsilon$$

$$(-1)^k \sinh\beta = \pm 1 / \varepsilon$$

$$\sinh\beta = \pm (-1)^k / \varepsilon$$

$$\sinh(\pm (-1)^k \beta) = 1 / \varepsilon$$

$$\pm (-1)^k \beta = \log[1 + (\varepsilon^2 + 1)^{1/2} / \varepsilon]$$

$$\beta = \pm (-1)^k \log[1 + (\varepsilon^2 + 1)^{1/2} / \varepsilon]$$

From this result and expression (11)

$$\phi + i\psi = (\pi / 2 + k\pi) / n$$

therefore

$$\phi = \alpha / n = (\pi / 2 + k\pi) / n$$

$$\psi = \beta / n = \pm (-1)^{k+1} \log[1 + (\varepsilon^2 + 1)^{1/2} / \varepsilon] / n \qquad (13)$$

Thus

$$\sigma_k = \cos[(2k + 1)\pi / 2n] \cosh\psi - i \sin[(2k + 1)\pi / 2n] \sinh\psi$$

Let $k + 1 = j$,

$$\sigma_j = \cos[(2j - 1)\pi / 2n] \cosh\psi - i \sin[(2j - 1)\pi / 2n] \sinh\psi \quad (14)$$

and

$$\psi = \pm (-1)^j \log[1 + (\varepsilon^2 + 1)^{1/2} / \varepsilon] \quad (15)$$

From (14) and (15), two values of $\psi$ can be defined for every $k$ ( $j$ ), they are a $\psi_0 > 0$ and a $\psi_1 < 0$. There are $4n$ poles [ 2 ($\psi_0$, $\psi_1$) * $2n$ ($j = 1, 2, \cdots, 2n$)]. But only a half of them actually appears since $\psi_1 = -\psi_0$ and $\sin[(2j - 1)\pi / 2n]$ has opposite signs as $j = l$ or $j = 2n - l$. If we choose the $\psi_1 < 0$, equation (14) and (15) are

$$\begin{aligned}
\sigma_j &= \cos[(2j - 1)\pi / 2n] \cosh(-|\psi|) - i \sin[(2j-1)\pi / 2n] \sinh(-|\psi|) \\
&= \cos[(2j - 1)\pi / 2n] \cosh\psi + i \sin[(2j-1)\pi / 2n] \sinh\psi \\
&= s_j + it_j \qquad (16) \\
\psi &= 1 / n \log\{[1 + (\varepsilon^2 + 1)] / \varepsilon\}
\end{aligned}$$

The poles fall in the upper half plane in the complex $\sigma$ plane when $j$ values are confined to 1, 2, $\cdots$, $n$. And at $j = n$, the denominator of equation (5) has a value ($2^{n-1}\varepsilon\sigma^n$). Thus the frequency response of the Chebyshev filter can be expressed as

$$C_n(\sigma) = \frac{1}{2^{n-1}\varepsilon} \prod_{j=1}^{n} \frac{1}{i\,(\sigma - \sigma_j)} \quad (17)$$

Filter's coefficients are obtained from the frequency response (17) with transformation

$$\sigma = \frac{\iota}{i}\,\frac{1-z}{1+z} \tag{18}$$

here, $\iota > 0$. First,

$$i(\sigma - \sigma_j) = \frac{\iota}{i}\,\frac{1-z}{1+z} - i\sigma_j$$

$$= \frac{(\iota - i\sigma_j) - z(\iota + i\sigma_j)}{1+z}$$

From (16), a pole $\sigma_{n-j+1}$ is

$$\sigma_{n-j+1} = -\sigma_j^* \tag{19}$$

where $\sigma_j^*$ is a conjugate complex number of $\sigma_j$. From (19),

$$i(\sigma - \sigma_{n-j+1}) = i(\sigma + \sigma_j^*) = \frac{(\iota + i\sigma_j^*) - z(\iota + i\sigma_j^*)}{1+z}$$

using pairs of $\sigma_j$ and $\sigma_{n-j+1}$, operation about $\prod$ in (17) can be calculated by the multiply of pairs of factors,

$$i(\sigma - \sigma_j)\cdot i(\sigma - \sigma_{n-j+1}) = i(\sigma - \sigma_j)\cdot i(\sigma + \sigma_j)$$

$$= \frac{1}{(1+z)^2}\{\iota^2 - i\iota(\sigma_j - \sigma_j^*) + \sigma_j\sigma_j^* - 2z[\iota^2 - \sigma_j\sigma_j^*]$$

$$+ z^2[\iota^2 + i\iota(\sigma_j - \sigma_j^*) + \sigma_j\sigma_j^*]\}$$

$$= \frac{1}{(1+z)^2} \{[(\iota + t_j)^2 + s_j^2] - 2z\,(\iota^2 - s_j^2 - t_j^2) + [(\iota - t_j)^2 + s_j^2\,]\}$$

If $n$ is odd number and equal to $2m + 1$, then $\sigma_{m+1}$ has no counterpart. Thus,

$$i\,(\sigma - \sigma_{m+1}) = \frac{(\iota - i\sigma_{m+1}) - z(\iota + i\sigma_{m+1})}{1+z}$$

$$= \frac{(\iota + t_{m+1}) - z(\iota - t_{m+1})}{1+z}$$

is remained. So as a result, a digital expression of a transfer function of a type 1 Chebyshev filter is generalized by

$$H(z) = \frac{1}{2^{n-1}\varepsilon} \cdot \frac{(\iota + t_{m+1}) - z(\iota - t_{m+1})}{1+z} \cdot$$

$$\prod_{j=1}^{m} \frac{(1+z)^2}{[(\iota + t_j)^2 + s_j^2] - 2z\,(\iota^2 - s_j^2 - t_j^2) + [(\iota - t_j)^2 + s_j^2]} \qquad (20)$$

where, $m$ is $(n\text{-}1) / 2$ when $n$ is odd number, or $n / 2$ when $n$ is equal number and then the second factor of $H(z)$ is neglected. The transfer function (20) is products of proportions of polynomials variable $z$ order 2. Coefficients of a filter are calculated from (20) and (3).

We obtain here a type 1 Chebyshev lowpass filter for the $\sigma$ variable. The type 1 Chebyshev filters have ripples in the passband, whose amplitude is constant (equiripple passband). Recursive filters have such ripples at the passband and/or stopband in the transfer function. Although this situation is of course undesirable, there is an advantage of allowing ripples in term of a narrow transfer band.

3) Saito's Algorithm

Saito (1978) described an automatic design algorithm for the type 1 Chebyshev filters. A complete Fortran program is also given. It allows us to obtain the design parameters of a filter, $\varepsilon$ and $n$, from critical frequencies at the edges of stopband ($f_s$ or $f_s$) and passband ($f_L$ and $f_H$) nondimensional parameters that specify maximum attenuation in the passband ($A_p$) and minimum attenuation in the stopband ($A_s$) for a bandpass filter (Fig. 1-3-5).

The transformation from the $\sigma$ variable to the $z$ variable is given with (18). The poles, $\sigma_j$, in the upper half plane in $\sigma$ are transformed into the outside of the unit circle in the $z$ plane. Let the unit circle in the $z$ plane,

$$z = \exp(-i\omega)$$

where $\omega$ is a nondimensional angular frequency defined as $\omega = 2\pi f \Delta t$. The circle transformed to the real axis of the $\sigma$ plane, and it can write with $\omega$,

$$\sigma = \iota \tan\omega / 2$$

As the original angular frequency, $\omega$, goes from 0 to $\pi$, the variable $\sigma$ goes from 0 to infinity. Thus the nature of lowpass filter is preserved through the transformation (18).

Using $\sigma_s$ , $A_p$ and $A_s$ , the frequency response $C_n(\sigma)$ is limited as,

$$1 / (1 + A_p^2) \le |C_n(\sigma)|^2 \le 1 \qquad |\sigma| \le \sigma_p < \sigma_s \qquad (21)$$

$$|C_n(\sigma)|^2 \le 1 / (1 + A_s^2) \qquad |\sigma| \ge \sigma_s \qquad (22)$$

and $\sigma_p$ is defined to 1 from (7) and (8). From (7) and (21), $\varepsilon$ is evidently limited that

$$\varepsilon \le A_p \qquad (23)$$

From (22),

$$\varepsilon T_n(\sigma_s) = \varepsilon \cos(n \cos^{-1}\sigma_s) \geq A_s \tag{24}$$

must be satisfied. If we now substitute

$$\theta_s = (1 / i)\cos^{-1}\sigma_s = \log[\sigma_s + (\sigma_s^2 - 1)^{1/2}] \tag{25}$$

into (24), we have

$$\varepsilon \cosh n\theta_s \geq A_s \tag{26}$$

From (23) and (26), a condition

$$\cosh n\theta_s \geq A_s / A_p \tag{27}$$

required to be satisfied. Recall that

$$\text{real}(\cos^{-1}x) = \log[x + (x^2 - 1)]$$

we obtain

$$n \geq (1 / \theta_s)\log\{A_s / A_p + [(A_s / A_p)^2 - 1]^{1/2}\} \tag{28}$$

from the condition (27) where, $\theta_s$ is calculated from $\sigma_s$ using equation (25). From (23) and (26), a maximum and a minimum values of $\varepsilon$ are given by

$$A_p \geq \varepsilon \geq A_s / \cosh n\theta_s$$

Then a constant parameter $\varepsilon$ of the filter may be estimated from a geometric mean of the both values,

$$\varepsilon^2 = A_p A_s \,/\, \cosh n\theta_s \tag{29}$$

Thus, if there are parameters $\sigma_s$, $A_s$, and $A_p$ are given, we get a minimum value of $n$ and a constant $\varepsilon$. As a result, all coefficients of digital expression of a type 1 Chebyshev lowpass filter (20) can be obtained.

For bandpass filter, we introduce a new variable $\lambda$ which is

$$\sigma = \frac{\lambda^2 - \lambda_0^2}{\lambda} \tag{30}$$

For a $\sigma = \sigma_P$ in (30), we have two roots of $\lambda$, they are $\lambda_H$ and $-\lambda_L$. A range of $|\sigma| \le \sigma_P$ is transformed to a range of $\lambda_L \le |\lambda| \le \lambda_H$ by the transformation (30). Thus the new filter about $\lambda$ has a nature of bandpass filter. Similarly, for a $\sigma = \sigma_s$, we have two roots of $\lambda$, they are $\lambda_S$ and $-\lambda_S'$. Then the ranges of stopband in $\lambda$ axis are $|\lambda| \ge \lambda_S$ and $|\lambda| \le \lambda_S'$. Thus, a lowpass filter for $\sigma$ variable is a bandpass filter for $\lambda$ variable, simultaneously. From (30),

$$\begin{aligned} \sigma_P &= \lambda_H - \lambda_L \\ \sigma_S &= \lambda_S - \lambda_S' \\ \lambda_0^2 &= \lambda_H \lambda_L = \lambda_S \lambda_S' \end{aligned} \tag{31}$$

are lead.

Filter's coefficients are obtained from (17) with transformation

$$\lambda = \frac{\iota}{i}\frac{1 - z}{1 + z} \qquad \iota > 0$$

As same as $\sigma$, $\lambda$ and $\omega$ has a relationship, that is

$$\lambda = \iota \tan(\omega / 2)$$

When we need a filter whose passband has a range of $\omega_L \le |\lambda| \le \omega_H$ and stopbands are $|\omega| \le \omega_S'$ and $|\omega| \ge \omega_S$. $\omega_L$, $\omega_H$, $\omega_S$ and $\omega_s'$ must satisfy the equations (31), so

$$\begin{aligned} \sigma_P &= \iota \, [\tan(\omega_H / 2) - \tan(\omega_L / 2)] \\ \sigma_S &= \iota \, [\tan(\omega_S / 2) - \tan(\omega_S' / 2)] \\ \lambda_0^2 &= \iota^2 \tan(\omega_H / 2) \cdot \tan(\omega_L / 2) = \iota^2 \tan(\omega_S / 2) \cdot \tan(\omega_S' / 2) \end{aligned} \tag{32}$$

The third equation of (32) means that $\omega_L$, $\omega_H$, $\omega_S$ and $\omega_s'$ are connected with one equation, thus they cannot be given independently. If $\omega_L$, $\omega_H$, and $\omega_S$ are given, $\omega_s'$ can be defined from the third equation of (32).

From equations of (32),

$$\frac{\sigma_S}{\sigma_P} = \frac{|\tan(\omega_S / 2) - \tan(\omega_H / 2) \cdot \tan(\omega_L / 2) \cdot \cot(\omega_S / 2)|}{\tan(\omega_H / 2) - \tan(\omega_L / 2)} \tag{33}$$

re given. Of course, for the type 1 Chebyshev filter, $\sigma_P$ is 1. Thus we obtain that

$$\begin{aligned} \iota &= [\tan(\omega_H / 2) - \tan(\omega_L / 2)]^{-1} \\ \sigma_S &= \iota |\tan(\omega_S / 2) - \tan(\omega_H / 2) \cdot \tan(\omega_L / 2) \cdot \cot(\omega_S / 2)| \\ \lambda_0^2 &= \iota^2 \tan(\omega_H / 2) \cdot \tan(\omega_L / 2) \end{aligned} \tag{34}$$

parameters $n$ and $\varepsilon$ can be calculated from $\sigma_S$ into (28) and (29).

From (30),

$$i(\sigma - \sigma_j) = \frac{i(\lambda^2 - \sigma_j\lambda - \lambda_0^2)}{\lambda} = \frac{i(\lambda - \lambda_{j1})(\lambda - \lambda_{j2})}{\lambda}$$

$$= \frac{1}{\imath(1 - z^2)} [(\imath - i\lambda_{j1}) - (\imath + i\lambda_{j1})z] \cdot [(\imath - i\lambda_{j2}) - (\imath + i\lambda_{j2})z]$$

where, $\lambda_{j1}$ and $\lambda_{j2}$ are roots of a equation

$$\lambda^2 - \sigma_j\lambda - \lambda_0^2 = 0$$

For a pole $\sigma_{n-j+1}$, $\sigma_{n-j+1} = -\sigma_j^*$ is held. Then

$$\lambda^2 + \sigma_j^*\lambda - \lambda_0^2 = 0$$

has two roots, $-\lambda_{j1}^*$ and $-\lambda_{j2}^*$. Thus

$$i(\sigma - \sigma_{n-j+1}) = \frac{1}{\imath(1 - z^2)} [(\imath + i\lambda_{j1}^*) - (\imath - i\lambda_{j1}^*)z]$$

$$\cdot [(\imath + i\lambda_{j2}^*) - (\imath - i\lambda_{j2}^*)z]$$

When $n = 2m + 1$, the term of $j = m + 1$ is

$$i(\sigma - \sigma_{m+1}) = i\sigma + t_{m+1}$$

$$= \frac{\imath^2(1 - z)^2 + \imath(1 - z^2)t_{m+1} + \lambda_0^2(1 + z)^2}{\imath(1 - z^2)}$$

The transfer function of the filter can be generalized as

$$H(z) = \frac{1}{2^{n-1}\varepsilon} \cdot \frac{\iota(1 - z^2)}{(\iota^2 + \iota t_{n+1} + \lambda_0^2) - 2(\iota^2 - \lambda_0^2)z + (\iota^2 - \iota t_{n+1} + \lambda_0^2)z^2}$$

$$\cdot \prod_{j=1}^{m}{}' \frac{(1 + z)^2}{[(\iota + v_j)^2 + \mu_j^2] - 2z\,(\iota^2 - |\lambda_j|^2)z + [(\iota - v_j)^2 + \mu_j^2]z^2} \qquad (35)$$

where $\lambda_j = \mu_j + \mathrm{i}v_j$ and operator $\prod'$ requires that the following calculation must be done for two roots for equation (35), $\lambda_j$ and $\lambda_j'$, and multiplied. As same as (20), $m$ is $(n\text{-}1) / 2$ when $n$ is odd number, or $n/2$ when $n$ is equal number and then the second factor of $H(z)$ is neglected.

*Application and Results*

Two bandpass filters were used to isolate the SV components obtained above. One passes the components of periods between 1200 years (= $1 / f_H$) to 3500 years (= $1 / f_L$). The edge of stopband is 1000 years (= $1 / f_S$). The other passes the periods between 600 years and 800 years, and the edge of stopband is 400 years. Nondimensional parameters are specified to 0.5 (= $A_P$) and 5 (= $A_S$) in both filters. The two SV components isolated by these filters were shown in Fig. 1-3-6. The component of longer period was named LPJPN and the component of shorter period was named SPJPN. Polar projections of these two SV components are exhibited in Figs. 1-3-7 and 1-3-8.

The SV component of longer period (LPJPN) shows smooth clockwise loops and some irregular motions (Fig. 1-3-7). During the times older than 8000 years B.P. and younger than 4500 years B.P., clear clockwise loops are traced out. Between 8000 years B.P. and 4500 years B.P., a counter-clockwise loop and cusps appear. This interval may be disturbed by a strong counter-clockwise motion added to smooth clockwise ones, considering that it is sandwiched by the two intervals

dominant with clockwise motions. This disturbed interval is started with the increase of amplitude of the U-D component.

The SV component of shorter period (SPJPN) represents thin ellipses (Fig. 1-3-8), suggesting rather oscillating motions than rotating ones. Such thin ellipsoidal features have been also suggested from the spectral analysis of the complex YZ-component. Linear motion of a field vector on the YZ-plane, regardless of its direction, yields a symmetrical spectrum in both clockwise and counter-clockwise rotations. Elliptical motion yields an asymmetrical spectrum weighted more heavily in the sense of looping (Denham, 1975). In both cases, spectral peaks appear at a same period for clockwise and counter-clockwise senses. The spectral peak of period about 700 years per cycle is stable for both clockwise and counter-clockwise senses, suggesting an oscillating or elliptic motion.

## 1-3-4. Sense of Rotation

### *Curvature of Vector Motion*

Sense of rotation can characterize the complex motions in the secular variation of field vectors. Curvature or second derivative of moving paths for a field vector represent sense of rotation. The curvature quantified by an angle $\theta$ that is,

$$\theta = \sin^{-1} \frac{(f_2 - f_1) * (f_3 - f_1)}{|f_2 - f_1| \, |f_3 - f_1|}$$

where $f_1$, $f_2$, and $f_3$ are three successive field vectors, an asterisk denotes a vector product.

### *Application and Results*

Curvatures were calculated for the data sets of HCJPN, LPJPN, and SPJPN. Fig. 1-3-9 shows plots of curvatures averaged within a three-points moving window. Clockwise and counter-clockwise senses are shown in white and black, respectively. When curvature maintains the value of nearly zero, the field vector moves linearly.

The curvature plot for HCJPN shows a complex pattern. The sense of rotation changes frequently and durations for persistence of one rotational sense are only about several hundred years. Further there seems to be no duration for linear movement.

The longer period SV components (LPJPN) is dominated by motions of clockwise sense, as in the middle of Fig. 1-3-9. Between 8000 years B.P. and 4500 years B.P., counter-clockwise pulses appear mixed with clockwise and linear motions. The motions with counter-clockwise sense seem to be added accidentally to the major motion with clockwise sense during only this time span.

In the shorter period SV components in the right of Fig. 1-3-9, clockwise and counter-clockwise senses persist for relatively long durations alternatively. Curvature of clockwise sense is maintained from 11000 to 8300 years B.P., followed by relatively short durations of counter-clockwise sense from 8300 to 6500 years B.P. and again clockwise sense from 6500 to 5300 years B.P.. A long duration of counter-clockwise sense appears from 5300 to 2200 years B.P., followed by a short duration of clockwise sense from 2200 to 1300 years B.P. and then a duration of counter-clockwise sense. The curvature for SPJPN is characterized by symmetrical appearance of both rotational senses with long durations > 1000 years.

Table 1-3-1. MEM spectral peak periods of HCJPN

| HCJPN | PEAK PERIODS (yrs/c) | | | |
|---|---|---|---|---|
| E-W comp. | | 2020 | 871 | |
| U-D comp. | 3700 | 1390 | | 716 |
| clockwise | | 1590 | | 750 |
| counter-clockwise | 3170 | | 945 | 716 |

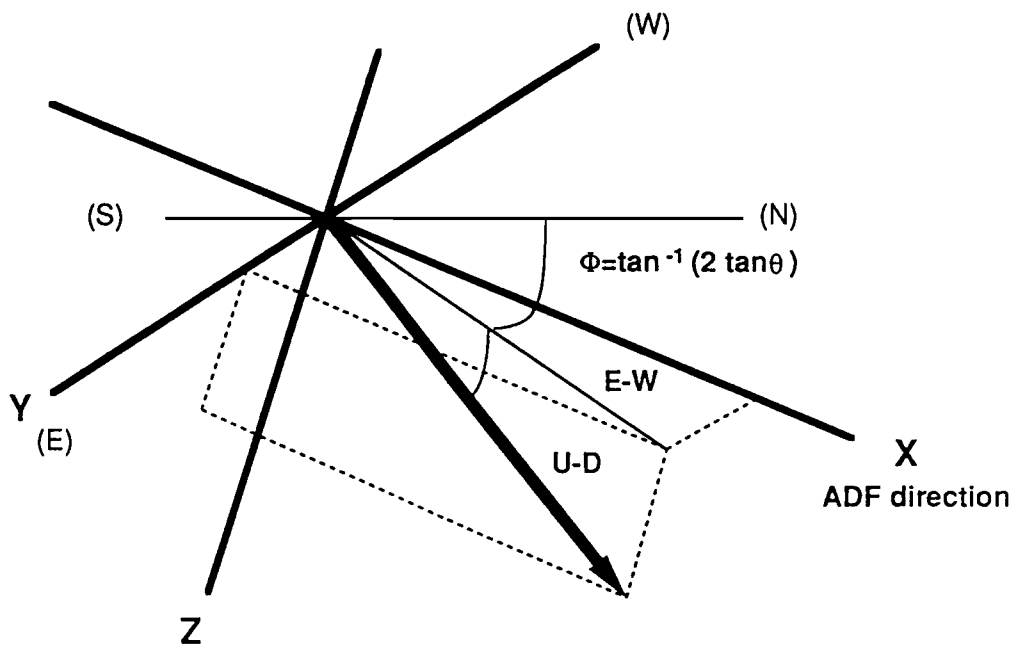


Fig. 1-3-1. The adopted reference frame (after Turner and Thompson ,1981). The X-axis coincides with the direction of the geocentric axial dipole field at a site. The Y-axis is a horizontal axis perpendicular to the X-axis. The Z-axis is perpendicular to the X- and Y-axes in the right hand system. The thick arrow shows the paleomagnetic field direction.

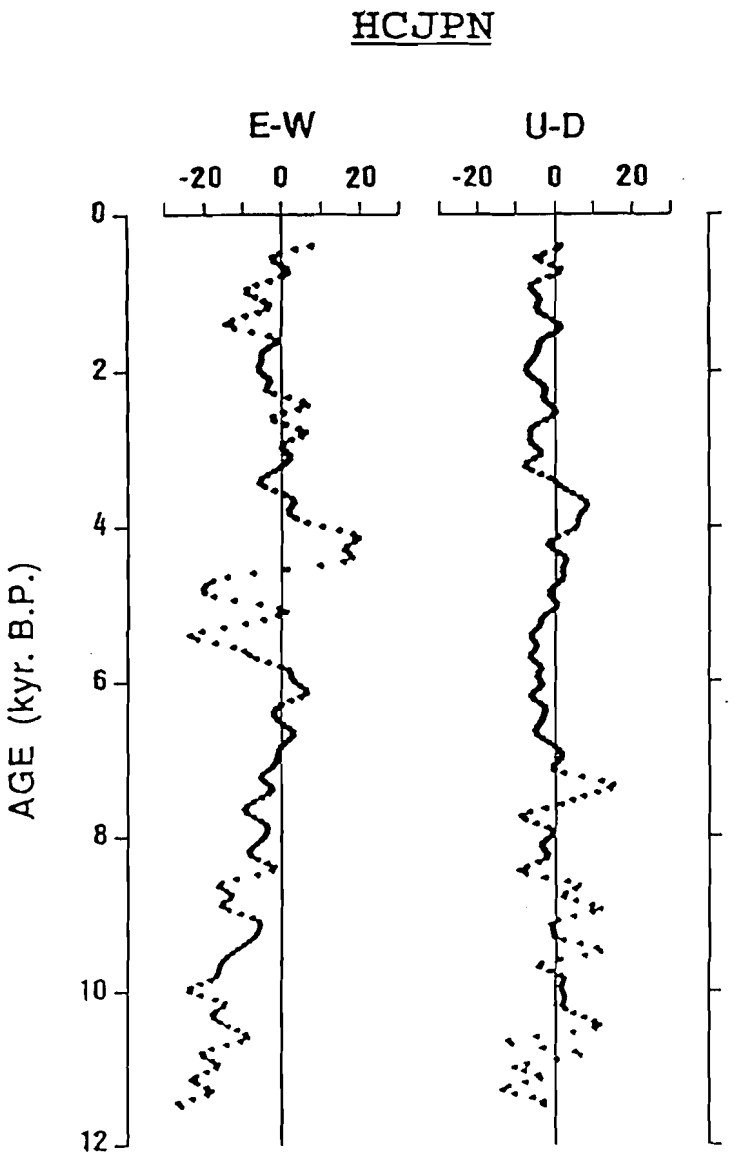


Fig. 1-3-2. Smoothed E-W and U-D components for the secular variation from central to southwest Japan, filtering frequencies higher than 5.0 cycles per kyr. The data points are at intervals of 50 years.

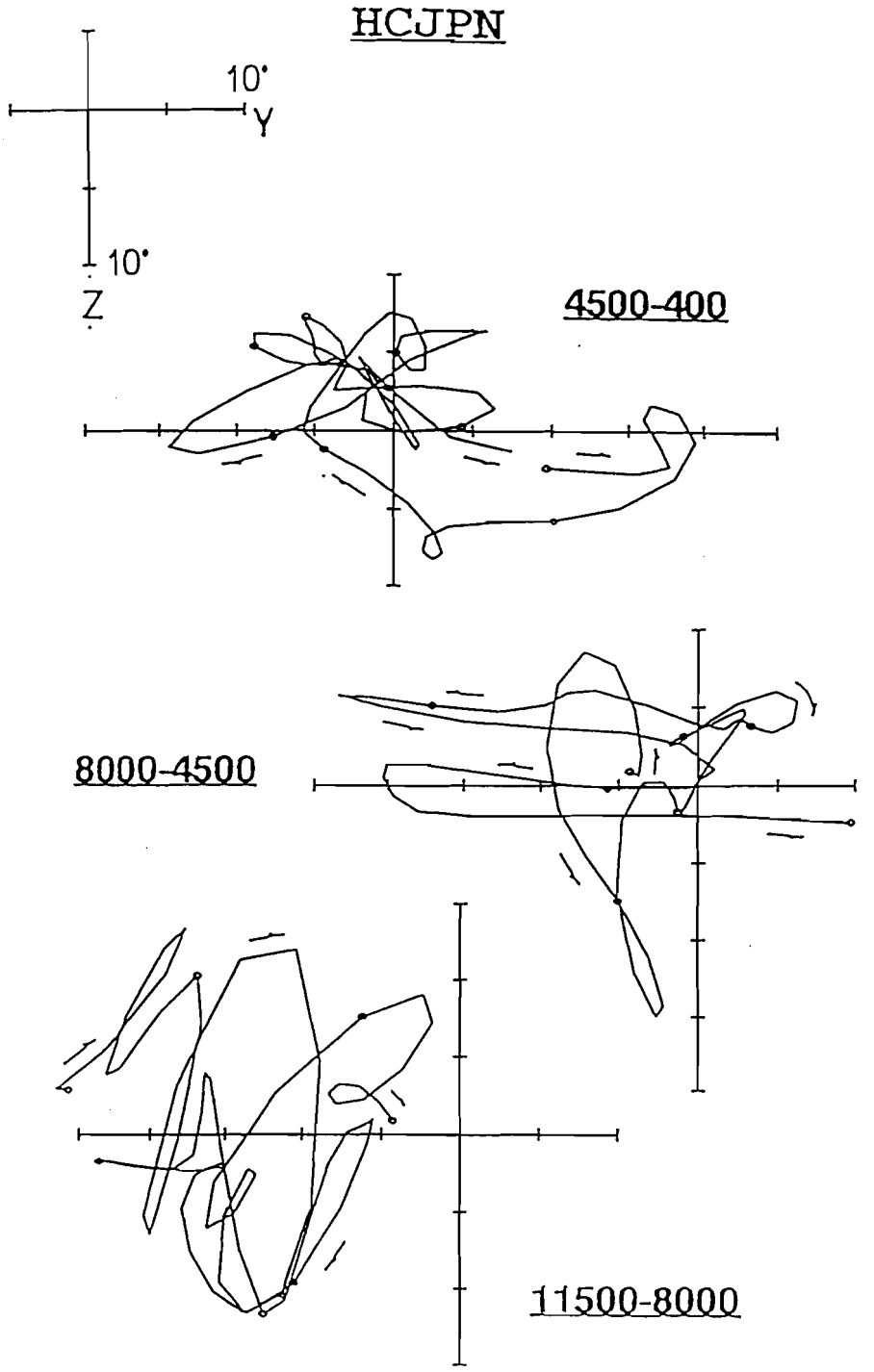


Fig. 1-3-3. Polar projections about the ADF of the secular variation from central to southwest Japan for separate intervals; 11500 - 8000 year B.P. (bottom), 8000 - 4500 year B.P. (middle) and 4500 - 400 year B.P. (top). The data points are at intervals of 50 years. Open circles show every 500 years data points from 11500 years B.P. to 500 years B.P.. The arrows show forward direction in time.

# Japan

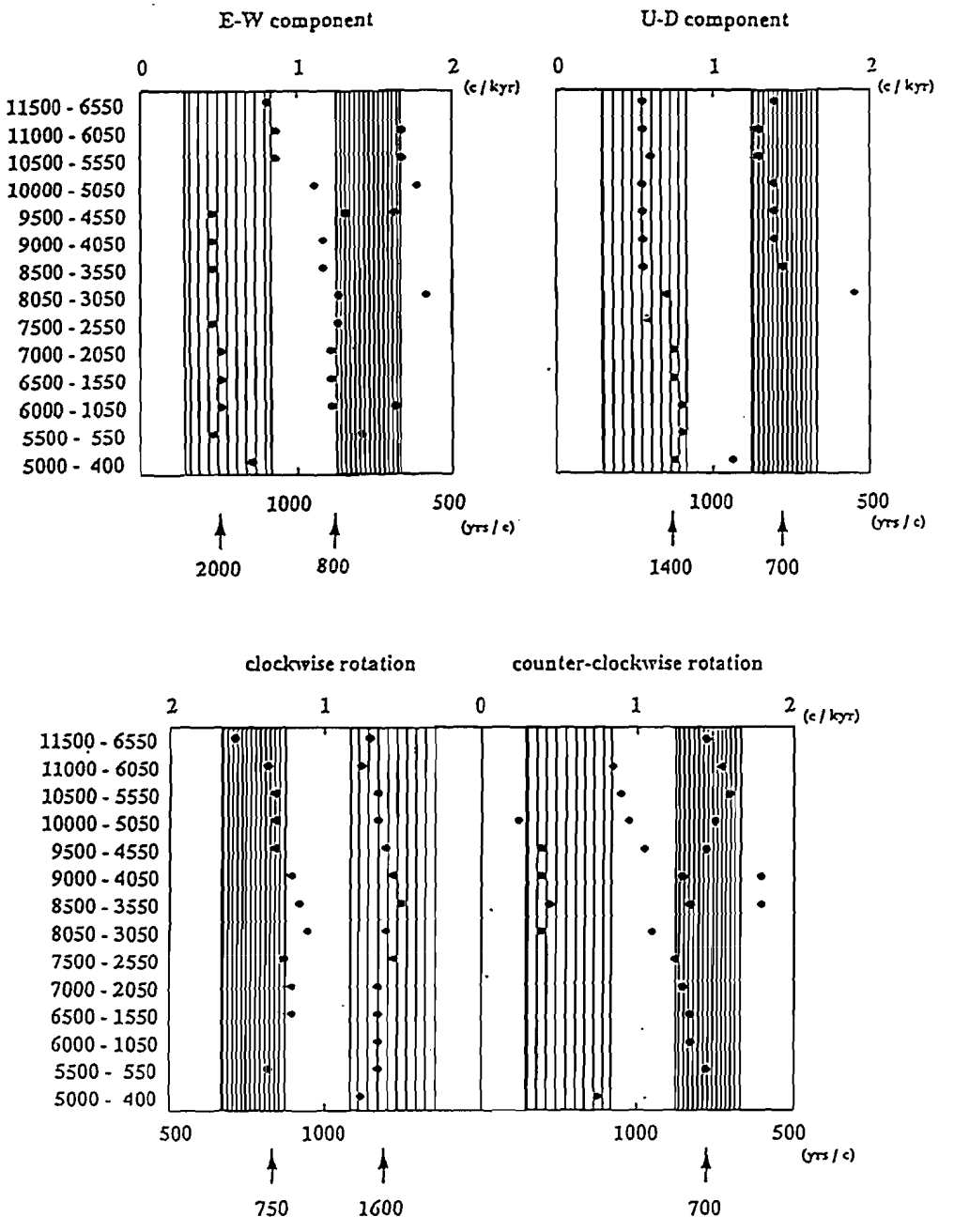


Fig. 1-3-4. MEM spectral peak periods of the HCJPN calculated within a moving window of 5000 years. Spectral peaks whose powers < 10% of the largest peak or whose periods > 5000 years are omitted. Stable existence of the period consistent with the whole data analyses (Table 1-3-1) are shown with arrows. The periods of spectral peaks are concentrated in two bands; 600 - 800 years per cycle (thin striped area) and 1200 - 3500 years per cycle (bold striped area).

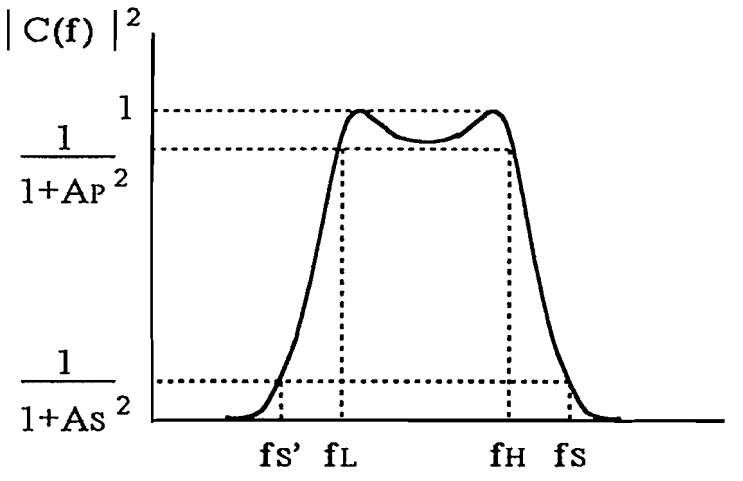


Fig. 1-3-5. A frequency response of bandpass filter. The frequency response is given by five parameters, three of which are critical frequencies at the edges of passband ($f_L$ and $f_H$), stopband ($f_S$ or $f_S'$), and two of which are nondimensional ones specifying maximum attenuation in the passband ($A_P$) and minimum attenuation in the stopband ($A_S$).

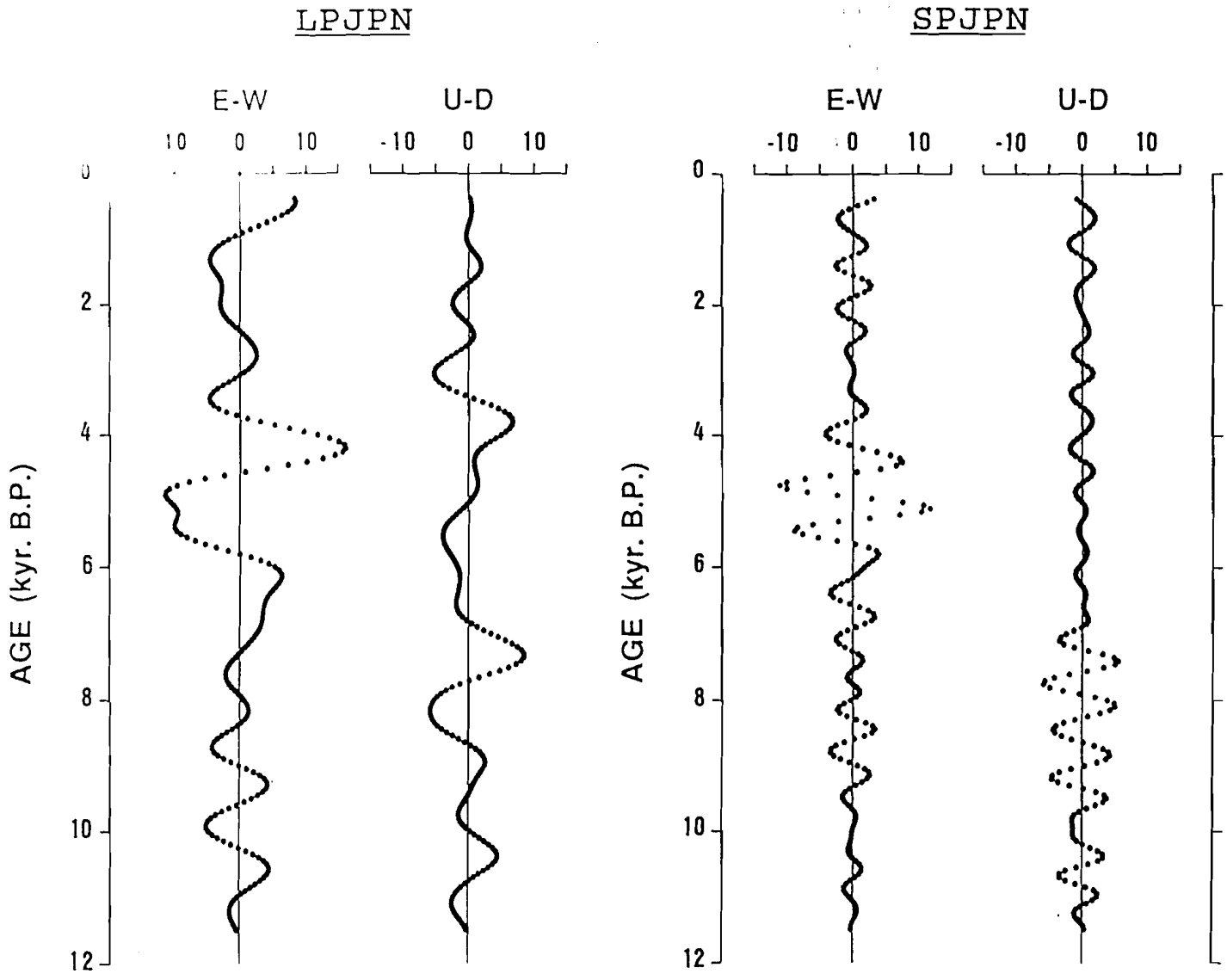


Fig. 1-3-6. E-W and U-D components of the secular variation for the bands of periods 1200 - 3500 years per cycle (LPJPN) and 600 - 800 years per cycle (SPJPN).

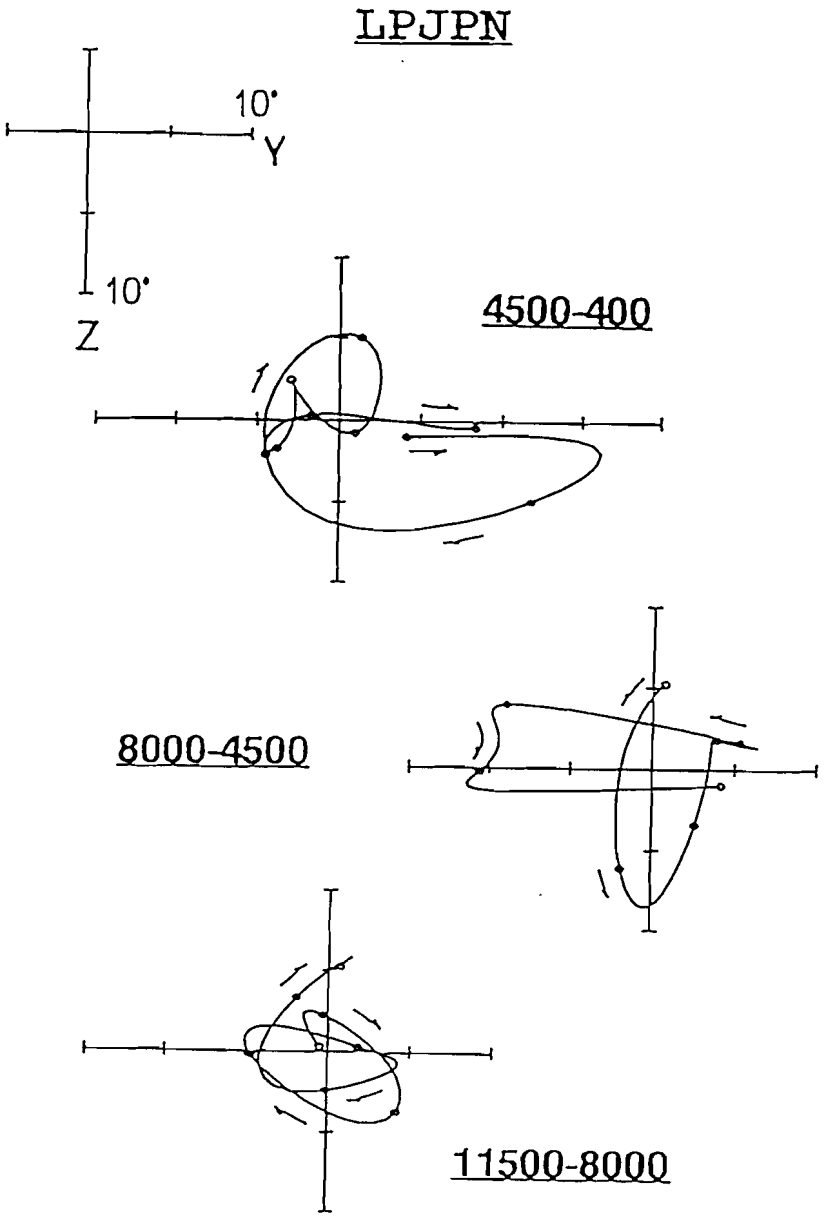


Fig. 1-3-7. Polar projections of the secular variation of band of periods 1200 - 3500 years per cycle for separate intervals. Open circles show every 500 years data points from 11500 years B.P. to 500 years B.P.. The arrows show forward direction in time.

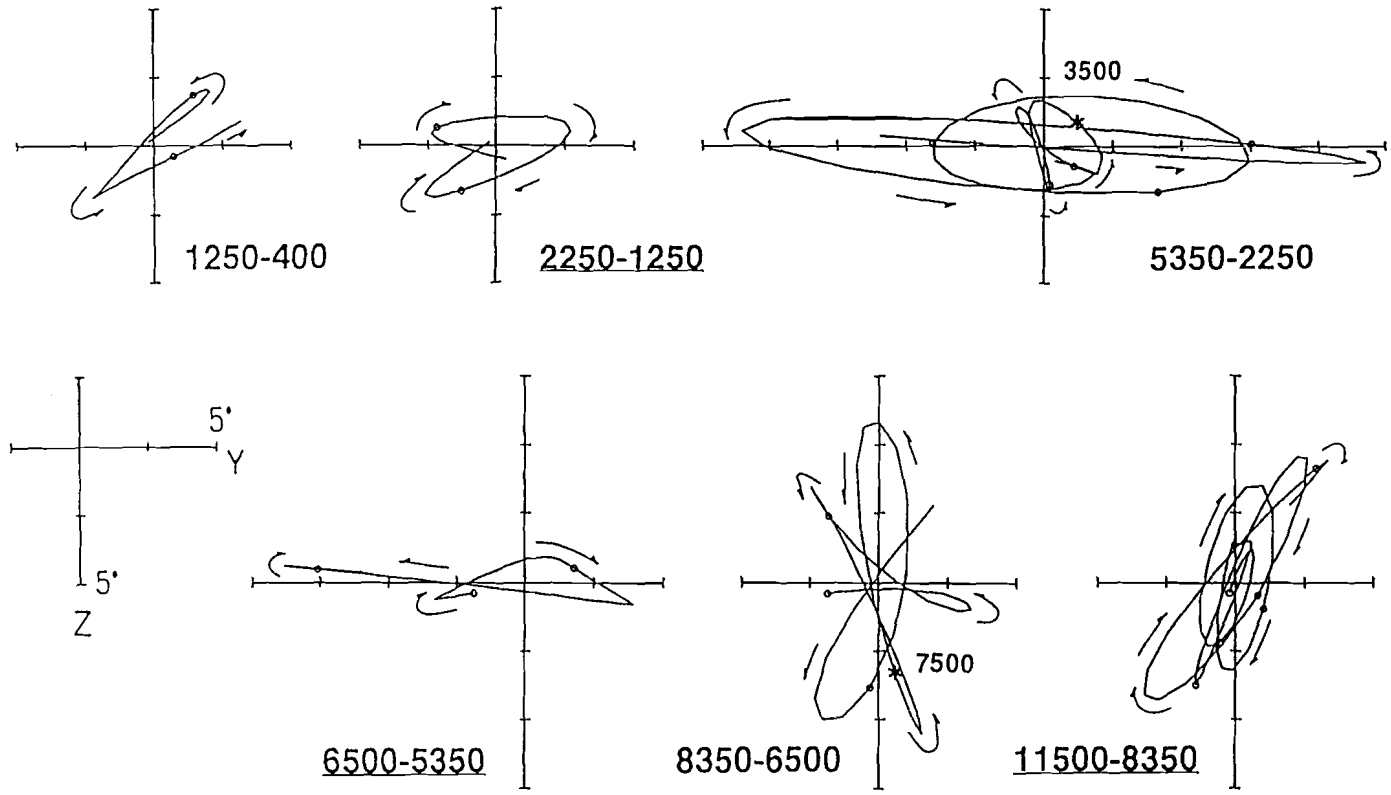


Fig. 1-3-8. Polar projections of the secular variation of the period band 600 - 800 years per cycle for separate intervals. The underlined intervals are dominated by clockwise motion. Open circles show every 500 years data points from 11500 years B.P. to 500 years B.P.. The arrows show forward direction in time. The asterisks (*) represent the data points of 7500 and 3500 years B.P..

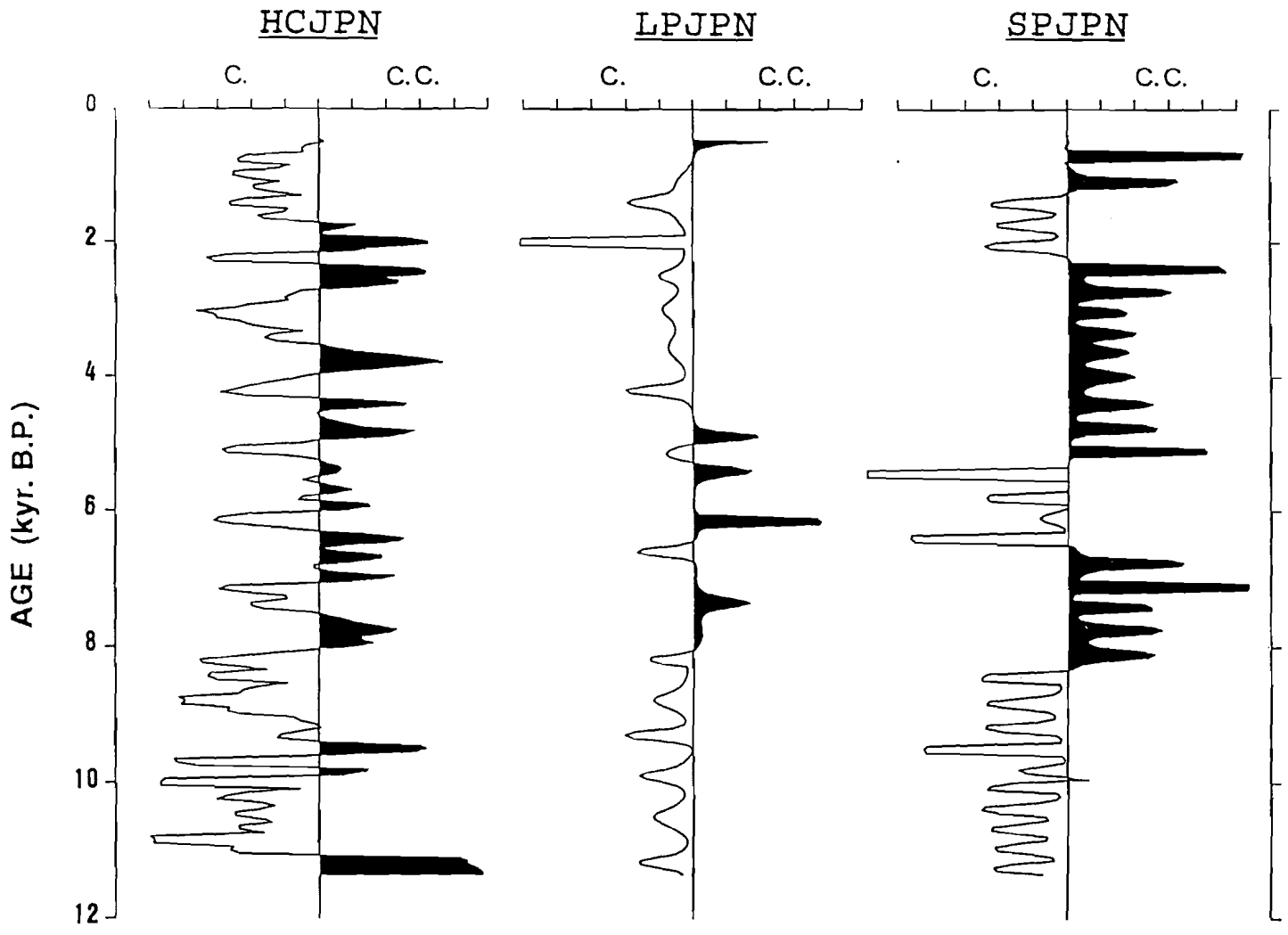


Fig. 1-3-9. Plots of curvature of field direction paths for the SV components of periods longer than 200 years per cycle (left), the SV components of band of periods 1200 - 3500 years per cycle (center) and the SV components of band of periods 600 - 800 years per cycle (right). Clockwise sense (C.) is shown in white and counter-clockwise sense (C.C.) is shown in black.

## 1-4. DISCUSSIONS

A local coordinate system whose one axis aligns with the normal polarity axial dipole field is useful to display a path of paleomagnetic directional change. A pair of E-W and U-D components is preferred to a pair of declination and inclination. Since the direction of time averaged field is approximately an ADF direction, E-W and U-D components can be regarded as deviations from a mean direction. The two components are compensated from the effect of latitude on the relative amplitude, so that they can describe most effectively a deviation from an average direction of field vectors at a single site. Hoffman (1984) applied the local ADF coordinate system to the data from polarity transitions and excursions, and illustrated the utility of the application. He used a polar stereographic display in the space perpendicular to the ADF direction for a given site. Our orthogonal projection in the YZ plane can represent the polar stereographic projection if the variational directions are not so far from the ADF direction.

The SV components of LPJPN and SPJPN represent most components in the original data, HCJPN. The two SV components have been isolated by band-pass filters with the frequency ranges around the two major spectral peaks. Powers of other peaks are negligibly small.

The results of complex MEM analyses show long term natures of field rotation as shown in Fig. 1-3-4. The nature are not represented in the curvature plots. It is because that the curvature plot can describe detailed structures of vector motion, but they are governed by instantaneous motions.

Origins of The Longer Period Variations

The secular variation component of the periodicity band between 1200 and 3500 years per cycle (LPJPN) is characterized by smooth clockwise loopings in the motion of field direction (Figs. 1-3-7, and 1-3-9). The periodicity of about 2000 years, at

which a spectral peak is obtained, is concordant with the length of time needed for a full axial rotation for the observed westward drifting fields. Smooth clockwise loops thus seem to be originated from continuous westward drifting anomaly. It seems reasonable to consider that the westward drift of field anomalies is an intrinsic behavior of the geomagnetic field for the last 11500 years.

A field vector can make an almost full loop while a drifting source moves only on the site's hemisphere. If a source drifts only on the anti-hemisphere of the site, looping features are hardly produced in the field vector. Therefore, it is reasonable to consider that the dominance of clockwise sense of rotation in the SV component of LPJPN verifies that westward drifting anomalies have existed in the Pacific hemisphere. Recent studies of the magnetic field at the core-mantle boundary have suggested that the westward drift is not global, and is almost completely absent from the Pacific region for last three centuries (Bloxham and Gubbins, 1985, 1987; Gubbins, 1991). Our result suggests that such a feature is instantaneous and the drifting feature have not been confined to the Atlantic hemisphere during the last 11500 years.

The curvature plot (Fig. 1-3-9) shows that the counter-clockwise motion of a field vector has been added irregularly to the steady clockwise motion. The historical geomagnetic data for the last 300 years show that drifting and standing field anomalies simultaneously exist and both anomalies have been varying with no interaction (Yukutake and Tachinaka, 1969). The standing fields are changed in their intensity. Intensity fluctuations of standing fields can disturb a smooth vector motion originated by steady westward drifting anomalies. The break up of the smooth clockwise motion may be explained by a large fluctuation of intensity of a standing field near Japan.

Origins of The Shorter Period Variation

The SV component of period about 700 years per cycle (SPJPN) is characterized by thin elliptic oscillation (Fig. 1-3-8). The elliptic pattern may be produced by intensity fluctuation of source fields. One ellipse corresponds to one cycle of growth and decay or growth to opposite sign. The peaks of curvature in Fig. 1-3-9 would coincide with the maxima and/or minima of source's intensity.

Matsushima and Honkura (1988) estimated the periods and amplitudes of non-dipole field fluctuations using Gauss coefficients during 1550 to 1980 A.D.. As a result, they clarified that there are large amplitude fluctuations of standing fields with periods about 600 years per cycle. This seems to be consistent with that the intensity fluctuations with period of about 700 years suggested by our data. This time scale motion is also proposed as an incidental feature to the geomagnetic dynamo implied from the frozen flux theorem (Hide, 1982).

Oscillation of a long axis of ellipse seems to be confined to certain regions (Fig. 1-3-8). In the first interval from 11500 to 7500 years B.P., the azimuth of long axes of ellipse seems almost confined to the Z-axis so that the amplitude of the U-D component is larger than that of the E-W component (Figs. 1-3-6 and 1-3-8). In the intervals from 6500 to 3500 years B.P. and from 2250 to 400 years B.P., the long axes are almost aligned along the Y-axis and then the amplitude of the E-W component is larger. These confined alignments imply that the source fields can not move freely, confined to certain places during these three intervals. The first two durations are 4000 and 3000 years long. A fluctuating standing field make a linear oscillation in field vector. If there are another drifting fields whose intensities are not so strong near the site, the linear motion would be changed to an elliptic orbit. A change of drifting direction may result in a change of sense of looping motion. Then it is reflected in the curvature pattern. One duration for persistence of one sense of curvature would indicate one stable stage of geomagnetic field variation pattern. Though the ellipses are very thin, the sense of curvature of SPJPN is critical.

There are two intervals characterized by peculiar motions of field vector; the intervals from 7500 to 6500 years B.P. and from 3500 to 2250 years B.P. (see Fig.

1-3-8). The motion is similar to the quasi-hypotrocoid motion proposed for the dipole wobble by Kawai and Hirooka (1967). They explained the motion of VGP from archaeomagnetic secular variation data by combing two different rotations of a main dipole; one rotation has a period longer than the other and its rotational sense is opposite to the other. The hypotrochoid motion in our data appears when the curvature changes the sense, that is regarded as the changes of drifting direction. The two intervals for such motions may be transitional for the change in drifting direction, then the existence of eastward and westward motions can be also explained. Simultaneous occurrence of both motions has been suggested by Yukutake (1987) in the historical geomagnetic data.

## 1-5. CONCLUSION

A method to analyze paleomagnetic secular variations was introduced. The method consists of four steps. First, a time series of a pair of declination and inclination is transformed to those of ADF reference frame. Second, characteristic periodicities are deduced by spectral analysis. Third, the secular variation components of the periodicities are isolated by band-pass filters. Last, motions of field vectors are investigated by polar projections and curvature calculations for each secular variation component. Application of this method to the Japanese secular variation for the last 11500 years was succeeded in characterizing two periodic motions of field vector.

The secular variation component of periodicity about 2000 years per cycle is dominated by smooth clockwise loops suggesting a steady westward drifting field. There is a break up of the smooth clockwise looping during the time from 8000 to 4500 years B.P., which may be generated by accidental occurrence or growing up of a standing field.

The secular variation component of periodicity about 700 years per cycle is characterized by thin elliptic motions, which are probably generated by the intensity fluctuation of source fields. The sense of curvature in this component is frequently changed and the azimuth of long axis of ellipse is remained constant for 3000 - 4000 years except two short intervals. The latter suggests that the source field is stationary. The component of periodicity about 700 years consists of succession of time spans of different regional geomagnetic field variations. During the intervals from 7500 to 6500 years B.P. and from 3500 to 2250 years B.P., the field vector shows a trochoidal motion. The intervals may be transitional from one steady state to the other.

# A Geomagnetic Secular Variation Study by Separation of A Field Variation into Its Spectral Components

## 2. Global Analyses of Paleosecular Variation

## 2-1. INTRODUCTION

In the previous chapter, we have succeeded in separation of secular variation components for the Japanese geomagnetic record. As a result, it was revealed that westward drifting of non-dipole fields is an intrinsic behavior of the geomagnetic field for the last 12000 years. In this chapter, the same method is applied to paleomagnetic secular variation records from other sites on the globe, in order to examine if the westward drifting is a global feature.

Reliable geomagnetic secular variation records have been obtained from lacustrine sediments in U.K. (Turner and Thompson ,1981), North America (Lund and Banerjee, 1985), and Australia (Burton and McElhinny, 1982). The sites of U.K. and North America, both of which are in the northern hemisphere, are equally separated from Japan in longitude and close to Japan in latitude (Fig. 2-1-1). The site of Australia is in the equatorial symmetric position to Japan in the same longitude.

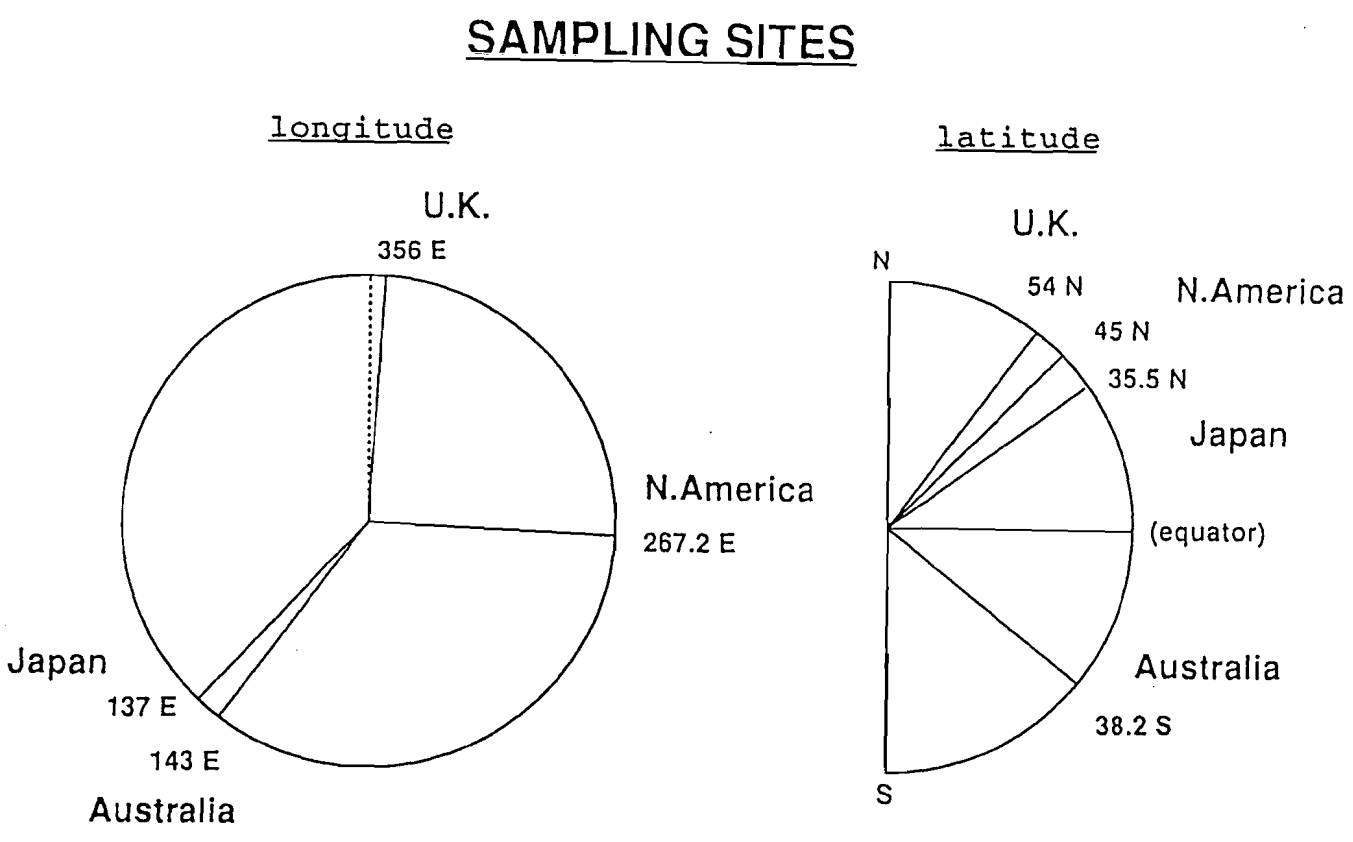


Fig. 2-1-1. Locations of field observation sites by sedimentary magnetism. Site longitudes are projected on a latitudinal plane (left) and site latitudes are projected on a longitudinal half plane (right).

## 2-2. SECULAR VARIATION RECORD FROM U.K.

### 2-2-1. Data

Turner and Thompson (1981, 1982) have published the paleomagnetic records of 10 unoriented cores from Loch Lomond in Scotland, Lake Windermere in North England, and Llyn Geirionydd in North Wales (Fig. 2-2-1). All sediment cores are fine-grained organic muds.

Age control is based on 19 preferred radiocarbon dates from 30 age determinations and pollen analyses on three cores: the elm decline, which is dated between 5000 to 5200 years b.p. ($^{14}C$) for the whole of northwest Europe. The conventional radiocarbon ages (years b.p.) have been calibrated to calender years (years B.P.) using Clark's (1975) treatment of the bristlecone pine tree ring data. The individual depth scales were connected with each lake from susceptibility and lithology correlations, and a preferred time scale was transformed to each core. Transformation was made by linear interpolations between the depths dated. Values of declination and inclination every 40 years were calculated by linear interpolation between the two original data points immediately above and below, and an equal interval data set of each core was obtained.

A composite record was obtained by averaging the dated records from 10 cores (UKDORG; Fig. 2-2-2). The sequence of unit vectors describing the magnetic direction record of each core was rotated so as to place its mean direction (the mean over the section of core between 0 and 7000 years B.P.) at zero transformation. The transformed coordinate frame of each core is thus assumed to represent the mean geomagnetic field direction during the last 7000 years. The 10 records can be averaged in this coordinate system. The averaged record has been detransformed to absolute declination and inclination system, so as to match the uppermost westerly swing to the London observatory swing which extends to 24°W (Turner and Thompson, 1982).

## 2-2-2. Analyses and Results

### *Transformation to The ADF Reference Frame*

The time series of unit field vector (UKDORG; Fig. 2-2-2) was transformed into an axial dipole reference frame. A site latitude was set to 54°N. The time series of E-W and U-D components were calculated by the procedure shown in the section 1-2-1. The data points were calculated at intervals of 50 years by linear interpolation between two adjacent data for the points having no original data. Smoothing was performed to the data set with a Chebyshev low-pass filter which cut the frequencies higher than 5.0 cycles per kyr (period = 200 years).

The time series of E-W and U-D components smoothed (HCUKD) are shown in Fig. 2-2-3. The amplitudes of change in the two components are almost equal. Both components seem to be consist of long wave length changes with large amplitudes and small fluctuations. The amplitude of variational features is somewhat reduced by treatments of stacking and averaging interpolations. Consequently, short-duration fluctuations become vague.

Polar projections about the axial dipole field direction (X-axis) clearly show remarkable characters of the variational features. There are two intervals of linear fluctuations, 8600 - 6000 years B.P. and 6000 - 1500 years B.P.. The azimuth of linear fluctuations in one interval is perpendicular to that in the other interval. Before 6000 years B.P., the field vector is limited in the far-sided area ($Z<0$). After 6000 years B.P., the field vector shows more broad variation.

### *Spectral Analyses*

Spectral analyses were carried on the scalar and vector time series of E-W and U-D components for HCUKD, using the maximum entropy method. Lengths of prediction error filter ($m$) were chosen satisfying the Akaike's final prediction error

criterion (Akaike, 1969a, b, 1970) and an empirical formula of $m < 3N^{1/2}$, where $N$ is number of data.

Results of spectral analyses are shown in table 2-2-1. The U-D component shows no clear spectral peak within the period bands shorter than the data-length and longer than 500 years per cycle. For the other three components, a periodicity about 1900 years per cycle is commonly obtained. It implies that the variational feature of periodicity about 1900 years is linear. A periodicity of about 4500 years per cycle is obtained for the E-W and the counter-clockwise rotational components. A periodicity of 1030 years is obtained only for the clockwise rotational component.

To test stability of the estimated spectra throughout the length of time span of data, spectral analyses were again carried out within a sliding window of 5000 years every 500 years. The results are summarized in Fig. 2-2-5, where each point shows a period of the spectral peak in each sliding window.

Stable spectral peaks are obtained at a periodicity of about 4000 years per cycle for the E-W component. The periodicity of about 1810 years per cycle is only in two windows, 9800 - 5050 years B.P. and 5500 - 550 years B.P.. Thus, the spectral analysis does not show stable periodicity of 1810 years per cycle, however, the wave morphology suggests its existence. There are four remarkable easterly deflections in the E-W component at ages 9200, 7200, 2700 and 1000 years B.P.. The interval between the older two deflected ages is 2000 years, and that between the younger two is 1700 years. They seem to fit to the periodicity of about 1810 years. There are no easterly swing between 7200 and 2700 years B.P., at which one or two easterly deflections are expected to appear if the variation of periodicity about 1810 years per cycle continued. In the interval from 7200 to 2700 years B.P., the variation of periodicity about 1810 years may be diminished. The spectrum for the youngest window has a peak whose periodicity is 2350 years per cycle. Two peaks of periodicities, 4000 years per cycle and 1810 years per cycle, may be failed to separate.

The U-D component has the periodicity of about 2000 years per cycle before 3050 years B.P. and the periodicity of about 1000 years per cycle after 7500 years

B.P.. Thus no clear peak periods are obtained from whole data analyses. Only in a window from 5000 to 300 years B.P., both periodicity peaks appear.

For clockwise rotation of a field vector on the Y-Z plane, the periodicity about 2110 years is stably obtained before 3550 years B.P. and the periodicity about 1030 years appears after 7500 years B.P.. For the counter-clockwise rotation, stable spectral peaks are not obtained at the two periods, 4750 and 1810 years per cycle, obtained from the whole data analysis. An intermediate periodicity of the two periods, 2200 years per cycle, is obtained in windows before 3050 years B.P.. After that, no stable periodicity is obtained. The estimation of prediction error filter may be too high in the whole data analysis of total vector series, so that the split of a spectral peaks occur.

Signals whose periods are in the bands from 4000 - 1800 years per cycle, which are shown by the bold striped areas in Fig. 2-2-5 exist in all of SV components. The periodicity about 1000 years per cycle is obtained for the windows after 7000 years B.P. of the U-D and clockwise components. The spectral power concentrates at the longer side of periodicity, consequently it is considered that the peak of periodicity about 1000 years per cycle becomes negligibly small in other windows after 7000 years B.P..

*Separation of Quasi Periodic Motions*

Spectral peaks are concentrated in a band of periods from 4000 -1800 years per cycle. The SV component of this band of periods was isolated using a Chebyshev band-pass filter, named LPUKD (Fig. 2-2-6). A polar projection of LPUKD is represented in separate intervals in Fig. 2-2-7. The plots suggest a change in the azimuth of linear fluctuations. The motion extends from west-down direction to east-up direction before 6000 years B.P.. After 5000 years B.P., it extends from west-up direction to east-down direction. After 1000 years B.P., the elongation direction returns to the direction before 6000 years B.P.. There are transitional intervals of about

1000 years long between them. Smooth loops are only seen between 7000 to 5500 years B.P. in the polar projection of LPUKD.

The SV component of period about 1000 years per cycle was also isolated from the original data, using a filter passing periodicities between 1200 to 800 years per cycle. This component was named SPUKD (Fig. 2-2-6). A polar projection of SPUKD is in Fig. 2-2-8. The plots of SPUKD in Fig. 2-2-6 show that the amplitude of U-D component gradually increases with time while the amplitude of E-W component is unchanged. The field vector traces triple clockwise loops in the interval from 4700 to 1500 years B.P., and then the motion is replaced by the counter-clockwise motion accompanied by amplification of U-D component. Before 4000 years B.P. the motion of this periodicity is very small.

*Sense of Rotation*

Instantaneous sense of rotation is defined with curvature. Curvatures were calculated for the data sets of HCUKD, LPUKD and SPUKD. Fig. 2-2-9 shows plots of curvatures averaged within a three-points moving window. Clockwise and counter-clockwise senses are shown in white and black, respectively.

HCUKD changes its rotational sense frequently. The durations for persistence of one rotational sense are < 1000 years. In the shorter period SV component (SPUKD), both of clockwise and counter-clockwise senses persist for relatively long durations alternatively. The durations for persistence of clockwise sense are about 3000 years, which are longer than those of counter-clockwise sense (< 2000 years). The curvature plot of the longer period SV components (LPUKD) shows pulse-like form, which can be easily expected from the linear motion in the Y-Z plane (Fig. 2-2-

2.2.3. Discussion

The original secular variation of U.K. does not show strong evidence for the persistence of non-dipole field westward drifting. The spectral analyses of HCUKD show a well resolved clockwise periodicity of about 2000 years per cycle, suggesting westward drifts. This component has a looping feature only in the interval between 7000 and 5500 years B.P.(Fig. 2-2-7), and the sense of rotation is clockwise during the interval (Fig. 2-2-9).

The elongation direction of linear motion of LPUKD in the YZ-plane may imply a direction of an active oscillating field. From 9800 to 6000 years B.P., an active oscillating field may have existed to the west of U.K. and then to the east till 2000 years B.P.. After 1000 years B.P., it returned to the west. It is possible that clockwise loopings caused by westward drifting fields are disturbed by field variations generated by such oscillating fields.

For the SV component of SPUKD, triple clockwise loops from 4700 to 1500 years B.P. may be caused by westward drifting fields. The clockwise sense is more stable than the counter-clockwise sense according to the lengths of persisting intervals. The geomagnetic field directions observed in London has been moving with clockwise sense during the last 300 years (Malin and Bullard, 1981; Fig. 2-2-10). This loop is considered to be a part of a clockwise looping of periodicity about 1000 years per cycle. The counter-clockwise motion since about 1500 years B.P. in the component of SPUKD may stop at about 300 years B.P. (1650 AD).

Table 2-2-1. MEM spectral peak periods of HCUKD

| HCUKD | PEAK PERIODS (yrs/c) | | |
|---|---|---|---|
| E-W comp.<br>U-D comp. | 4220 | 1810 | |
| clockwise | | 2110 | 1030 |
| counter-clockwise | 4750 | 1810 | |

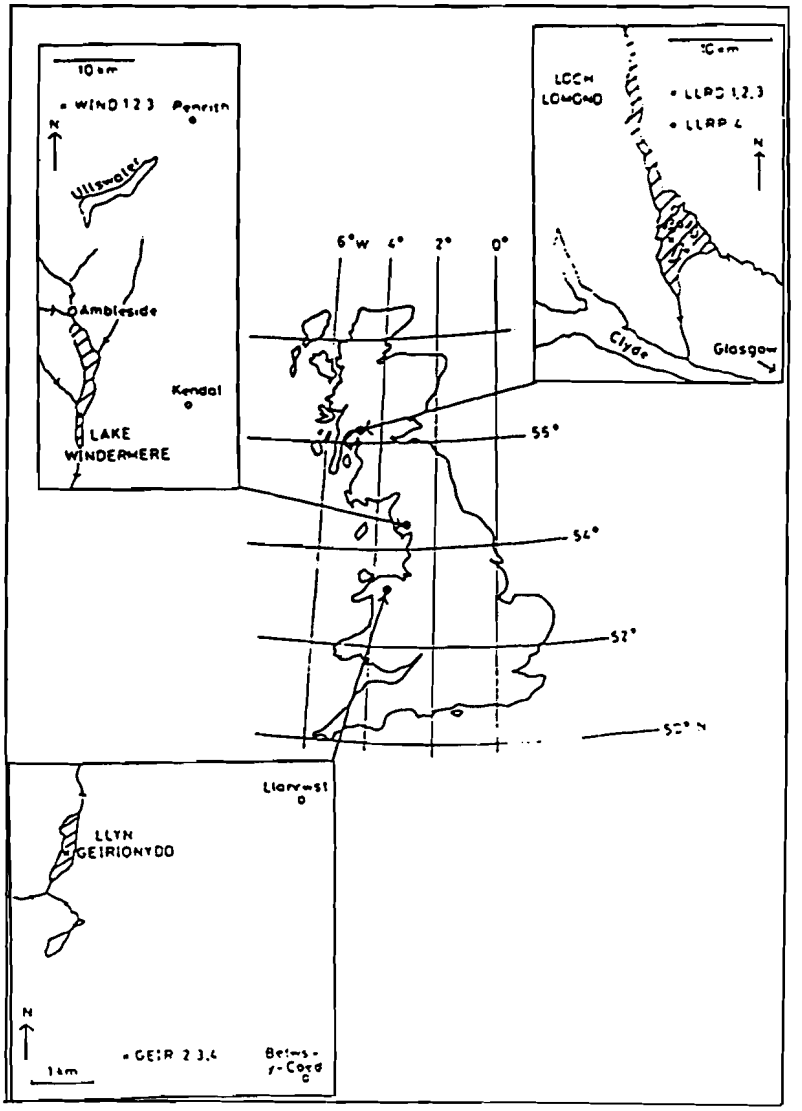


Fig. 2-2-1. Great Britain, showing localities of Loch Lomond, Lake Windermere and Llyn Geirionydd, and Coring sites (after Turner and Thompson, 1981).

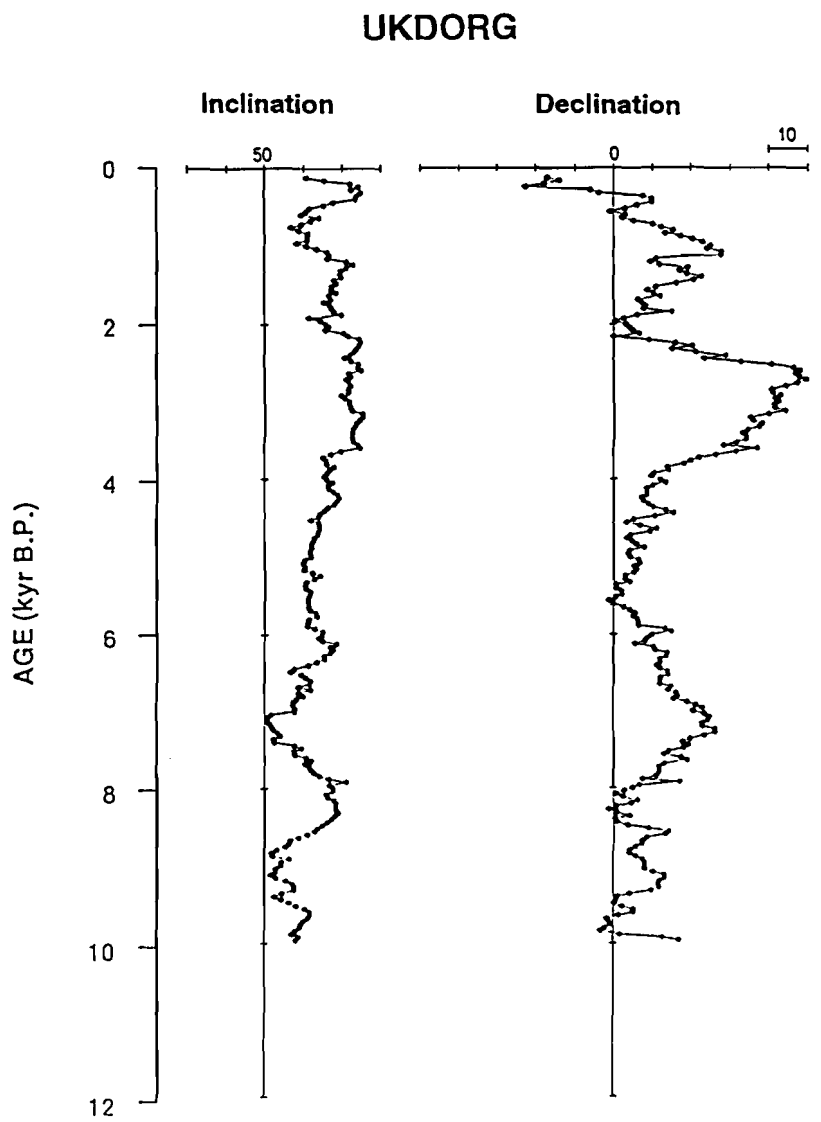


Fig. 2-2-2. Averaged inclination and declination of ten cores from three lakes plotted against age at 40 years intervals (after Turner and Thompson, 1982).

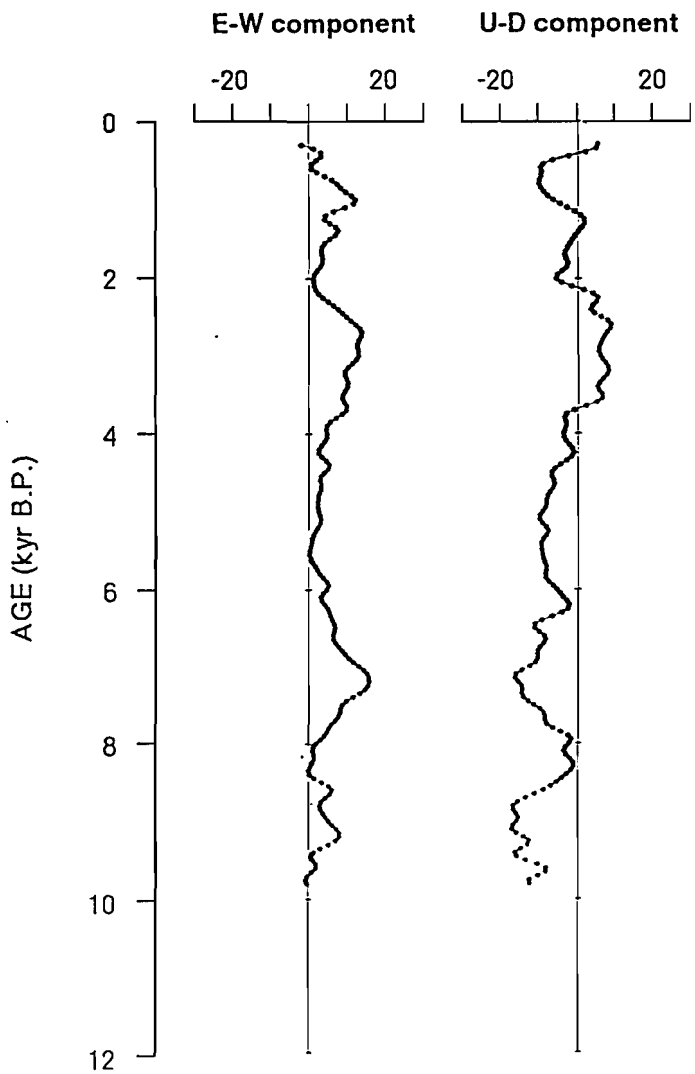


Fig. 2-2-3. Smoothed E-W and U-D components for the secular variation from U.K., filtering frequencies higher than 5.0 cycles per kyr. The data points are at intervals of 50 years.

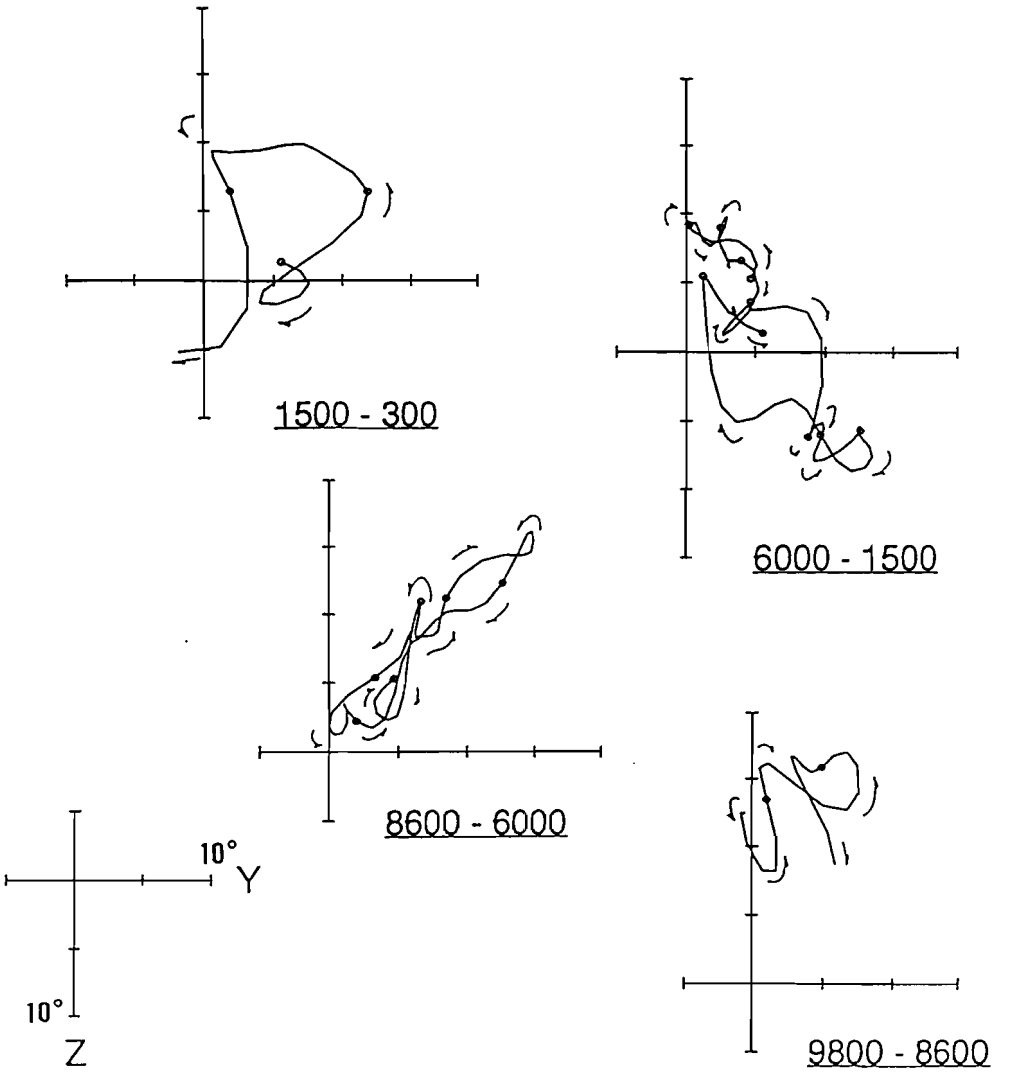


Fig. 2-2-4. Polar projections about the ADF of the secular variation from U.K. for separate intervals; 9800 - 8600 year B.P. (bottom right), 8600 - 6000 year B.P. (bottom left), 6000 - 1500 years B.P. (top right), and 4500 - 300 year B.P. (top left). The data points are at intervals of 50 years. Open circles show every 500 years data points from 9500 years B.P. to 500 years B.P.. The arrows show forward direction in time.

# U.K.

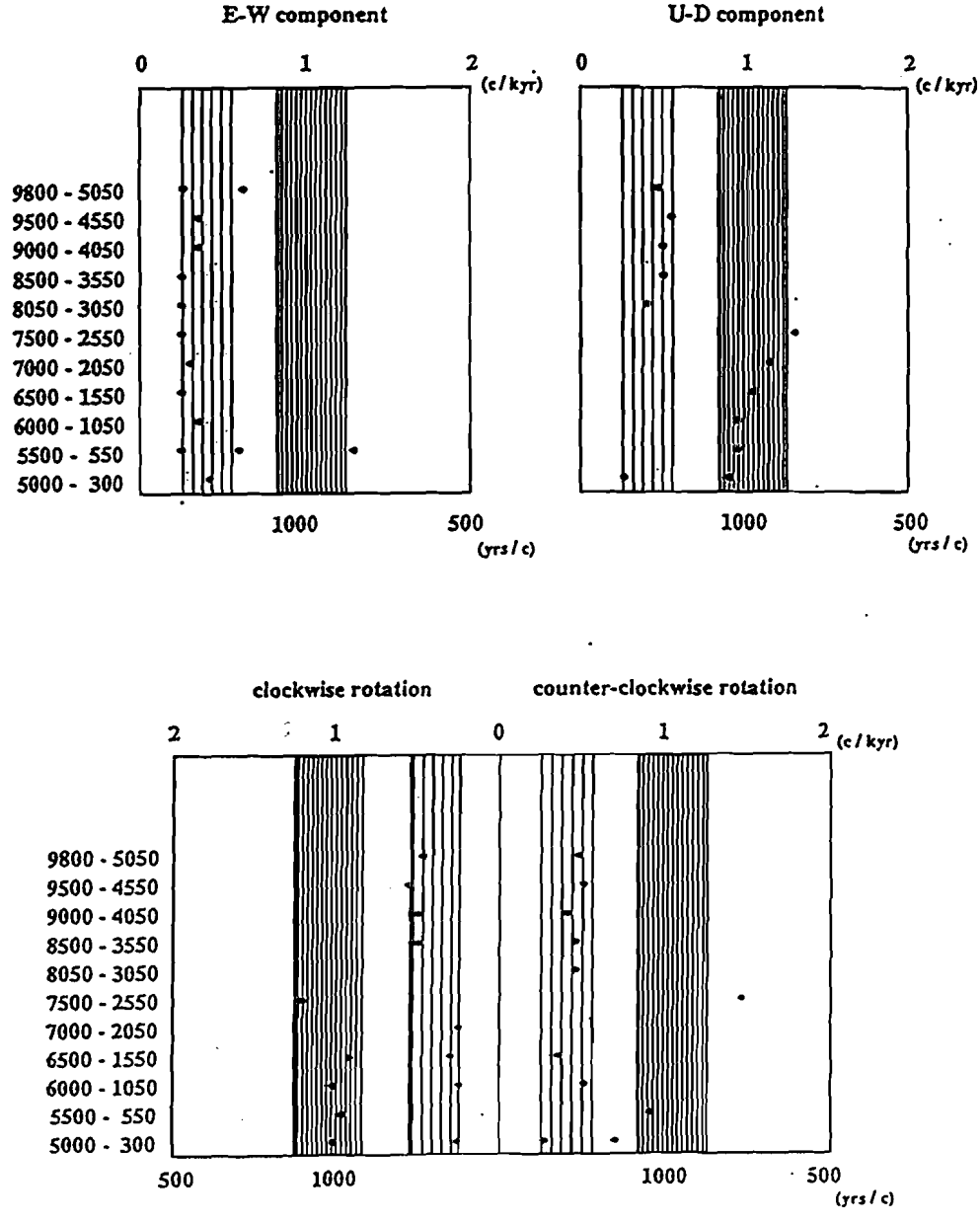


Fig. 2-2-5. MEM spectral peak periods of the HCUKD calculated within a moving window of 5000 years. Spectral peaks whose powers < 10% of the largest peak or whose periods > 5000 years are omitted. The periods of spectral peaks are concentrated in two bands; 1200 - 800 years per cycle (thin striped area) and 4000 - 1800 years per cycle (bold striped area).

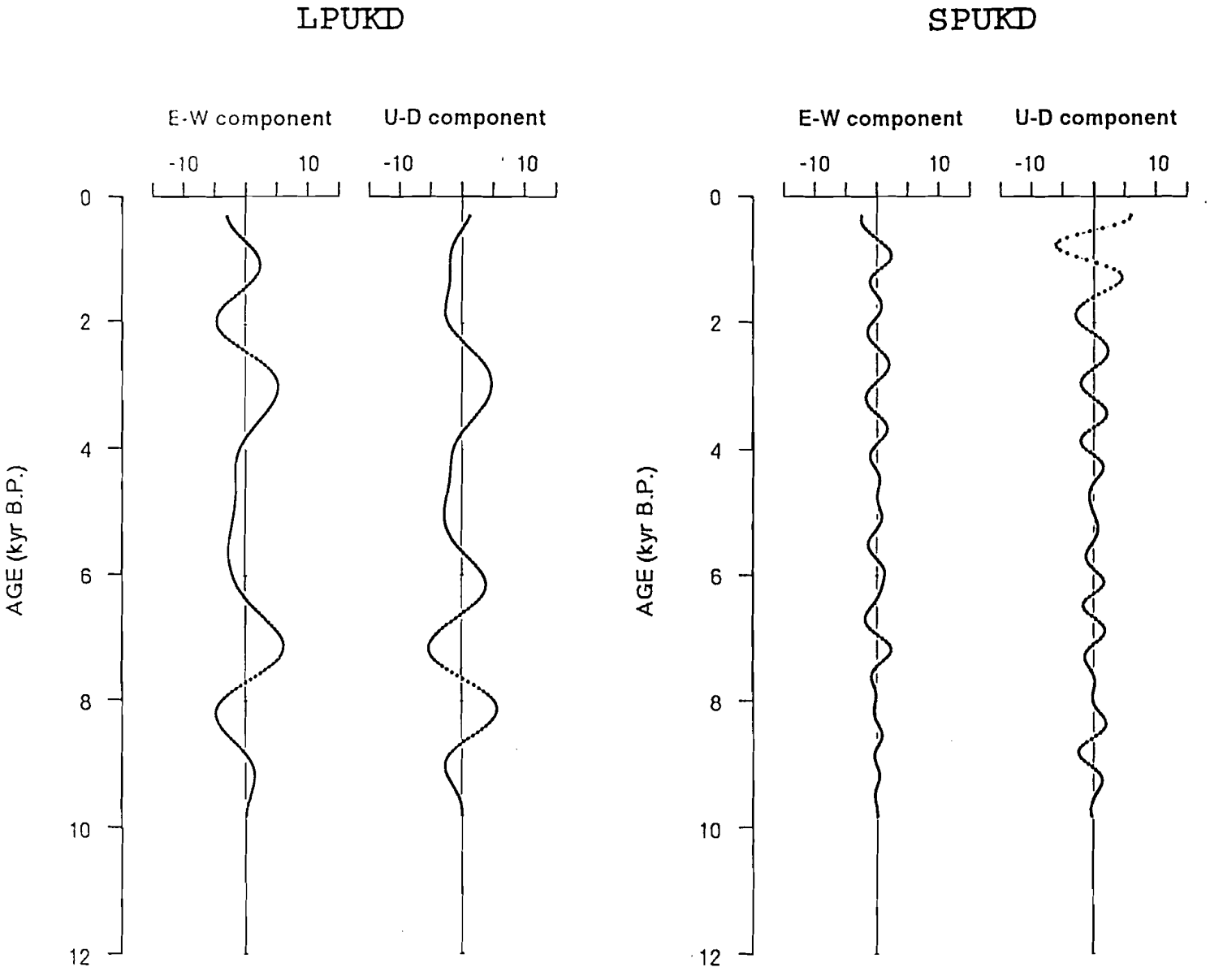


Fig. 2-2-6. E-W and U-D components of the secular variation for the bands of periods 4000 - 1800 years per cycle (LPUKD) and 1200 - 800 years per cycle (SPUKD).

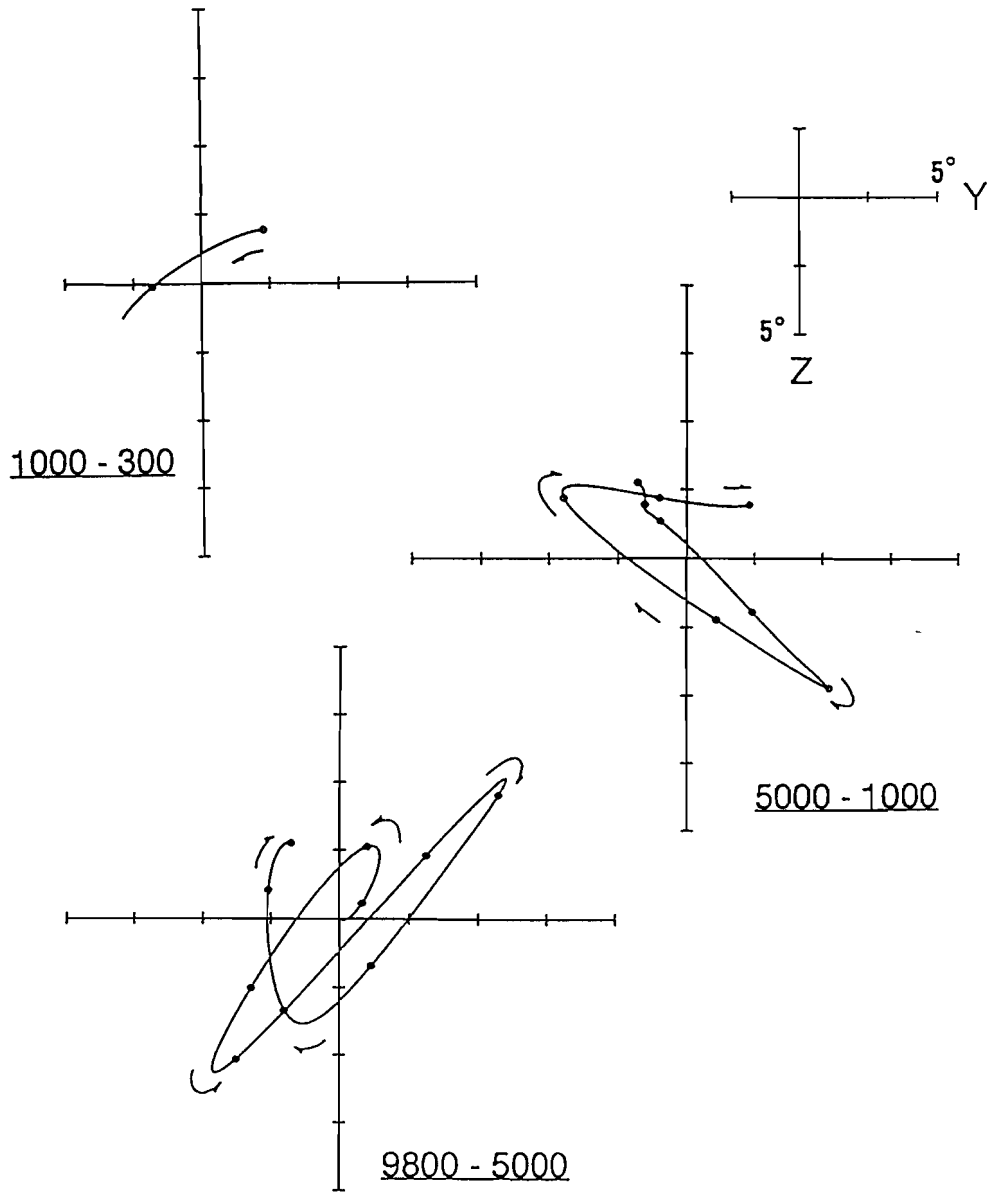


Fig. 2-2-7. Polar projections of the secular variation of band of periods 4000 - 1800 years per cycle (LPUKD) for separate intervals. Open circles show every 500 years data points from 9500 years B.P. to 500 years B.P.. The arrows show forward direction in time.

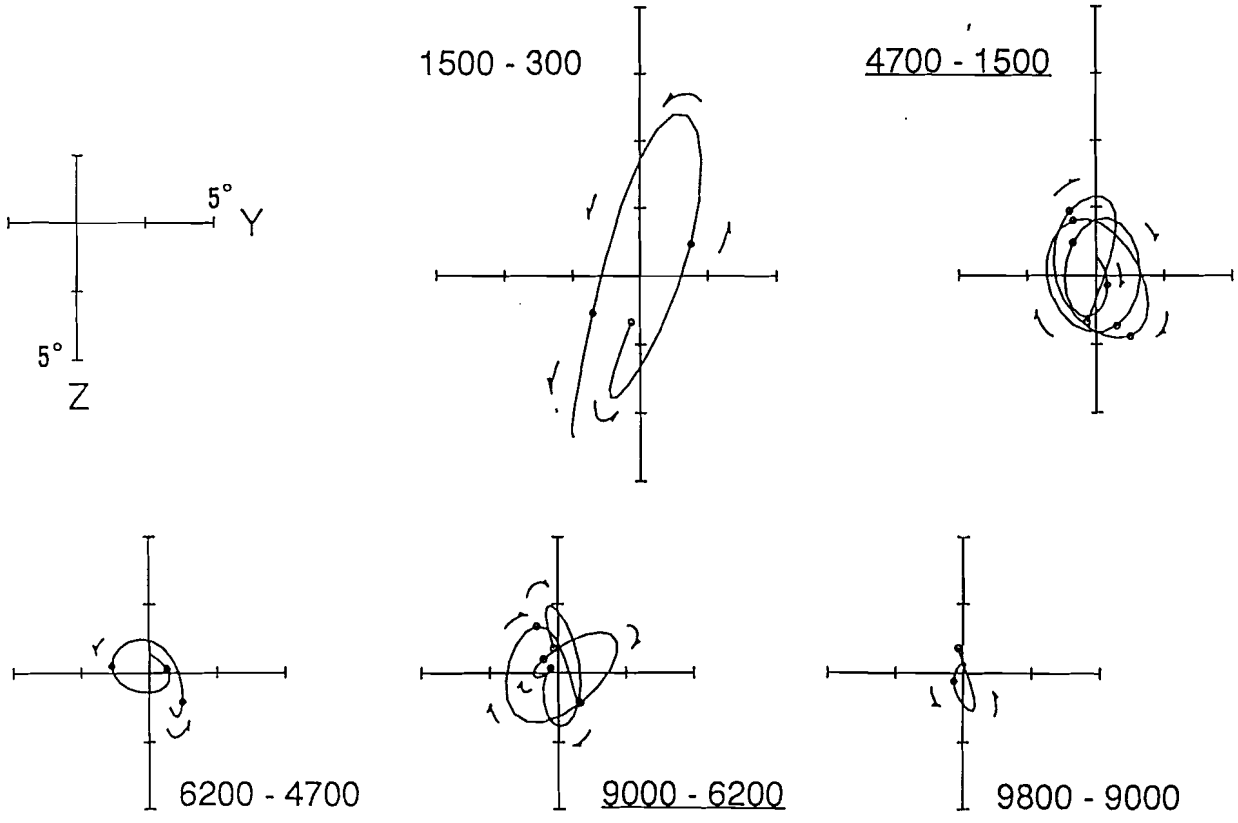


Fig. 2-2-8. Polar projections of the secular variation of the period band 1200 - 800 years per cycle (SPUKD). The underlined intervals are dominated by clockwise motion. Open circles show every 500 years data points from 9500 years B.P. to 500 years B.P.. The arrows show forward direction in time.

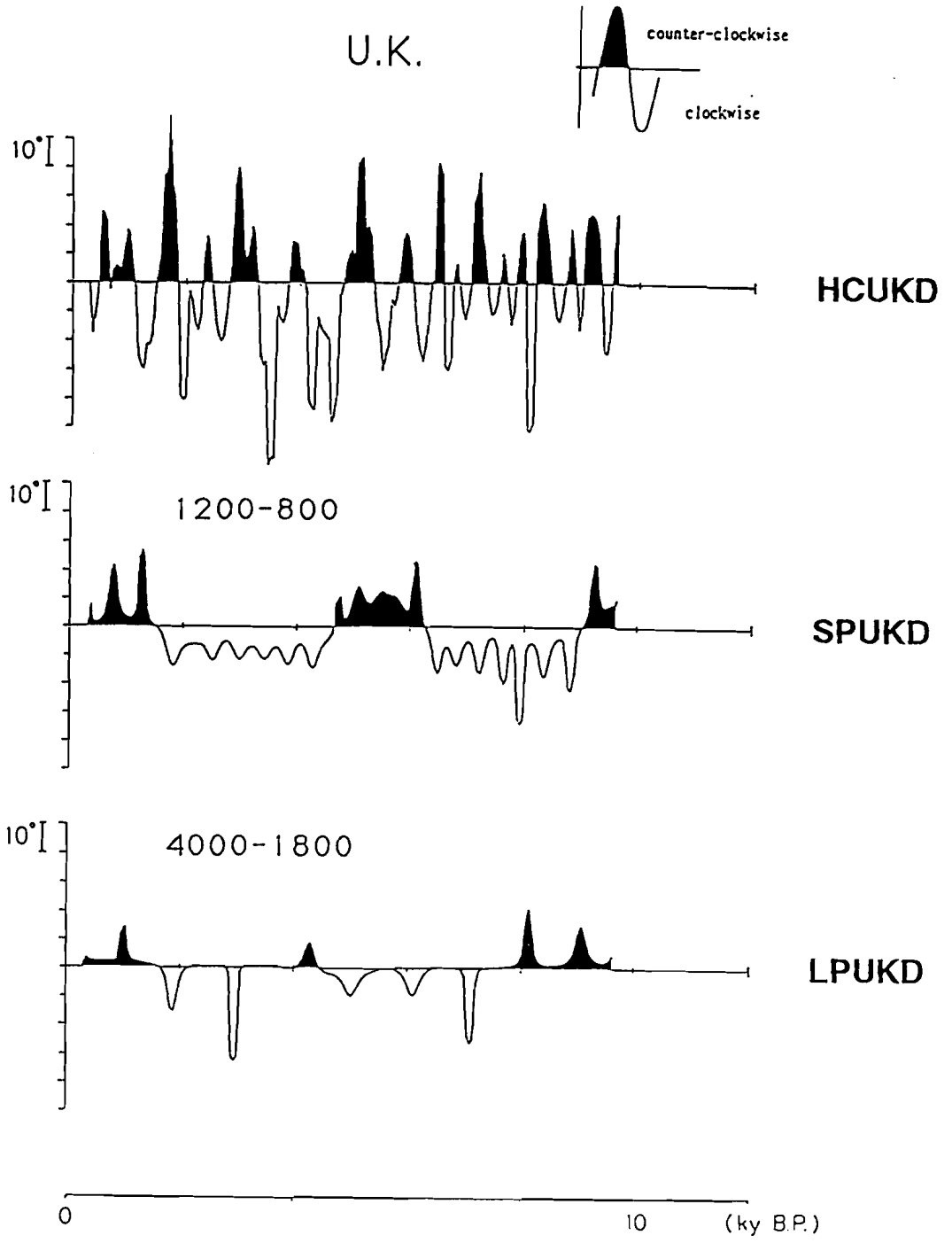


Fig. 2-2-9. Plots of curvature of field direction paths for the SV components of band of periods 4000 - 1800 years per cycle (bottom) and the SV components of band of periods 1200 - 800 years per cycle (middle), and the SV components of periods longer than 200 years per cycle (upper), Clockwise sense is shown in white and counter-clockwise sense is shown in black.

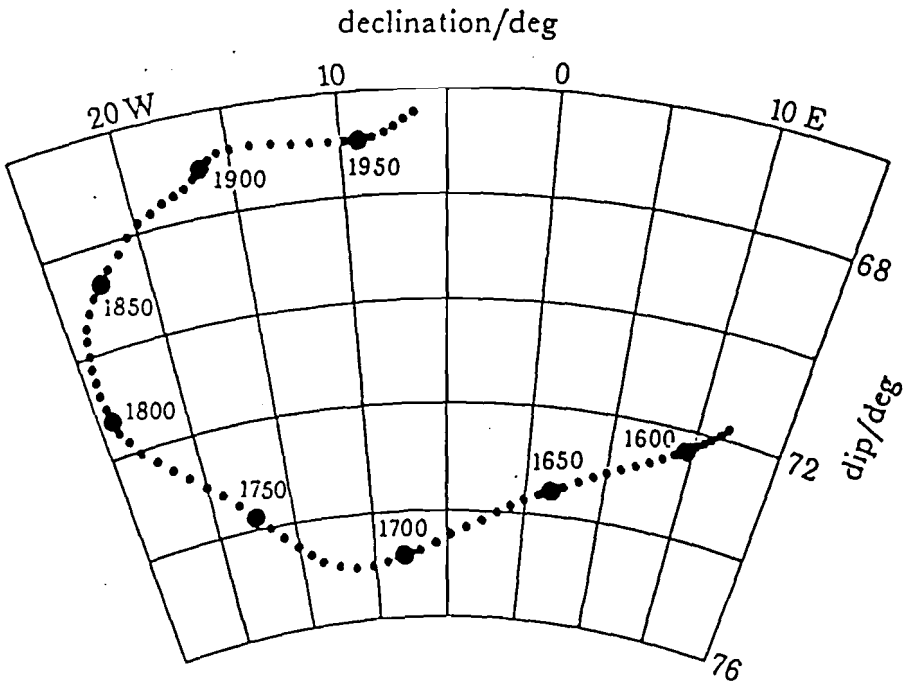


Fig. 2-2-10. The direction of the Earth's magnetic field at London, 1570 - 1975 AD (after Malin and Bullard, 1981).

## 2-3. SECULAR VARIATION RECORD FROM NORTH AMERICA

### 2-3-1. Data

Lund and Banerjee (1985) have published a geomagnetic secular variation record from remanence of sediments in Lake St. Croix, Minnesota (Fig. 2-3-1). The secular variation record is recovered from two replicated cores consisting of successive 1- or 3-m core segments. The segment boundaries in one core correspond to the middle of core segments in the other core. The cores are composed of dark brown clayey gyttja.

The age control is based on nine radiocarbon dates determined for one of the cores. Pollen analysis has established that the percentage of Ambrosia (ragweed) pollen rises sharply at 70 cm below the sediment / water interface. This pollen rise is normally attributed to cultural influences that began about 1850 A.D. in east-central Minnesota. The radiocarbon ages have been corrected using the error calculated at the Ambrosia rise to provide a time frame for the paleomagnetic results. The core extends from 0 to 9600 years B.P..

Reorientation of declination records have been performed by cross-correlating within segments from different cores. The uppermost segments were related to true north by comparing their declinations within the last 150 years to historical records.

A composite data set, LSCSUM (I, D), was formed by stacking the inclinations and the declinations reconstructed from the two cores. The composite secular variation versus time is plotted in Fig. 2-3-2. The data points become sparse at older parts because of the change of sedimentation rate.

### 2-3-2. Analyses and Results

*Transformation to The ADF Reference Frame*

A time series of unit field vector at intervals of 50 years (LSCORG) was constructed by linear interpolation (Fig. 2-3-3). The time series of LSCORG was transformed into the axial dipole field reference frame at a site latitude of 45°N. Time series of E-W and U-D components were obtained by the procedure shown in section 1-2-1. Smoothing was performed to the data sets with a Chebyshev low-pass filter cutting frequencies higher than 5.0 cycle per kyr (period = 200 years).

The E-W and U-D components of smoothed time series (HCLSC) are shown in Fig. 2-3-4. The amplitudes of long duration swings of E-W component are slightly larger than those of U-D component. The variation of U-D component is characterized by short duration fluctuations. A polar projection about the ADF direction for the last 8200 years (Fig. 2-3-5) shows dominant clockwise looping of field motion. From 8200 to 4550 years B.P., the field directions are westerly deflected, and after 4550 years B.P., they are easterly deflected.

*Spectral Analyses*

Spectral analyses were carried on the scalar and vector time series of the E-W and U-D components for HCLSC, using the maximum entropy method. Lengths of prediction error filter ($m$) were chosen satisfying Akaike's final prediction error criterion (Akaike, 1969a, b, and 1970) and an empirical formula of $m < 3N^{1/2}$, where $N$ is number of data. The results are shown in Table 2-3-1. The resultant spectra obtained from three data sets have one common peak periods about 1000 years per cycle.

To test stability of the estimated spectra throughout the length of time span of data, spectral analyses were again carried out within a sliding window of 5000 years every 500 years. The results are summarized in Fig. 2-3-6, where each point shows a period of a spectral peak in each sliding window.

The periodicity of about 1150 years per cycle for the E-W component was stably obtained from the windowed data. Stable spectral peaks were obtained at about 2150 and 1010 years per cycle for the U-D component. The periodicity of about 700 years appeared only in younger three windows. Two spectral peak periods of clockwise rotation at about 2480 and 1150 years per cycle were stably obtained. The period about 1240 years per cycle of counter-clockwise rotation was stable recalculated, however, the periodicities of 4530, 836, and 608 years per cycle obtained from whole data analysis were not obtained stably.

The periodicities obtained from the analyses without using a window (Table 2-3-1) are classified into two. One is the periods > 1000 years per cycle. These are stably recalculated for the windowed data sets. The other is the periods < 1000 years per cycle. These seem unstable because they are not obtained for all data sets, and the analyses using a sliding window show inconsistent results. The periods > 1000 years per cycle are further divided into two groups. One is limited in a band of periods about 4000 - 2000 years per cycle, which is shown with a bold striped area in Fig. 2-3-6. The other is about 1600 - 1000 years per cycle, that corresponds to the thin striped area in Fig. 2-3-6.

*Separation of Quasi Periodic Motions*

The results of spectral analyses for the full-length data sets and for the windowed data sets revealed two bands of period, within which spectral peaks are concentrated. The SV components of each band were isolated using Chebyshev band-pass filters (Fig. 2-3-7). The SV component of longer period band, 4000 - 2000 years per cycle, was named LPLSC. The polar projections of LPLSC are shown in Fig. 2-3-8. The SV component of shorter period band, 1600 - 1000 years per cycle, was named SPLSC. The polar projections of SPLSC are shown in Fig. 2-3-9.

The SV component of LPLSC shows smooth clockwise loops from 8200 years B.P. to 1700 years B.P. (Fig. 2-3-8). The loops exhibit a slight elongation along the

direction about 40 degrees from the Y-axis. Between 2000 and 1500 years B.P., the motion changed to counter-clockwise rotation. The amplitudes of change in both components are uniform over the whole data length (Fig. 2-3-7).

The SV component of SPLSC has large amplitude changes in the E-W component between 1000 and 3000 years B.P. (Fig. 2-3-7). On the other hand, the U-D component shows slightly large amplitude changes before 6000 years B.P.. From 8200 to 3500 years B.P., the SV component of SPLSC on the YZ-plane represents linear field motions. The lineation is almost confined to the Z-axis in the duration of 8200 - 5300 years B.P., and then it tilts clockwise by about 45 degrees (Fig. 2-3-9). After 3500 years B.P., the field motion shows large clockwise loop till about 1700 years B.P., associated with the increase of variation amplitude of E-W component. From 2500 to 1000 years B.P., the field direction represents a linear motion confined to the Y-axis. During the last 1000 years, it shows a linear motion confined to the direction about -45 or 135 degrees from the Z-axis.

*Sense of Rotation*

Instantaneous sense of rotation is defined with curvature. Curvatures were calculated for the data sets of HCLSC, LPLSC and SPLSC. Fig. 2-3-10 shows plots of curvatures averaged within a three-points moving window. Clockwise and counter-clockwise senses are shown in white and black, respectively.

Predominance of clockwise sense is seen in the curvature plots for HCLSC and LPLSC (Fig. 2-3-10). The durations of persisting one sense are at most 1000 years for HCLSC. Dominance of clockwise sense persists till 1500 years B.P., 6700 years long, for the curvature plot of the longer period SV component, LPLSC. After that counter-clockwise sense of motion appeared. The appearance of counter-clockwise motion seems to be triggered by a sudden change of field variation toward negative Z direction between 2000 and 1000 years B.P. (Fig. 2-3-8). In the shorter period SV component (SPLSC), clockwise and counter-clockwise senses are frequently

alternated. From 4200 to 1700 years B.P., smooth clockwise looping motions are implied by the curvature pattern. On the contrary, in the intervals of counter-clockwise sense, linear motions are suggested by the pulse-like features of curvature features.

## 2-3-3. Discussion

The SV component of LPLSC suggests the existence of a steady westward drifting field at least till 2000 years B.P.. If the intensity of the drifting field is unchanged , then the resultant secular variation is symmetric about Y-axis. The clockwise loops are somewhat elongated, suggesting intensity changes of the drifting field or other components of geomagnetic field variation.

After 2000 years B.P., the field vector is suddenly pulled up toward negative Z direction, followed by a counter-clockwise rotation. The counter-clockwise loop is elliptic and its long axis is confined to the Z axis. The motion may be caused by an intensity fluctuation of a standing field. The whole area of the North American Continent is dominated by non-dipole field anomaly at least since 16th century (Yukutake and Tachinaka, 1968). The center of the anomaly is located at latitude of 40°N and longitude of 265°E. It is very close to the site of Lake St. Croix (267.2°E, 45°N). The vector motion confined to the Z axis can be explained by an intensity fluctuation of a standing field below the site. This may suggest an appearance of a standing field. Sudden occurrence of a standing field has been observed in Japan during the interval from 8000 to 3500 years B.P. in the longer-period SV component of LPJPN (Fig. 1-3-7).

The SV component of SPLSC has large amplitude changes and shows complex field motions on the YZ-plane, during the interval from 4200 - 800 years B.P.. Before this interval the elongating direction of motion has been fixed. After this interval the direction is changed to the direction perpendicular to previous elongating axis. The sense of rotation changes at about 1700 years B.P. from clockwise to counter-

clockwise. This may be associated with the sudden break of steady motion at 2000 - 1500 years B.P.in the curve of LPLSC. The pattern of the field variation of North America may have largely changed at about 2000 years B.P..

Table 2-3-1. MEM spectral peak periods of HCLSC

| HCLSC | PEAK PERIODS (yrs/c) |
|---|---|
| E-W comp. | 1150 |
| U-D comp. | 2150 1010 700 |
| clockwise | 2480 1150 |
| counter-clockwise | 4030 1240 836 608 |

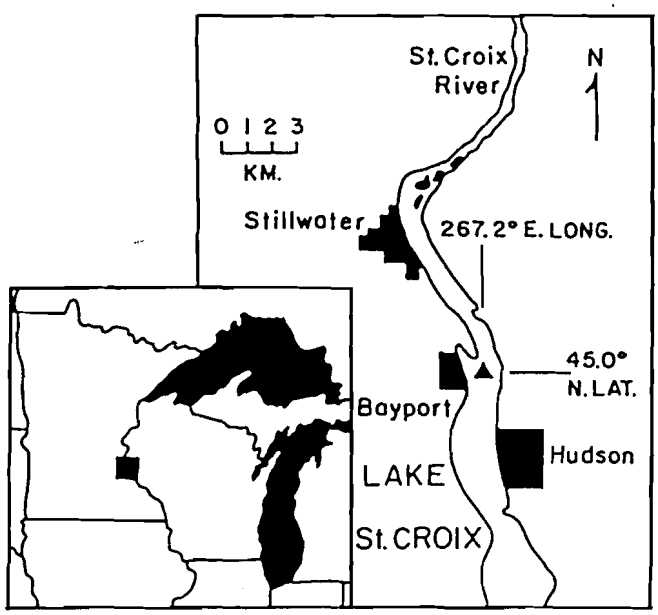


Fig. 2-3-1. Location map for Lake St. Croix, Minnesota. The solid triangle shows the coring site (after Lund and Banerjee, 1985).

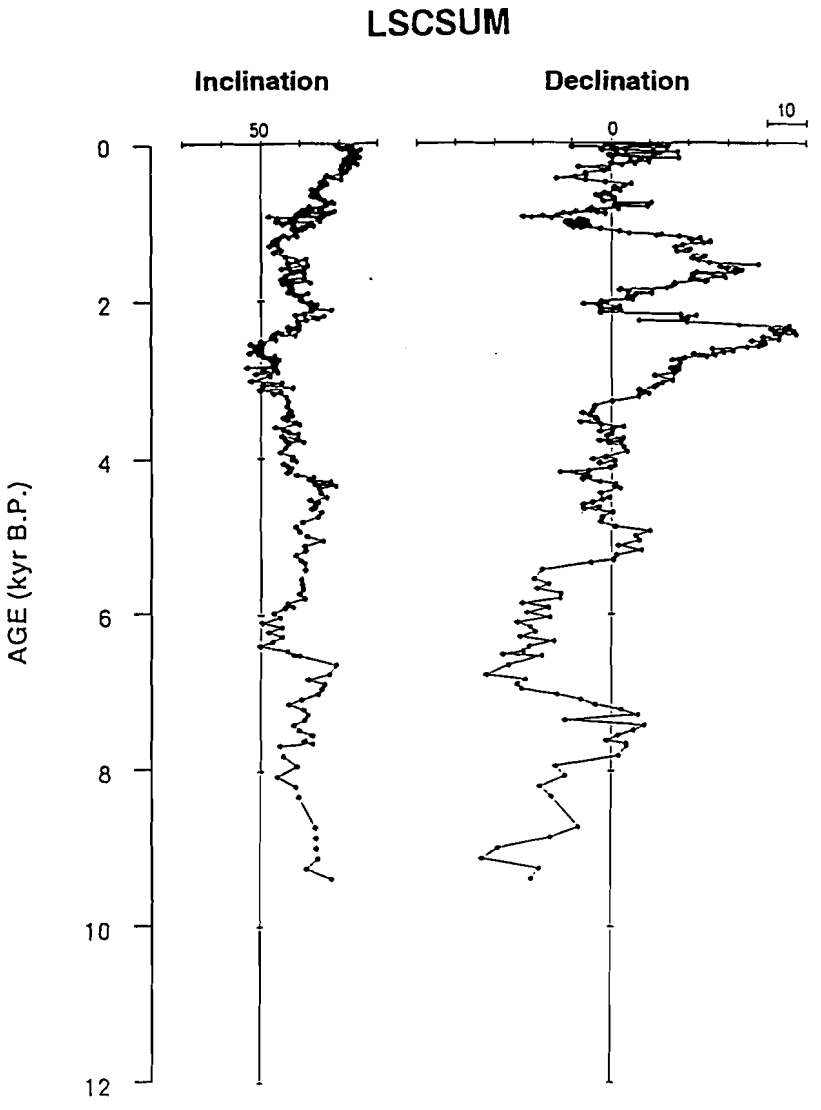


Fig. 2-3-2. Combined inclination and declination data from two cores (after Lund and Banerjee, 1985).

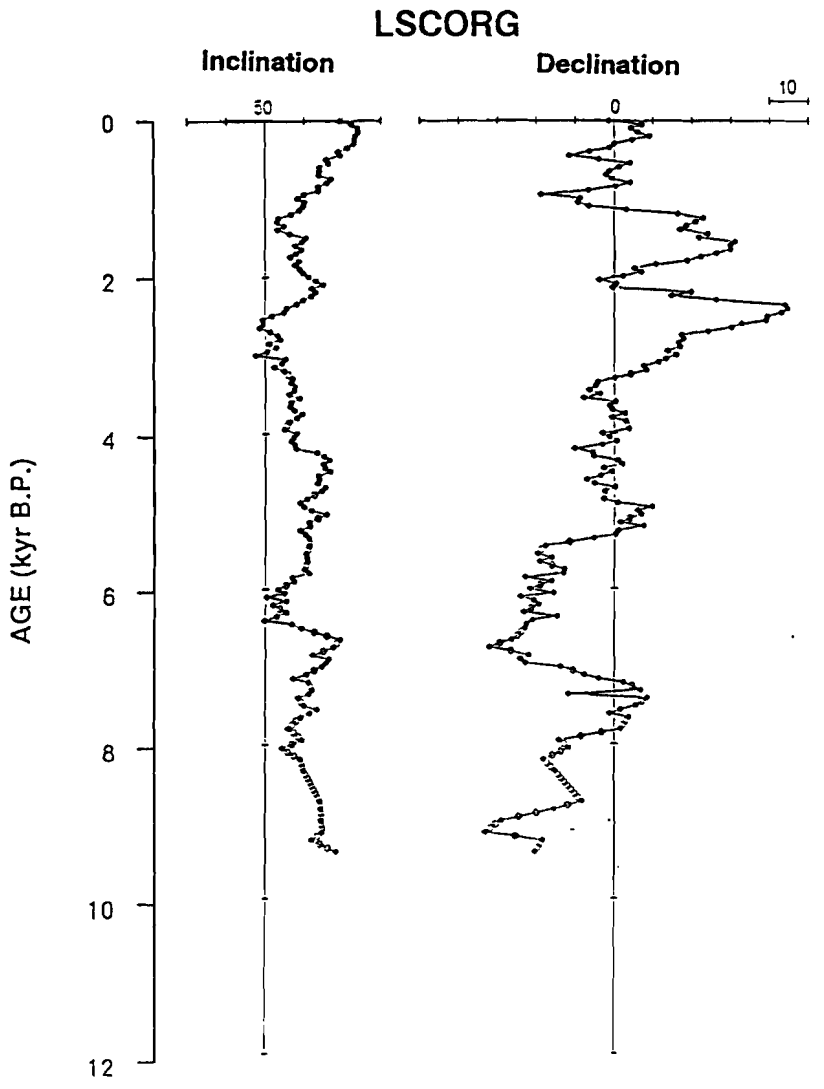


Fig. 2-3-3. Averaged inclination and declination records constructed every 50 years intervals. Open circles are interpolated data.

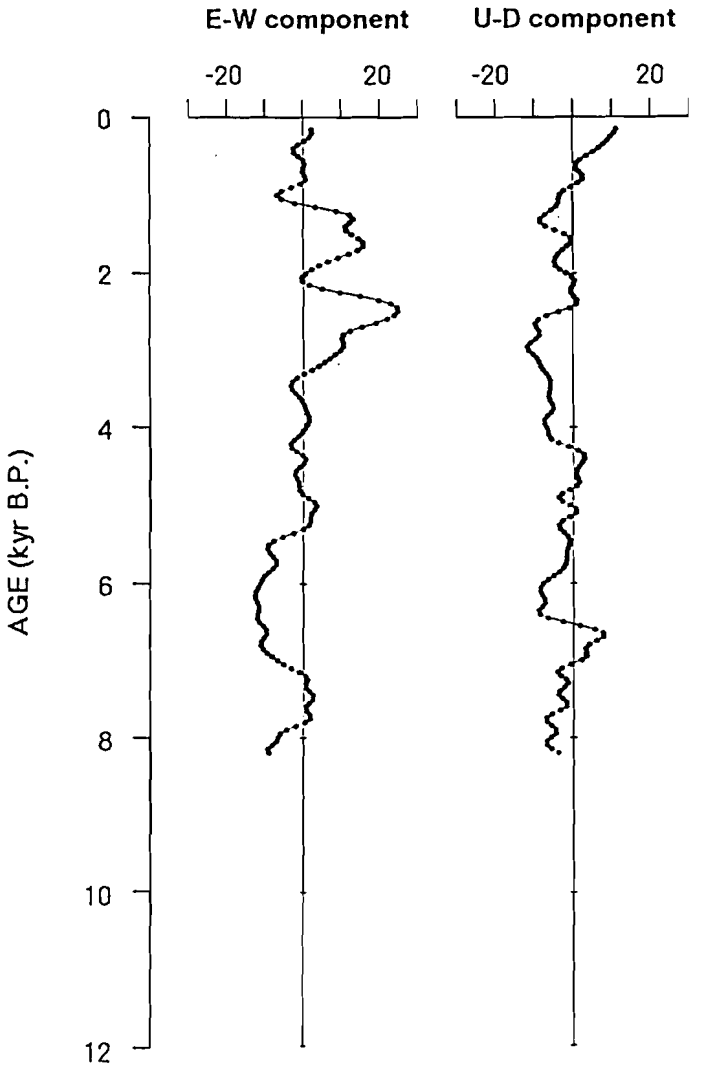


Fig. 2-3-4. Smoothed E-W and U-D components for the secular variation from North America, filtering frequencies higher than 5.0 cycles per kyr. The data points are at intervals of 50 years.

# HCLSC

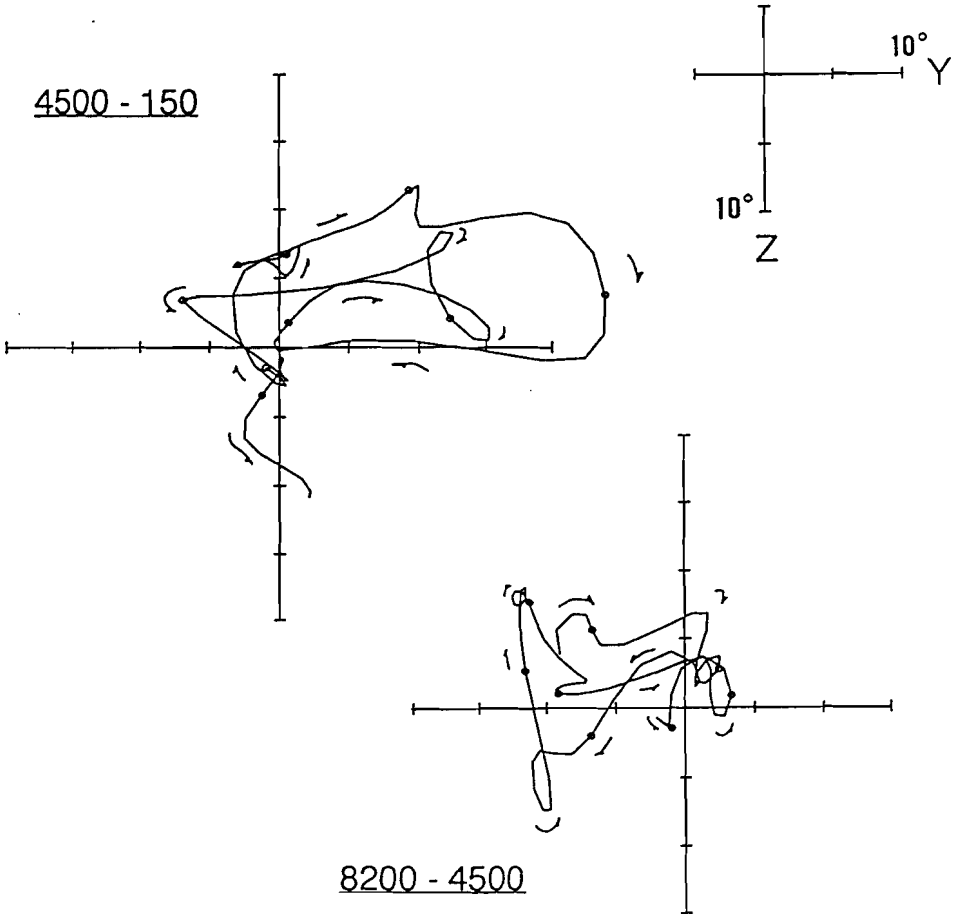


Fig. 2-3-5. Polar projections about the ADF of the secular variation from North America for separate intervals; 8200 - 4500 year B.P. (bottom), 4500 - 150 year B.P. (top). The data points are at intervals of 50 years. Open circles show every 500 years data points from 8000 years B.P. to 500 years B.P.. The arrows show forward direction in time.

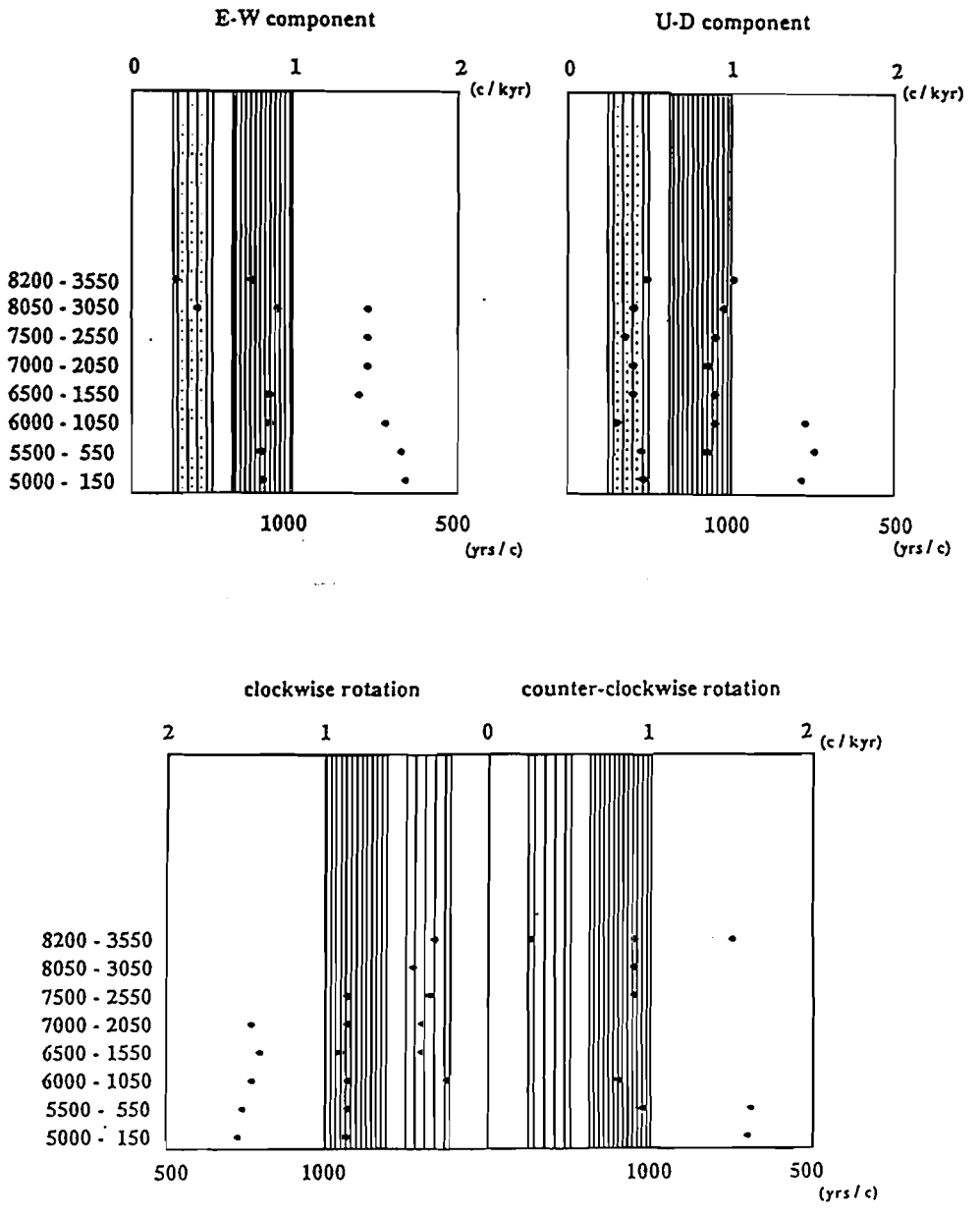


Fig. 2-3-6. MEM spectral peak periods of the HCLSC calculated within a moving window of 5000 years. Spectral peaks whose powers < 10% of the largest peak or whose periods > 5000 years are omitted. The periods of spectral peaks are concentrated in two bands; 1600 - 1000 years per cycle (thin striped area) and 4000 - 2000 years per cycle (bold striped area).

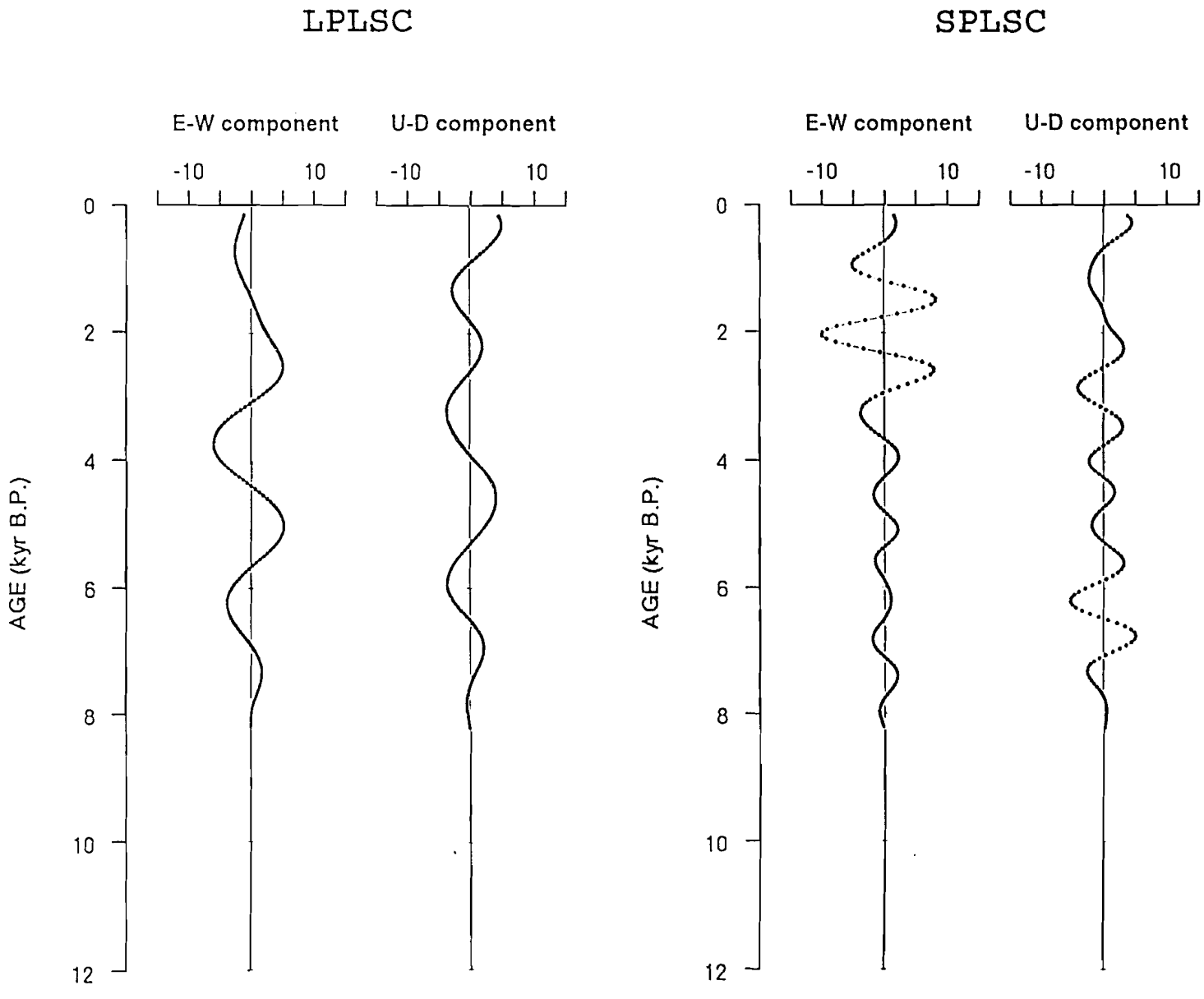


Fig. 2-3-7. E-W and U-D components of the secular variation for the bands of periods 4000 - 2000 years per cycle (LPLSC) and 1600 - 1000 years per cycle (SPLSC).

# LPLSC

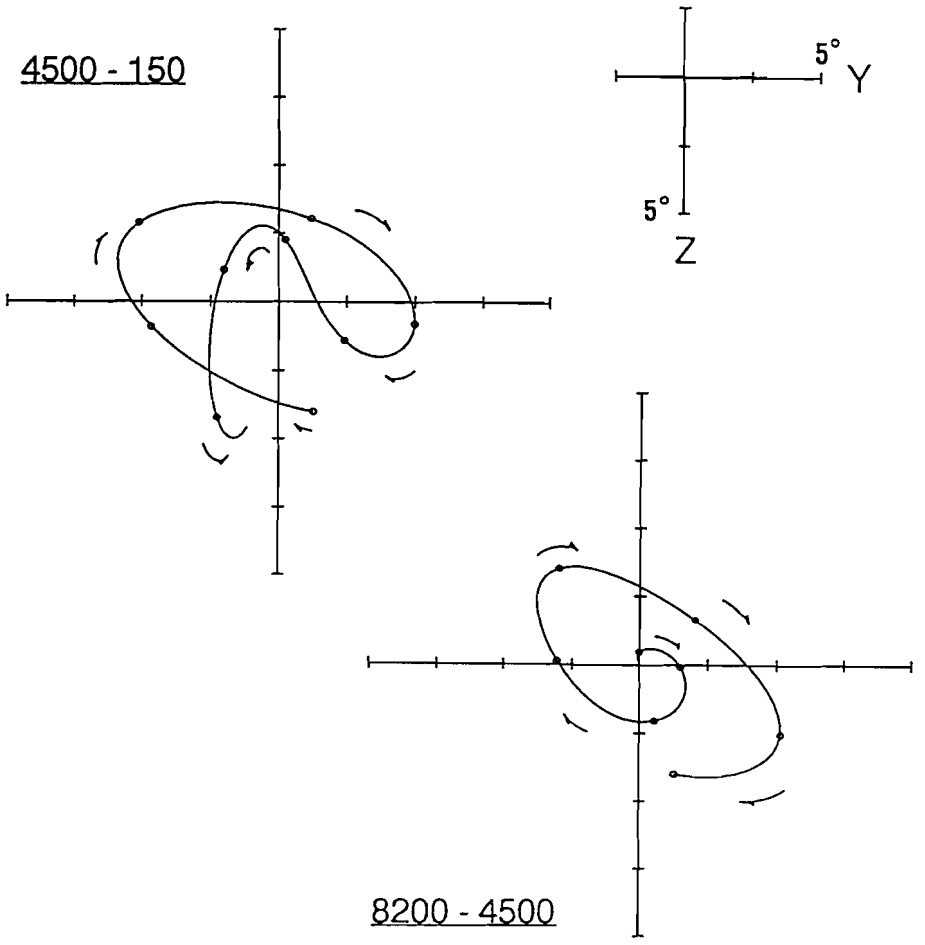


Fig. 2-3-8. Polar projections of the secular variation of band of periods 4000 - 2000 years per cycle (LPLSC) for separate intervals. Open circles show every 500 years data points from 8000 years B.P. to 500 years B.P.. The arrows show forward direction in time.

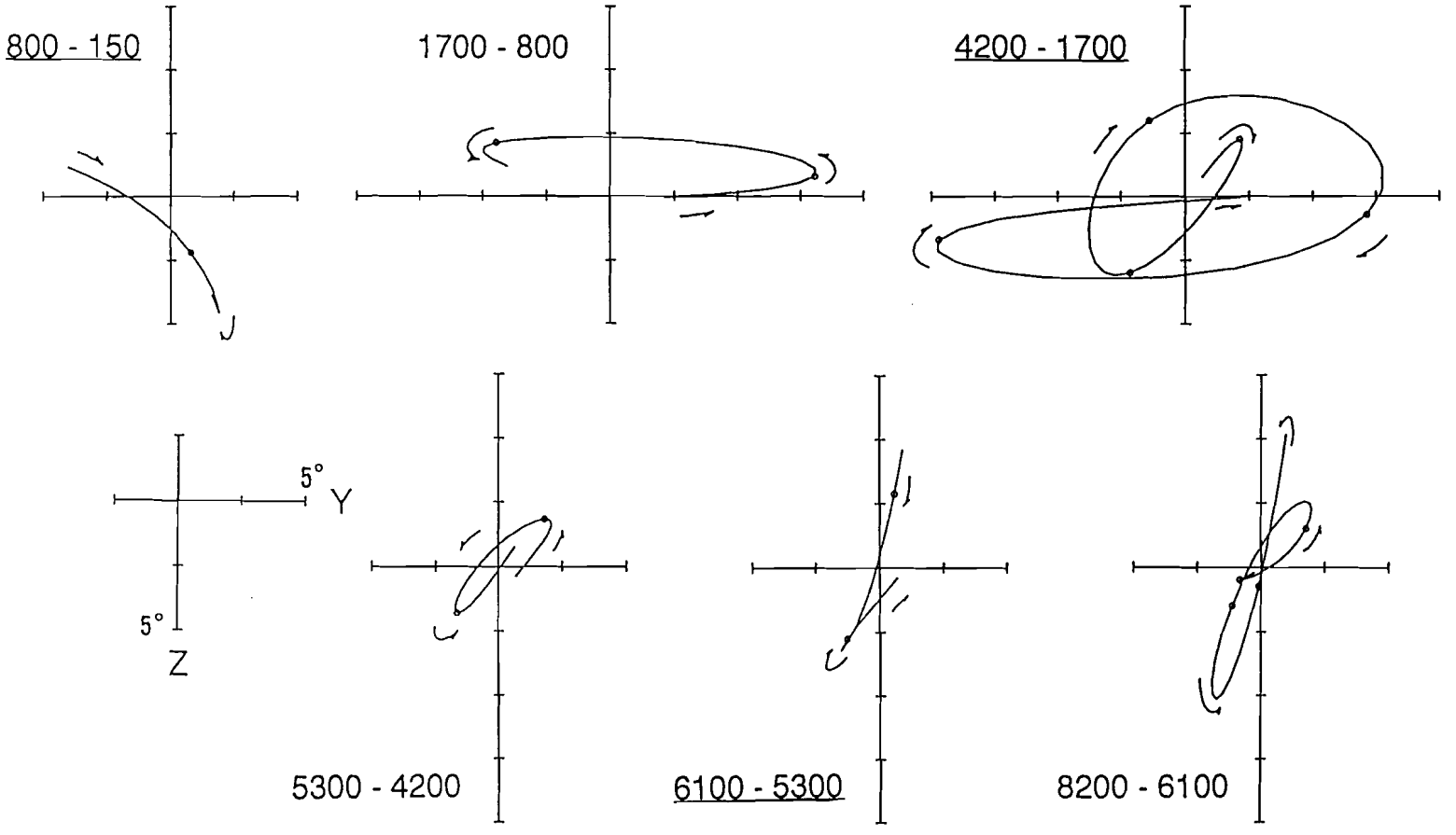


Fig. 2-3-9. Polar projections of the secular variation of the period band 1600 - 1000 years per cycle (SPLSC).The underlined intervals are dominated by clockwise motion. Open circles show every 500 years data points from 8000 years B.P. to 500 years B.P.. The arrows show forward direction in time.

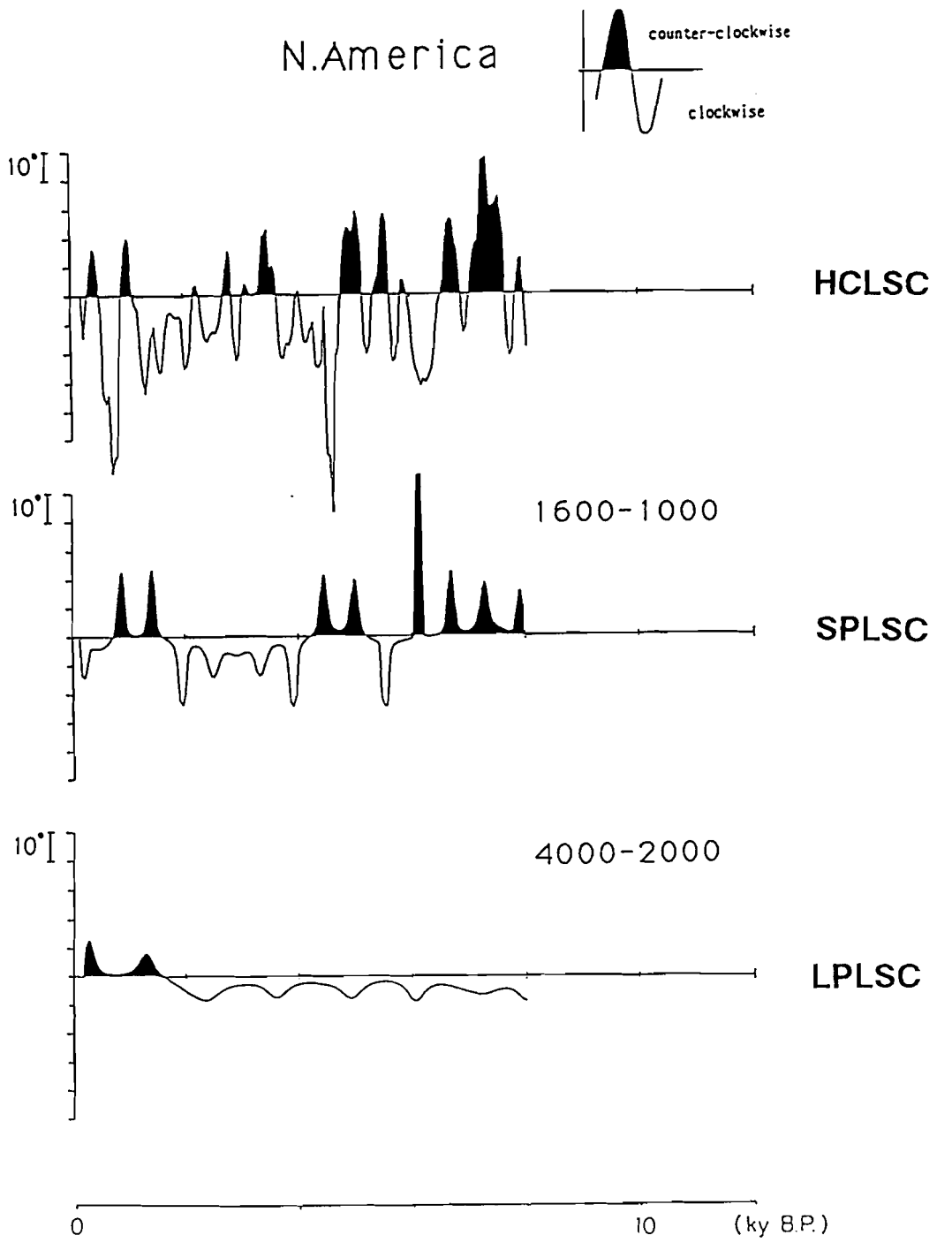


Fig. 2-3-10. Plots of curvature of field direction paths for the SV components of band of periods 4000 - 2000 years per cycle (bottom) and the SV components of band of periods 1600 - 1000 years per cycle (middle), and the SV components of periods longer than 200 years per cycle (upper), Clockwise sense is shown in white and counter-clockwise sense is shown in black.

## 2-4. SECULAR VARIATION RECORD FROM AUSTRALIA

### 2-4-1. Data

Barton and McElhinny (1981) have published a paleomagnetic secular variation record from remanence of sediments in Lake Keilambete (38°13'S, 142°52'E), Lake Bullenmerri (38°15'S, 142°06'E), Lake Gnotuk (38°14'S, 143°06'E) in southeast Australia.

Eight to thirty-two horizons from each lake have been radiocarbon dated (Barton et al., 1981). The radiocarbon ages were calibrated according to Clark (1975). Transformation from a depth scale to a time scale was accomplished by assuming linear sedimentation rates between dated levels. It is expected that small scale fluctuations in sedimentation rate are averaged out by this interpolation. It is therefore improbable that useful information can be expected about periodicities shorter than 400 years (Barton and McElhinny, 1981).

Each sequence agrees well with the between-lakes correlation of secular variation curves. Barton and McElhinny (1981, 1982) obtained the composite records by taking 100 years means of the combined set of stacked data from three lakes (ASTCOM; Fig. 2-4-1). All declination results of each core were detrended, i.e., a least-squares linear fit to the declination values v.s. depth was removed before stacking. Means were calculated after discarding the upper and lower quartiles per 100 years interval (a robust smoothing technique). Declinations were reset about the scalar mean value.

### 2-4-2. Analyses and Results

*Transformation to The ADF Reference Frame*

The time series of unit field vector ASTORG (Fig. 2-4-2) was transformed into an axial dipole reference frame. The site latitude was set to 38°14'S. The series of E-W and U-D components were obtained by the procedure shown in section 1-2-1. For consistency with the SV records of other three sites on the globe, the Australian data were interpolated every 50 years intervals. The data sets were subjected to smoothing with a Chebyshev low-pass filter which cut the frequencies higher than 5.0 cycles per kyr (period = 200 years). The resultant time series of E-W and U-D components (HCAST) are shown in figure 2-4-2.

The amplitude of secular variation in Australia for the last 10 000 years is very small. Especially, between 8000 and 4000 years B.P., the E-W component shows almost no variation. A polar projection about the axial dipole field direction (X-axis) is shown in Fig. 2-4-3. From 8000 years B.P., the field vector is confined to the Z-axis. This also suggests the absence of E-W component in the variation.

*Spectral Analyses*

Spectral analyses were carried on the scalar and vector time series of HCAST, using the maximum entropy method. Lengths of prediction error filter ($m$) used in the analyses were chosen satisfying Akaike's final prediction error criterion (Akaike, 1969a, b, and 1970) and an empirical formula of $m < 3N^{1/2}$, where $N$ is number of data.

Results of spectral estimates are shown in Table 2-4-1. The periodicity about 2500 years per cycle is obtained for both of the E-W and U-D components. The spectra of 2710 and 2380 years per cycle for clockwise and counter-clockwise rotations, respectively, may correspond to this periodicity. The E-W component and counter-clockwise rotational component have a spectral peak at a period of 1230 years per cycle. Counter-clockwise rotational component has a spectral peak at a period of 927 years per cycle, which may be distinct from the period of 1230 years per cycle. Both periods are somewhat shorter than the peak periods obtained for clockwise rotation.

To test the stability of the obtained spectra throughout the length of the time series, spectral estimation within a sliding window of 5000 years every 500 years was performed to the data set of HCAST. The results are summarized in Fig. 2-4-4, where each point shows a period of spectral peak. The periods about 2240 years per cycle were stably calculated for the U-D, clockwise rotational, and counter-clockwise rotational components. They probably correspond to the periods obtained for the three components of full data length, 2500, 2710, and 2380 years per cycle, respectively. For the E-W component, this peak period was not obtained from all sets of windowed data, which may caused by the power shift to the high frequency side of spectrum. The E-W component has a stable period of about 1200 years. Though the period of about 800 years per cycle also seems to be stable for E-W component, it is not obtained for the whole data. For the clockwise rotational component, within the five younger windows the period about 1200 years per cycle exists. The period about 1200 years per cycle is stably recalculated only for the E-W component.

*Separation of Quasi Periodic Motions*

The SV component whose period is about 2500 years per cycle was isolated from ASTORG using a Chebyshev bandpass filter. The filter passes the components of periods between 3000 to 1600 years per cycle. This component was named LPAST. As shown in Fig. 2-4-5, the amplitude of E-W component is almost zero, representing absence of components in this periodicity band. Polar projections of LPAST are shown in Fig. 2-4-6. It is clearly shown that the vector motion on the YZ-plane is confined to the Z-axis.

The SV component of period about 1200 years per cycle, which is expected to exist stably in the E-W component, was also isolated using a filter which passes periodicities 1500 - 800 years per cycle. This component was named SPAST. As shown in Fig. 2-4-5, the E-W component of SPAST has large amplitude variations than that of LPAST. Polar projections of SPAST are shown in Fig. 2-4-7. The vector

motion on the YZ-plane shows two-dimensional variation unlike that of LPAST. Most of the intervals separated in Fig. 2-4-7 are dominated by clockwise looping motions of a field vector. Especially, from 3950 to 1500 years B.P., two large clockwise full-loops are there. After 1500 years B.P., the motion changes to counter-clockwise looping.

*Sense of Rotation*

Instantaneous sense of rotation is defined with curvature. Curvatures were calculated for the data sets of HCAST, LPAST, and SPAST. Fig. 2-4-8 shows plots of the curvatures averaged within a three-points moving window. Clockwise and counter-clockwise senses are shown in white and black, respectively.

The curvature plot for HCAST shows complex pattern. There seems to be no systematic pattern in the changes of rotational sense. The durations for persistence of one rotational sense are shorter than 1000 years.

The SV component of longer periods (LPAST) are dominated by the linear motions as mentioned above. Therefore peaks of curvature plot correspond to turns or changes of moving direction of vector on the YZ plane. The turning points are mainly dominated by clockwise sense. It should be noted that the turning points of counter-clockwise sense are at every 2500 years intervals.

The SV component of shorter periods (SPAST) is dominated by the motion of clockwise sense. Counter-clockwise sense is obtained only before 8500 years B.P. and after 1500 years B.P..

2-4-3. Discussion

The low-amplitude secular variation in southeast Australia is mainly caused by small amplitude of the declination variation. Barton and McElhinny (1982) asserted

that it is a real SV feature in Australia because of reproducible variation features in individual cores. However, all the cores were twisted in declination, and it was corrected approximating equally apparent by linear trends. It is reasonable that the treatment by detrending affect the SV record. Small variations of the declination and the E-W component may be caused by unnecessary correction by detrending. Linear drift of the geomagnetic field variation about depth was also cleaned when the twisting of core was removed. The longer period variations are considered to be affected more strongly by the detrending treatment.

An alternative interpretation for the low-amplitude SV is that Australia may belong to the area of the Pacific dipole window (Dowell and Cox, 1971; Hyodo, 1989). The field variation in Australia caused by non-dipole components may be reduced by a magnetic insulator under the Pacific area (Hyodo, 1989). Possibility of this interpretation is still remained.

Table 2-4-1. MEM spectral peak periods of HCAST

| HCAST | PEAK PERIODS (yrs/c) |
|---|---|
| E-W comp. | 2530 1230 514 |
| U-D comp. | 2530 |
| clockwise | 2710 1230 |
| counter-clockwise | 2380 927 |

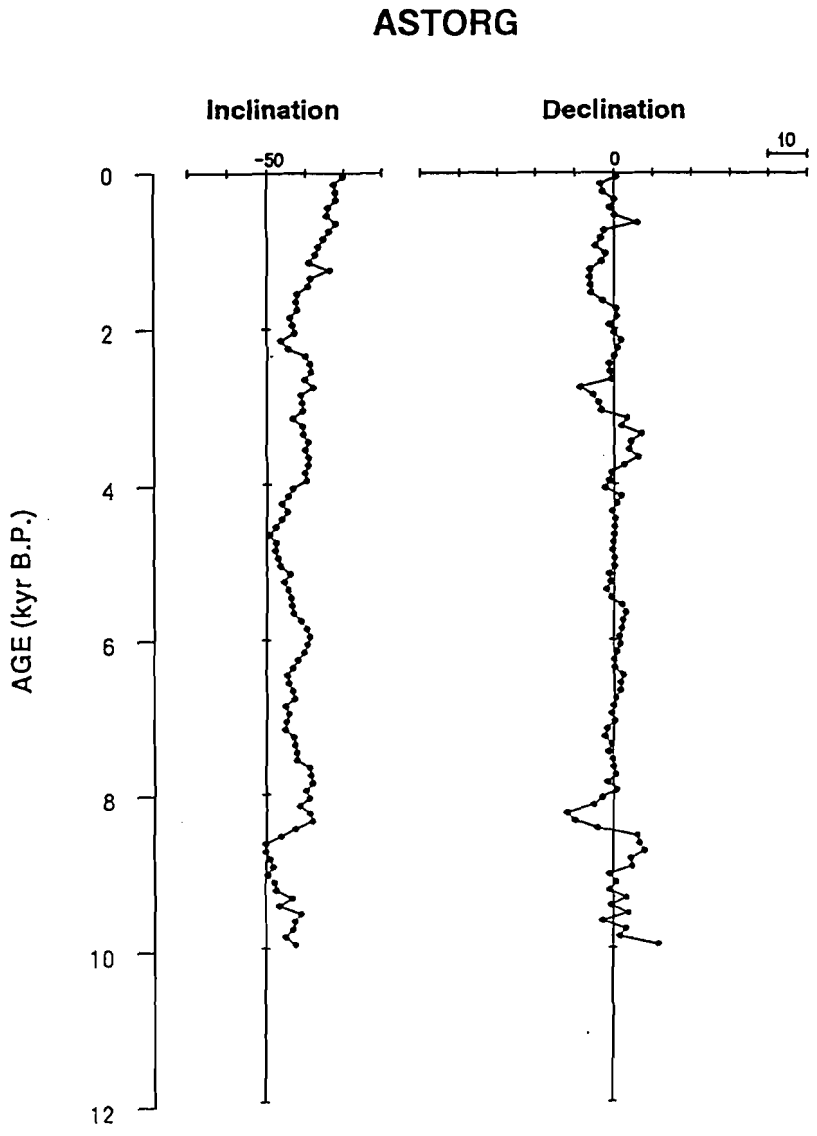


Fig. 2-4-1. Combined inclination and declination data obtained by 100 years means of the stacked data from Lake Keilambete, Lake Bullenmerri and Lake Gnotuk, Southeast Australia (after Barton and McElhinny, 1982).

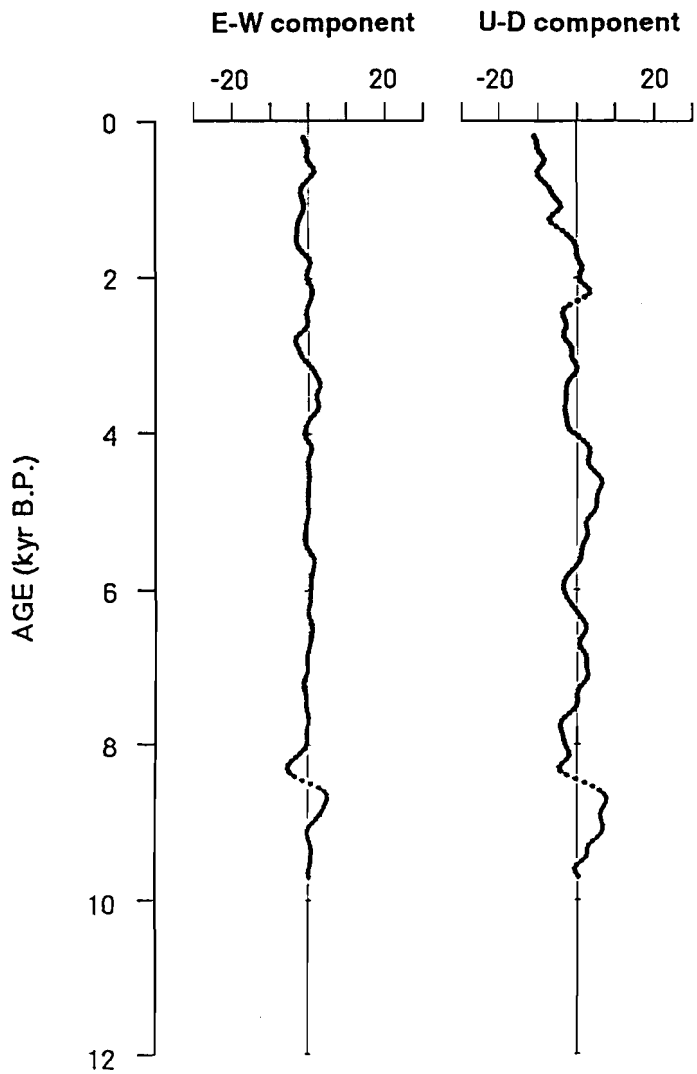


Fig. 2-4-2. Smoothed E-W and U-D components for the secular variation from Southeast Australia, filtering frequencies higher than 5.0 cycles per kyr. The data points are at intervals of 50 years.

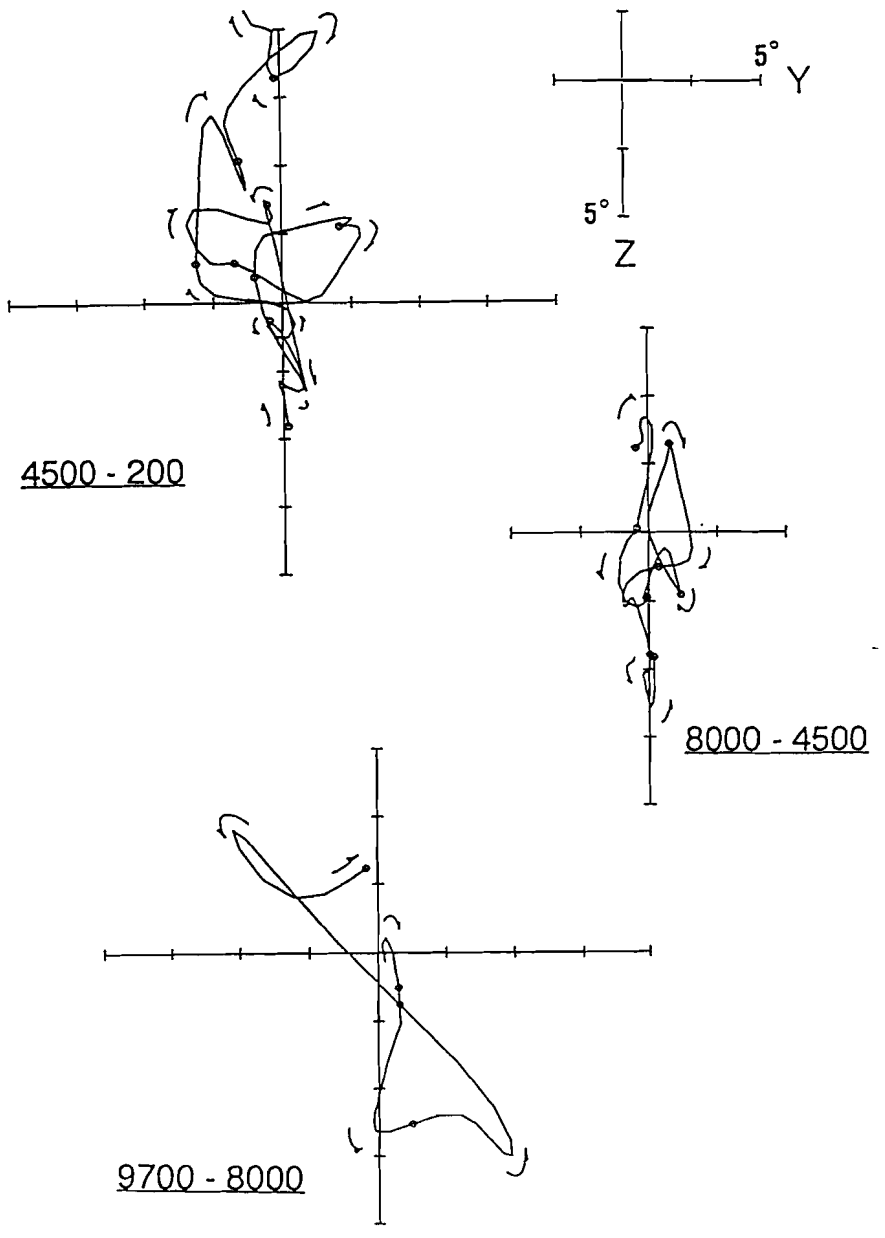


Fig. 2-4-3. Polar projections about the ADF of the secular variation from southeast Australia for separate intervals; 9700 - 8000 year B.P. (bottom), 8000 - 4500 year B.P. (middle), 4500 - 200 year B.P. (top). The data points are at intervals of 50 years. Open circles show every 500 years data points from 9500 years B.P. to 500 years B.P.. The arrows show forward direction in time.

# Australia

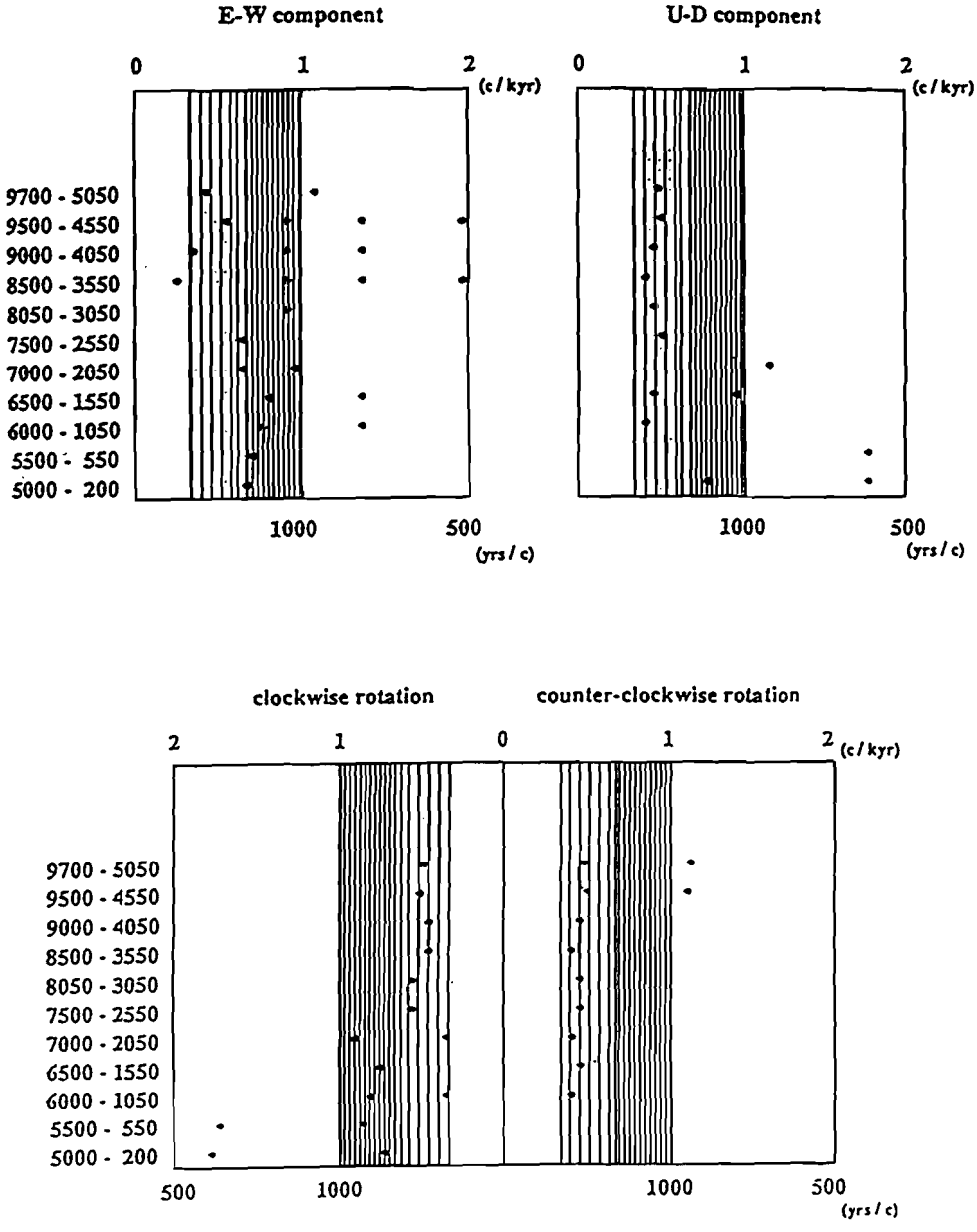


Fig. 2-4-4. MEM spectral peak periods of the HCAST calculated within a moving window of 5000 years. Spectral peaks whose powers < 10% of the largest peak or whose periods > 5000 years are omitted. The periods of spectral peaks are concentrated in two bands; 1500 - 800 years per cycle (thin striped area) and 3000 - 1600 years per cycle (bold striped area).

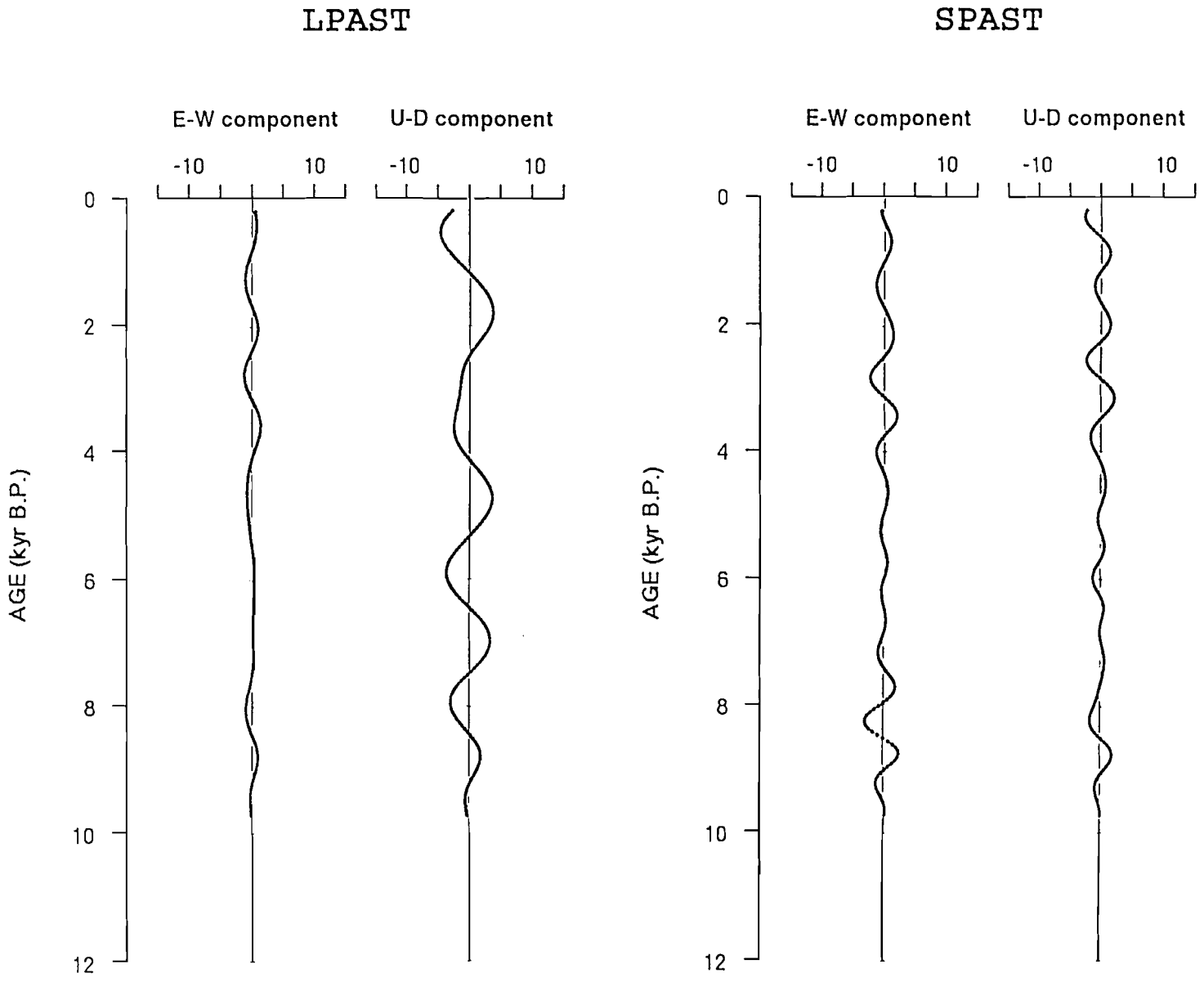


Fig. 2-4-5. E-W and U-D components of the secular variation for the bands of periods 3000 - 1600 years per cycle (LPAST) and 1500 - 800 years per cycle (SPAST).

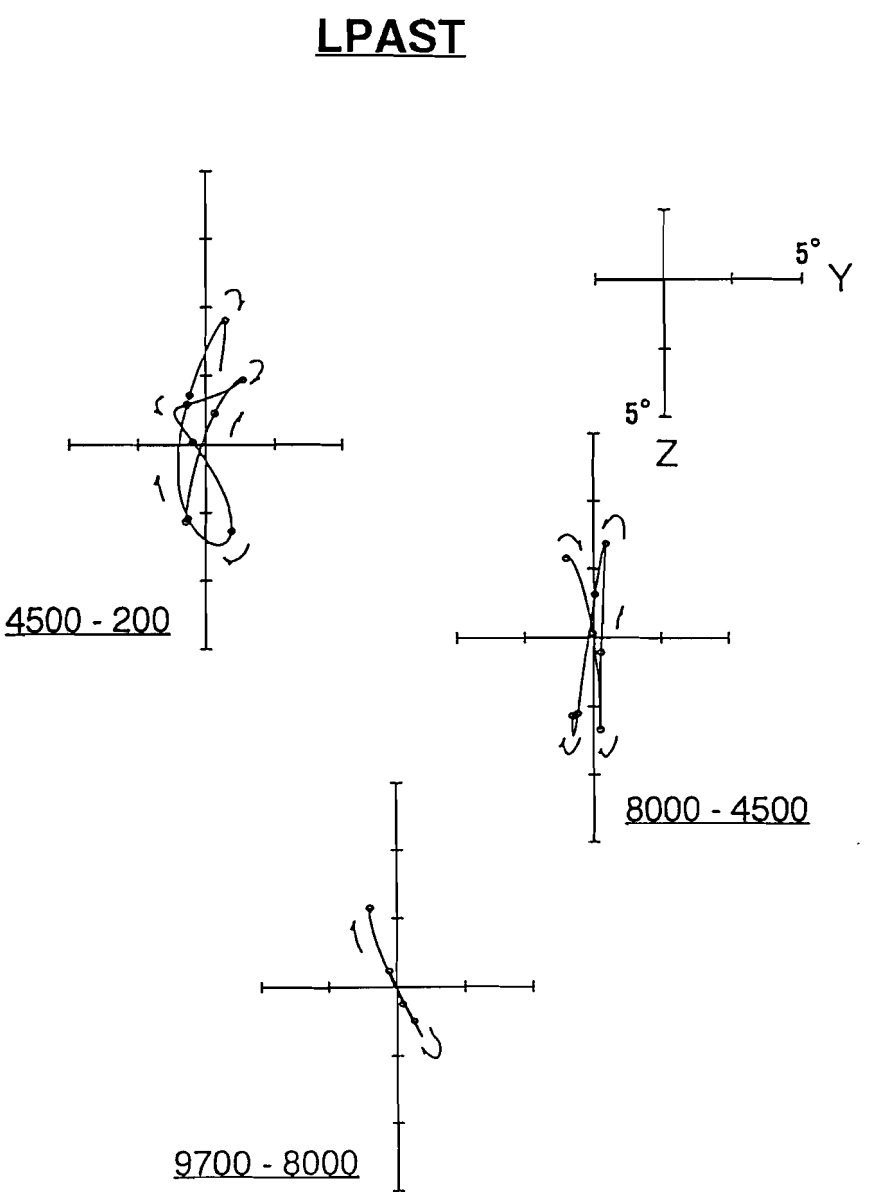


Fig. 2-4-6. Polar projections of the secular variation of band of periods 3000 - 1600 years per cycle (LPAST) for separate intervals. Open circles show every 500 years data points from 9500 years B.P. to 500 years B.P.. The arrows show forward direction in time.

# SPAST

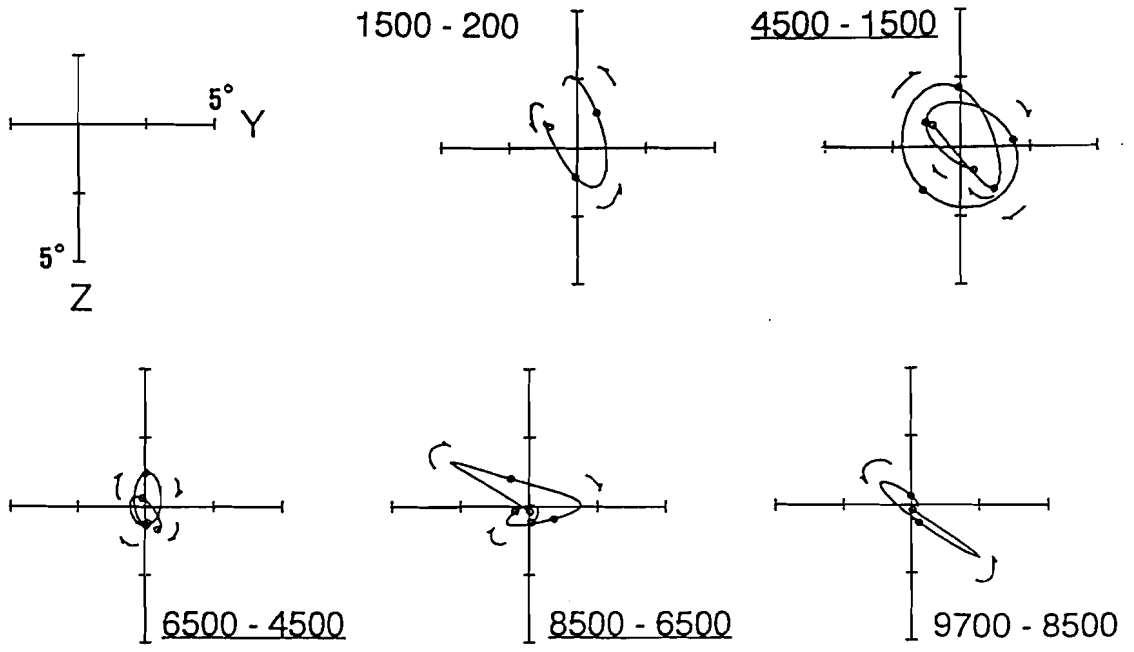


Fig. 2-4-7. Polar projections of the secular variation of the period band 1500 - 800 years per cycle (SPAST).The underlined intervals are dominated by clockwise motion. Open circles show every 500 years data points from 9500 years B.P. to 500 years B.P.. The arrows show forward direction in time.

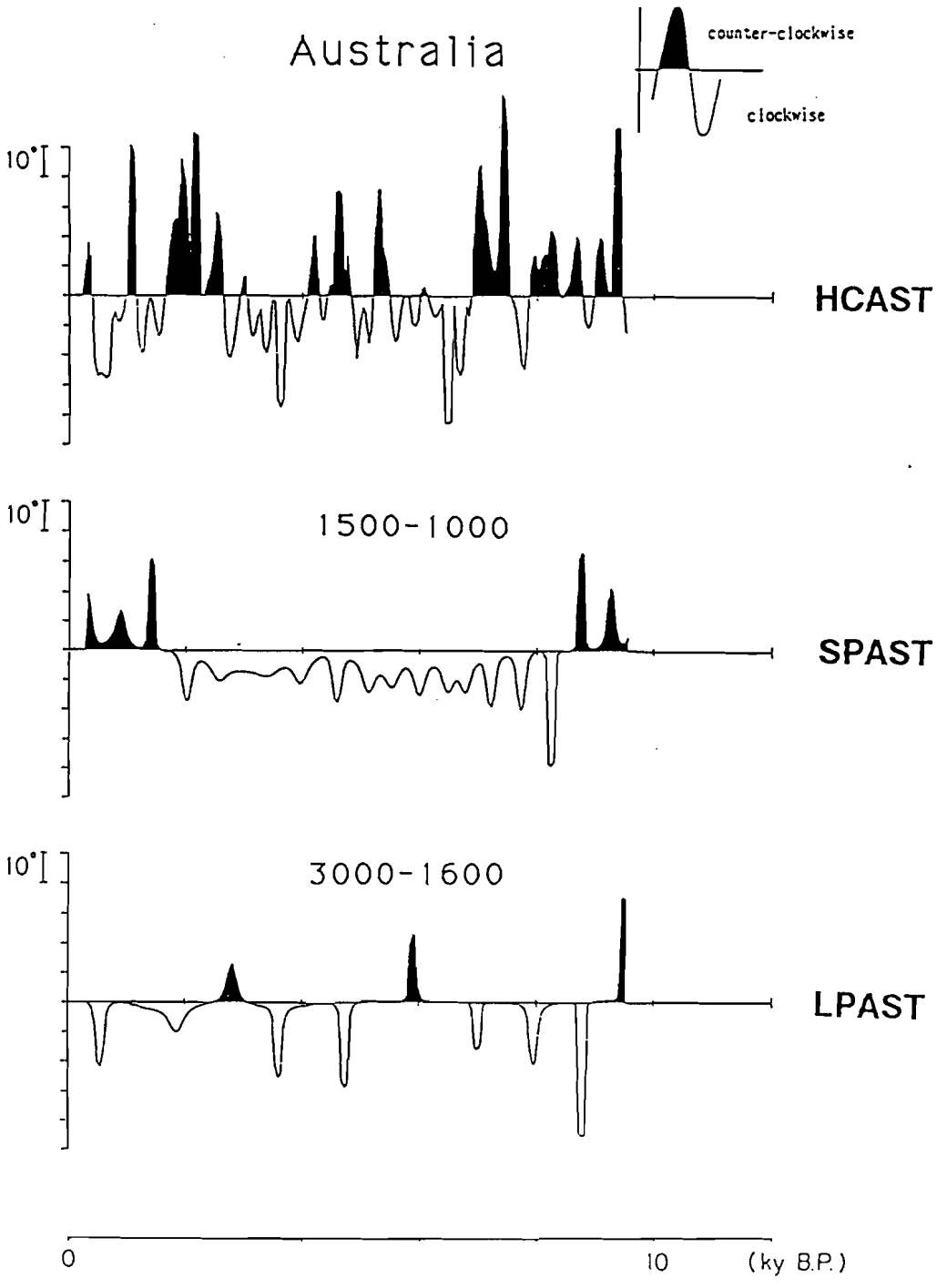


Fig. 2-4-8. Plots of curvature of field direction paths for the SV components of band of periods 3000 - 1600 years per cycle (bottom) and the SV components of band of periods 1500 - 800 years per cycle (middle), and the SV components of periods longer than 200 years per cycle (upper), Clockwise sense is shown in white and counter-clockwise sense is shown in black.

## 2-5. CORRELATIONS BETWEEN FOUR RECORDS

Common features in the secular variations observed at the four sites can be derived by calculating correlation functions. The three sites in the Northern Hemisphere, U.K., North America, and Japan, locate within a thin latitudinal band (Fig. 2-1-1). If some latitudinal drifting fields pass through the three sites, then correlating features will appear in the SVs at all the sites. The record from Australia, the Southern Hemisphere, is near Japan. Latitudinal drifting fields affect SVs at Japan and Australia simultaneously. Correlation functions of the E-W, the U-D and the vector components were calculated between records of the three sites in the Northern Hemisphere. Correlation functions between records of Japan and Australia were also calculated.

### 2-5-1. Correlation Function

A correlation function $C(\tau')$ between two time series $a_1, a_2, \ldots,$ and $b_1, b_2, \ldots,$ is defined as

$$C(\tau') = \frac{\sum (a_i \cdot b_{i-\tau'})}{[\ \sum a_i^2 \cdot \sum b_i^2\ ]^{1/2}} \qquad (1)$$

where $\tau'$ is a lag between two records. Mean values for each time series are 0.

The vector correlation is measured by cosine of angle between two vectors (Watson and Beran, 1967). A serial correlation between two unit vector time series $\boldsymbol{a}_i$, $\boldsymbol{b}_i$, is given as

$$L = \frac{\Sigma \cos \theta_i}{N} = \frac{\Sigma (a_i \cdot b_i)}{N} \qquad (2)$$

So the correlation function $C(\tau')$ is calculated by

$$C(\tau') = \frac{\Sigma (a_i \cdot b_{i-\tau'})}{N - \tau'} \qquad (3)$$

Time lag $\tau$ is defined as

$$\tau = \tau' \cdot \Delta t - [T(a_i) - T(b_i)]$$

where $T(a_i)$ and $T(b_i)$ are times of $i$'th data; $a_i$ and $b_i$ (Fig.2-5-1), $\Delta t$ is time interval of data.

Numbers of our data are limited. When the number of overlapped data was less than a half of the total number of data, then calculation of correlation coefficients was stopped.

2-5-2. Results of correlations

Fig. 2-5-2, parts 1, 2, 3, and 4, show the correlation functions calculated for pairs of HCJPN - HCLSC, HCLSC - HCUKD, HCUKD - HCJPN and HCJPN - HCUST. Time lags at which correlation functions have maxima disagree between the E-W and the U-D components. Therefore the correlation of vector pairs tend to be low.

For the pair of HCJPN and HCLSC (Fig. 2-5-2, part 1), remarkably high correlation is obtained at time-lags 1600 years and 4400 years for the E-W component. The latter may be correlated with the maximum peak of vectorial correlation at time-lag

4350 years. The correlation function of the U-D component generally shows small amplitude changes. A maximum correlation is obtained at time-lag -2950 years.

For the pair of HCLSC and HCUKD (Fig. 2-5-2, part 2), correlation functions of three components tend to have larger values at negative time-lags than positive ones. Major characteristic features may have been transmitted from U.K. to North America. Remarkably large peaks are obtained at time-lags -4650 for the E-W component, and -3800 years for the U-D component.

For the pair of HCUKD and HCJPN (Fig. 2-5-2, part 3), the correlation of vector pairs is very small. At time-lag 3000 years, the correlation function of the E-W component shows clear maximum.

For the pair of HCJPN and HCAST (Fig. 2-5-2, part 4), the correlation of the U-D component is higher than those of the other two components. Clear peak is obtained at time-lag 5250 years for the U-D component.

The correlation functions obtained above from the SV records without band-pass filters generally have small values. Correlation maxima were usually obtained at large time-lags. This may be due to small number of data were used for calculation of correlation coefficients.

Paleomagnetic secular variation records consists of many components, in which some are global and some are local, so that they show complex variations. The low correlation may be caused by local field variation components.

The four SV records have a spectral component of period about 3000 ~ 2000 years per cycle, as revealed above. This component in the Japanese SV has been explained by a steady westward drifting field, based on the consistency of the period with the estimate from the present field drifting rate, and the clockwise sense of the vector motion (Itota et al., 1982). The component in the North American record has been also considered to be generated by westward drifting field at least till 2000 years B.P.. To confirm this component global, correlation functions were calculated from isolating longer periodicity components. Fig 2-5-3, parts 1,2,3, and 4, shows

correlation functions calculated for pairs of LPJPN - LPLSC, LPLSC - LPUKD, LPUKD - LPJPN and LPJPN - LPAST.

For the pair of LPJPN and LPLSC (Fig. 2-5-3, part 1), the correlation coefficient at time-lag 1500 years for the E-W component is especially large. This maximum is also obtained from the correlation function of the E-W component between HCJPN and HCLSC (Fig. 2-5-2, part1). Other two peaks are at -1000 and 4300 years. Maximum correlations are obtained every 2500 years intervals. Maxima in the correlation function of the U-D component are obtained at time-lags of intervals 2000 - 2500 years. The E-W and the U-D components have consistent maxima at time-lags $1825 \pm 325$ and $-725 \pm 275$ years. The former maximum also corresponds to the maximum in the correlation function at 1800 years of the vector pairs. Values of the correlation function of vector pairs are generally small.

For the pair of LPLSC and LPUKD (Fig. 2-5-3, part 2), the correlation functions for all of three components show quite strong correlations at some time-lags. The maxima of E-W component at time-lags 1800 and -1900 years may correspond to the maxima obtained for the vector pairs at time-lags 1700 and -1450 years, respectively. They may also correspond to those for the U-D component at time-lags 1500 and -1200 years. The time-lag about $1650 \pm 150$ years is consisted among three components.

For the pair of LPUKD and LPJPN (Fig. 2-5-3, part 3), an extremely high correlation is obtained at a time-lag of 3000 years for the E-W component. Correlation maxima are obtained at time-lags -4250, -1050, and 4250 years for the U-D component with large values. For the vector pairs, the highest correlation is at time-lag 2950 years. Thus the highest correlation is obtained for the vector and the E-W components at time-lag about 3000 years. The U-D component has no such correlation. At time-lag about $-1125 \pm 75$ years, the three correlation functions commonly take a maximum.

The correlation functions of three component for the pair of LPJPN and LPAST show symmetric pattern (Fig. 2-5-3, part 4). All maxima of correlation except one of

E-W component (3900 years) simultaneously appear for other correlation functions. The maximum peaks obtained at time-lags near zero for three components are notable.

2-5-3. Discussion

The correlation functions calculated for the pairs of the low frequency components from the Northern Hemisphere have notable time-lags at which maximum correlations were commonly obtained with respect to three components. For the pair of LPJPN and LPLSC, the notable maxima is at $1825 \pm 325$ years. It means that the SV features are transferred from Japan to North America delayed by about 1825 years. A notable time-lag is $1650 \pm 150$ years for the pair of LPLSC and LPUKD, suggesting that the SV features are transferred from North America to U.K. delayed by about 1650 years. The pair of LPUKD and LPJPN has a notable time-lag at about $-1125 \pm 75$ years, that is, the SV features move from Japan to U.K. delayed by about 1125 years.

The SV components of LPJPN and LPLSC are dominated by clockwise looping, suggesting the existence of westward drifting fields. If the notable time-lags are attributed to the westward drift, a drifting rate is estimated from the time-lags as 0.16°/year - 0.13°/year. Then the time span for full rotation is 2300 - 2800 years. This is consistent with the period of the isolated components. Thus westward drifting fields seem to persist at least through the past 8000 years, and they have rotated all around the earth.

It is strange that the correlation maxima at time-lag about -525 years is not commonly obtained for the pair of LPJPN - LPLSC. The maxima at time-lag 525 years is expected from the notable time-lags of LPLSC - LPUKD and LPUKD - LPJPN, if their correlations are resulted in the westward drift. The correlation functions for the E-W and the U-D components obtained for the pair of LPJPN - LPLSC have a maxima at time lag $-725 \pm 275$. This time-lag may corresponds to the expected one. For the vector component, the peaks in the correlation functions are negligibly small at negative

time-lags. In the low frequency components of the three sites, variations generated by standing fields are included. So, only rough estimation of the westward drifting rate is probable.

In the polar projections of low frequency components in the three sites, counter-clockwise loops are observed only at the interval between 8000 - 7000 years B.P. in LPJPN and after 1500 years B.P. in LPUKD. Consequently, it is unrealistic to consider that the transformations of SV features are due to the eastward drifting non-dipole fields.

The correlation functions calculated for the pair of LPJPN and LPAST show high correlation at time-lag about 100 ~ 550 years. Although a slow eastward drift or a quite fast westward drift seem possible, it is reasonable to consider that this may be due to the effect of the detrending in the declination of Australian SV record. The U-D component is less affected by the detrending. The correlation function of the U-D component shows high correlation at time-lag only 100 years, which may be within dating error. The SV features should have occurred simultaneously at Japan and Australia. Consequently, the result of correlation function between LPJPN and LPAST is roughly consistent with the results from the Northern Hemisphere.

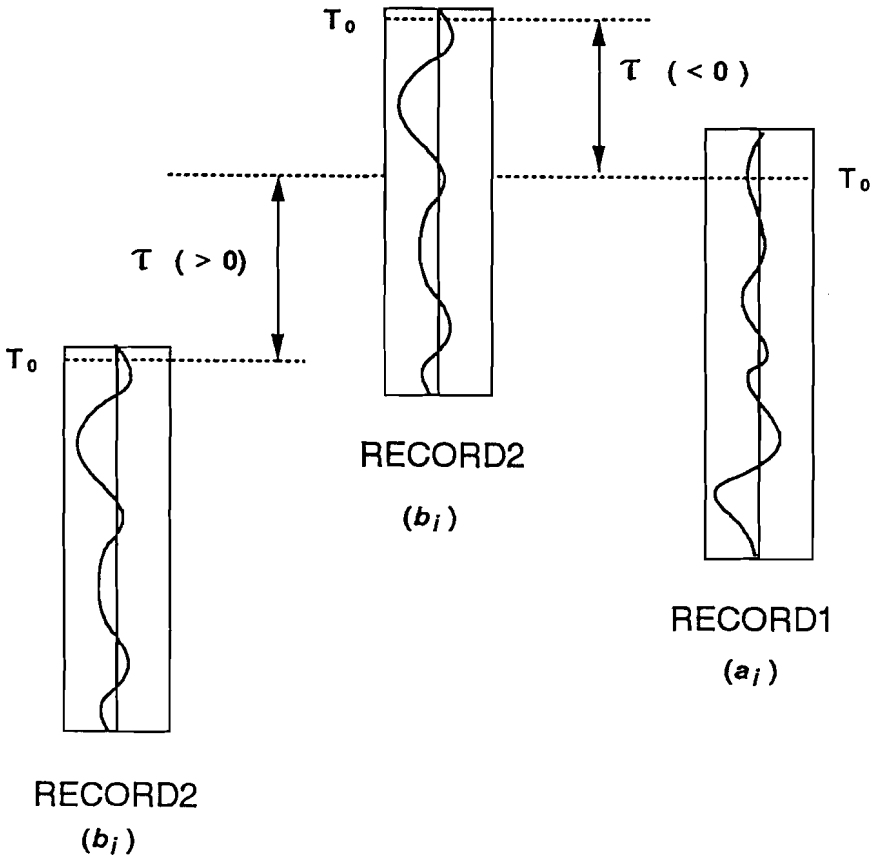


Fig. 2-5-1. Correlation function $C(\tau)$ is calculated from overlapped data of two records. Positive time-lags ($\tau > 0$) means that a certain SV feature in Record 1 precedes the same feature in Record 2. Negative time-lags ($\tau < 0$) means its opposite case.

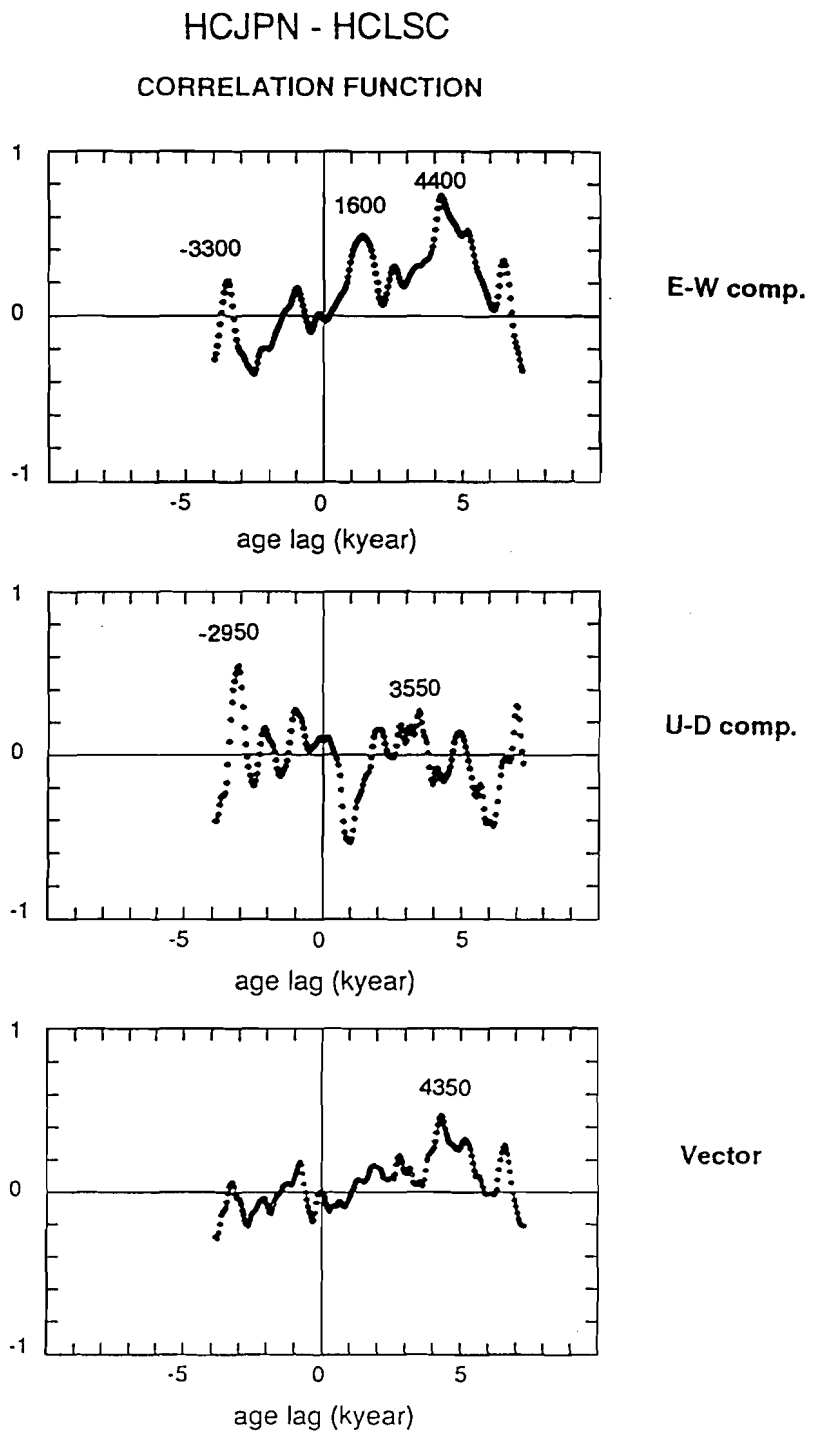


Fig. 2-5-2. (1) Correlation functions calculated between HCJPN and HCLSC for E-W (upper), U-D (middle) and vector components (bottom). Positive time-lags mean that the variational patterns appear in HCJPN transform to HCLSC. Negative time-lags mean that the variational patterns appear in HCLSC transform to HCJPN.

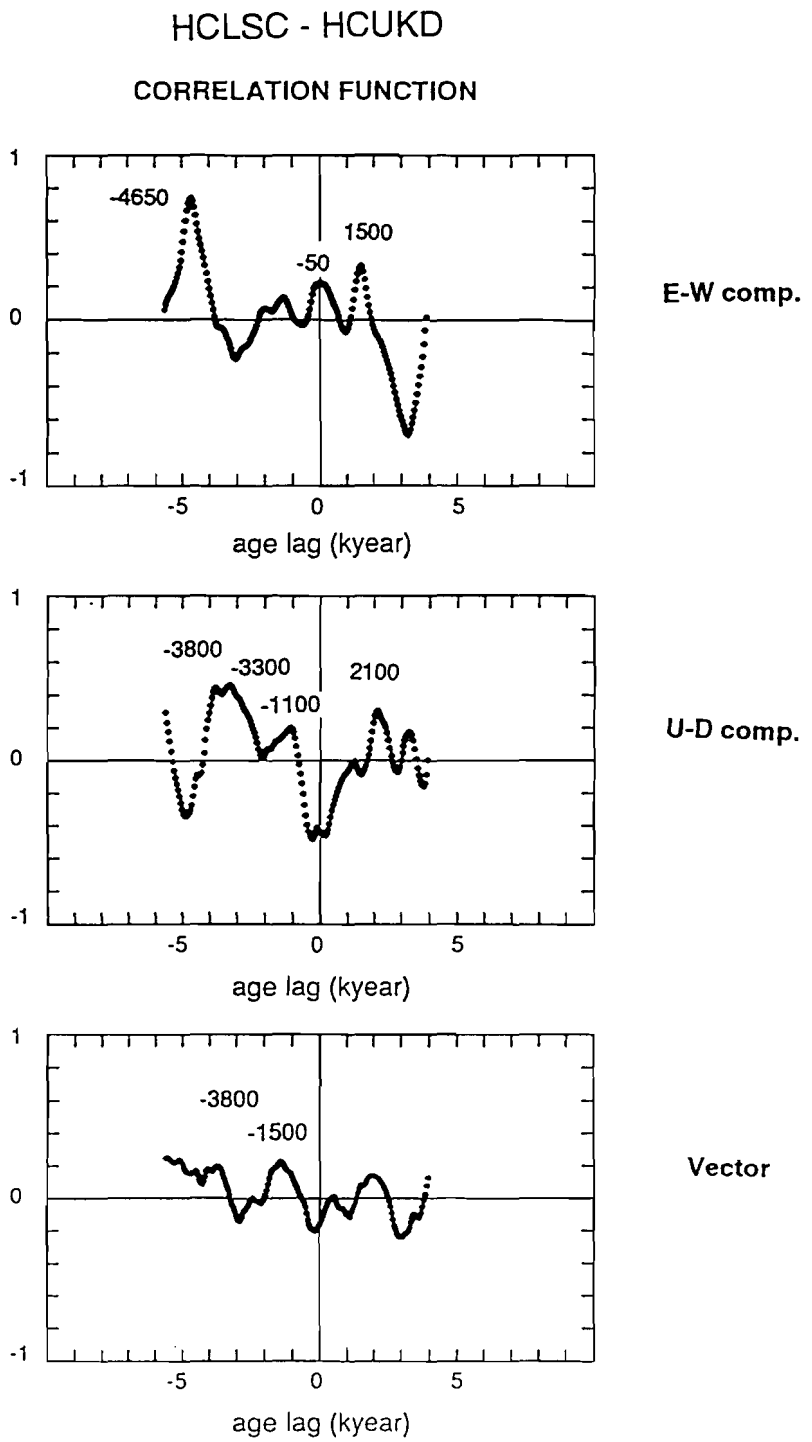


Fig. 2-5-2. (2) Correlation functions calculated between HCLSC and HCUKD for E-W (upper), U-D (middle) and vector components (bottom). Positive time-lags mean that the variational patterns appear in HCLSC transform to HCUKD. Negative time-lags mean that the variational patterns appear in HCUKD transform to HCLSC.

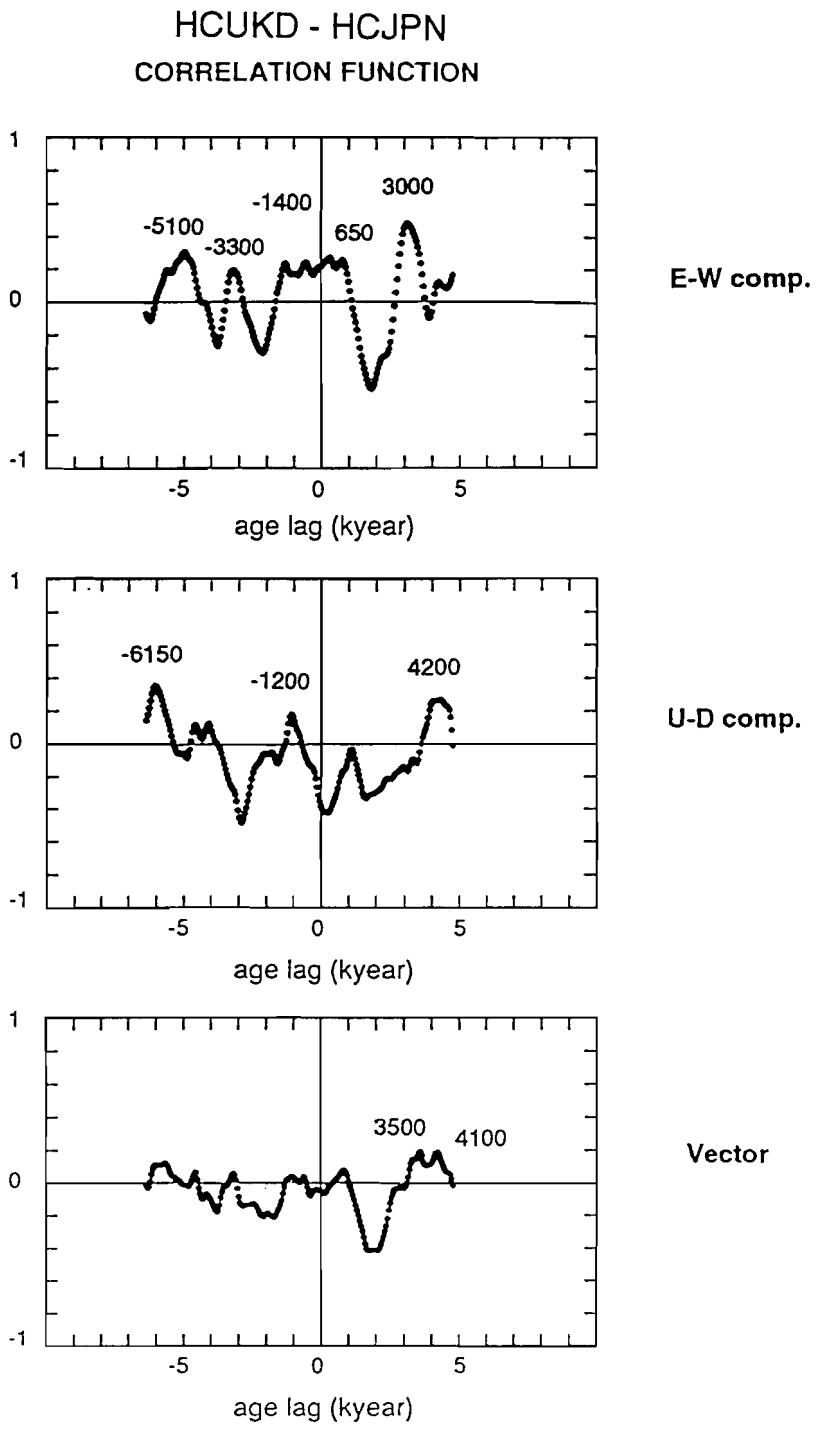


Fig. 2-5-2. (3) Correlation functions calculated between HCUKD and HCJPN for E-W (upper), U-D (middle) and vector components (bottom). Positive time-lags mean that the variational patterns appear in HCUKD transform to HCJPN. Negative time-lags mean that the variational patterns appear in HCJPN transform to HCUKD.

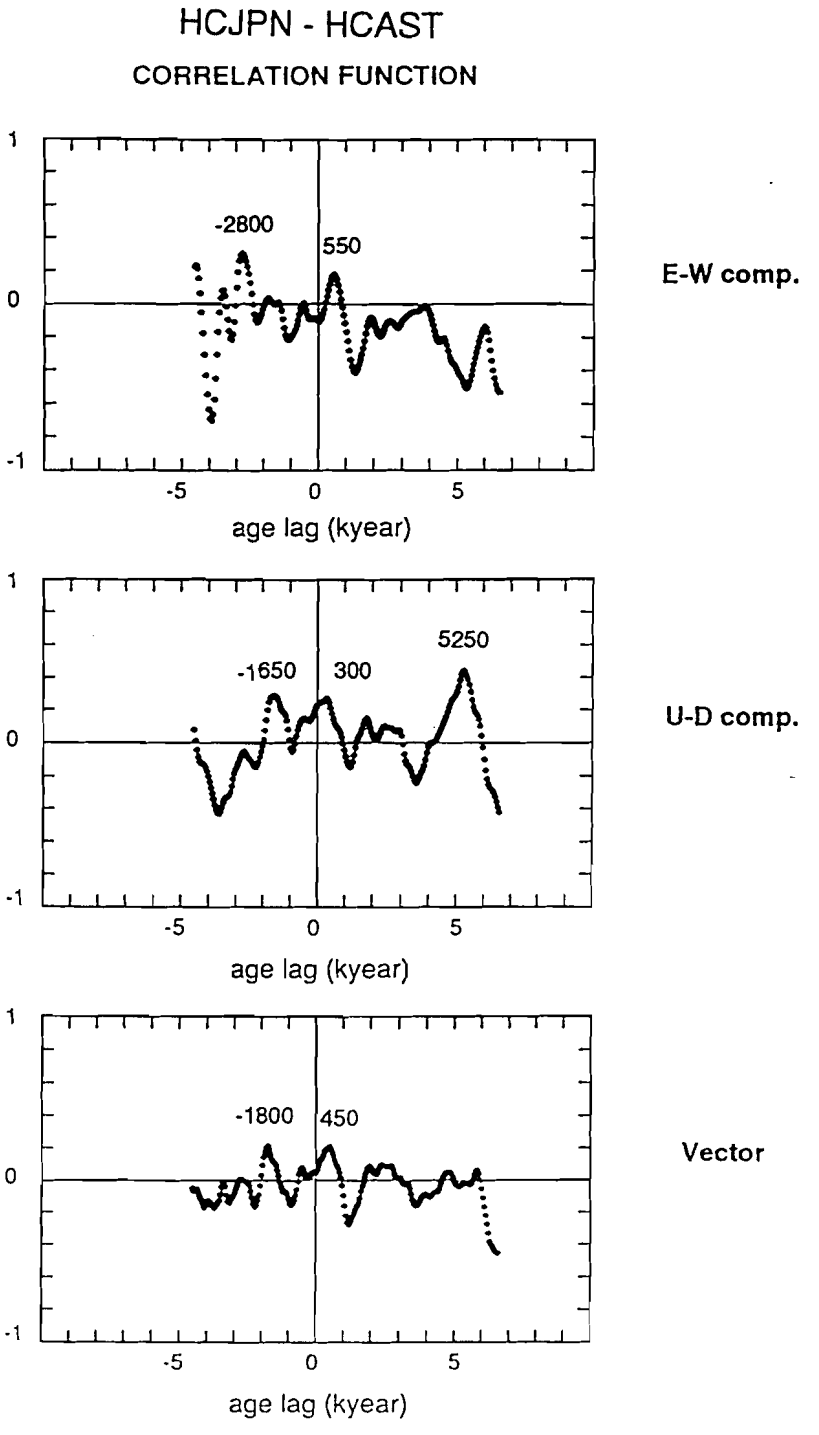


Fig. 2-5-2. (4) Correlation functions calculated between HCJPN and HCAST for E-W (upper), U-D (middle) and vector components (bottom). Positive time-lags mean that the variational patterns appear in HCJPN transform to HCAST. Negative time-lags mean that the variational patterns appear in HCAST transform to HCJPN.

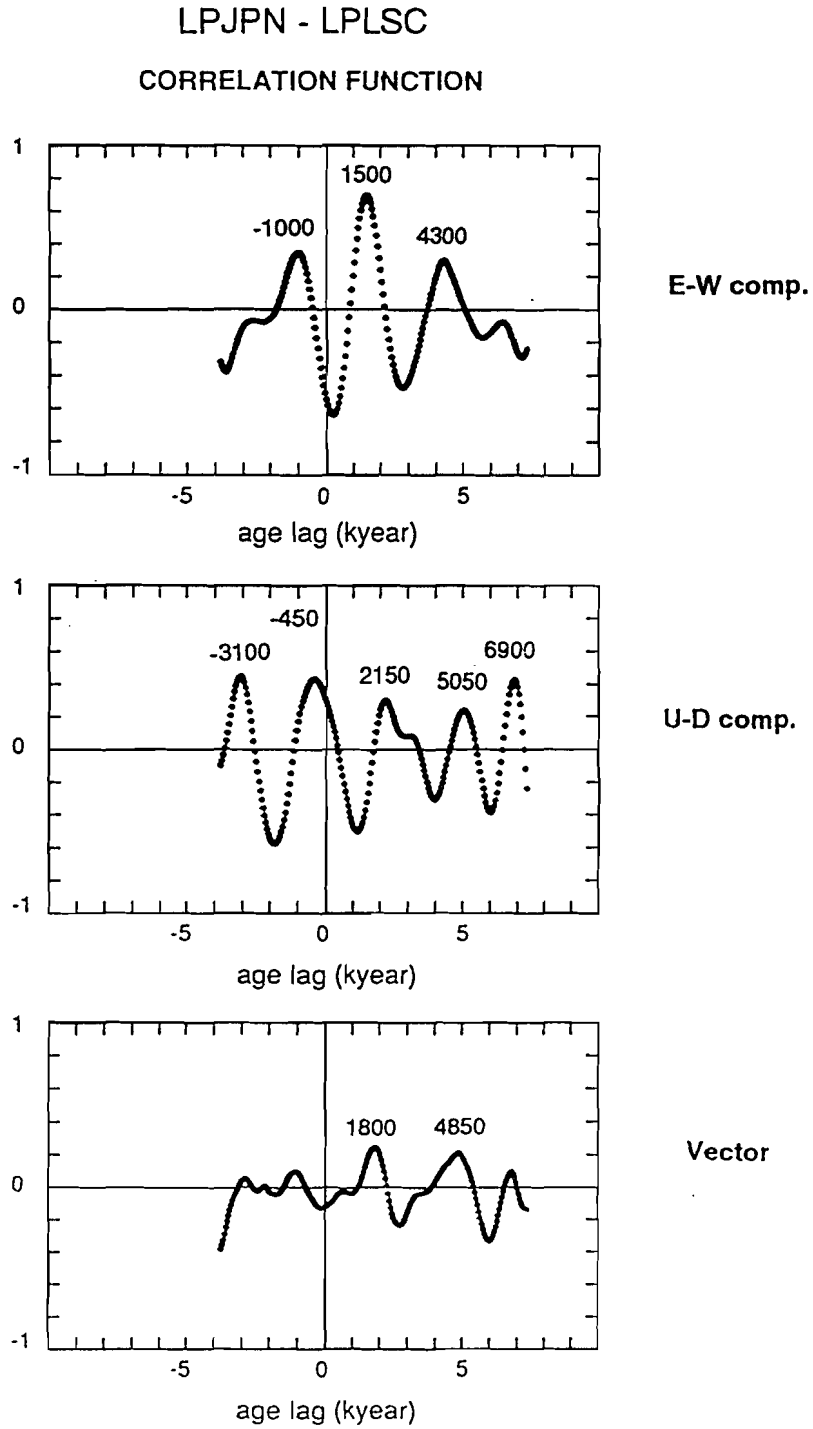


Fig. 2-5-3. (1) Correlation functions calculated between LPJPN and LPLSC for E-W (upper), U-D (middle) and vector components (bottom). Positive time-lags mean that the variational patterns appear in LPJPN transform to LPLSC. Negative time-lags mean that the variational patterns appear in LPLSC transform to LPJPN.

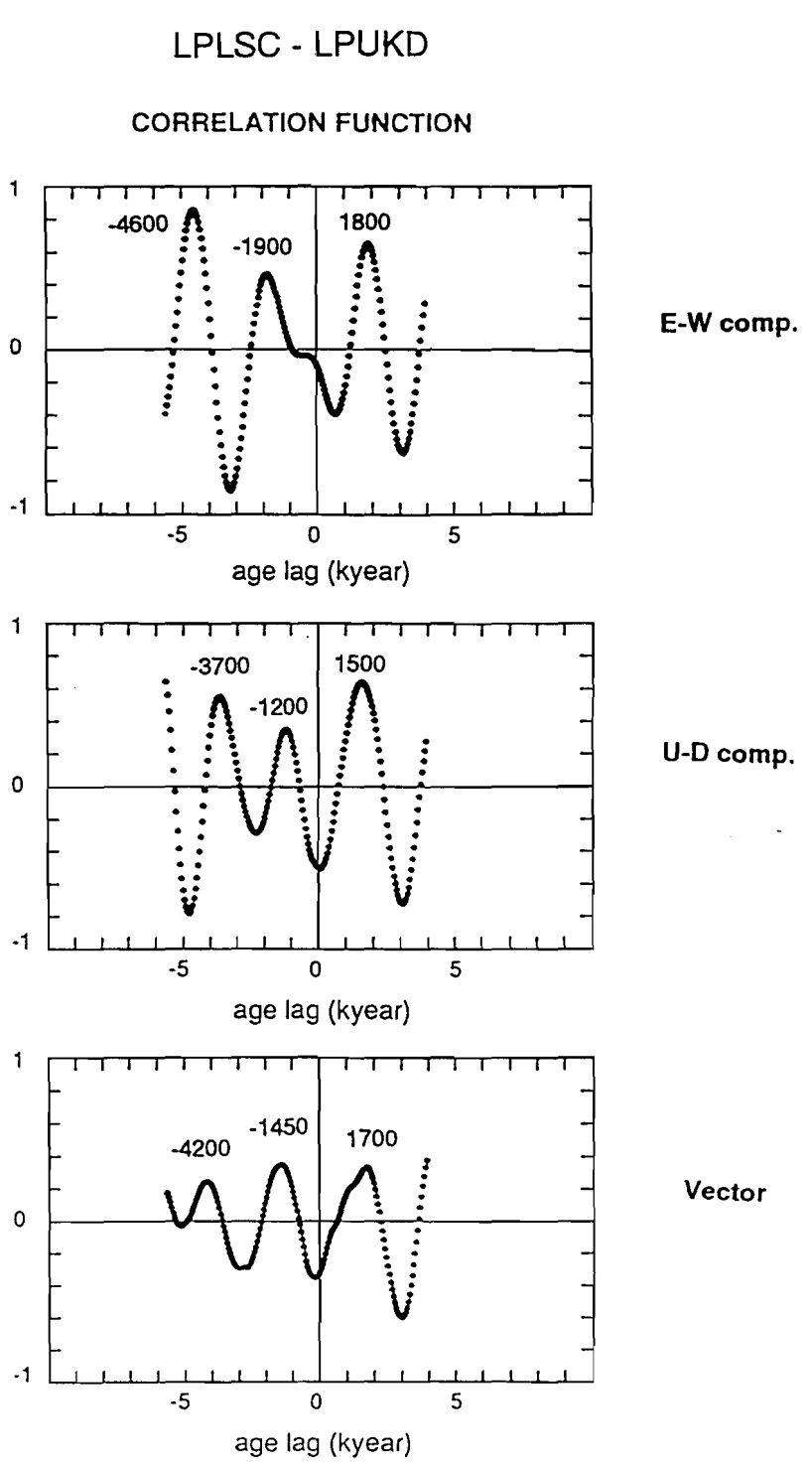


Fig. 2-5-3. (2) Correlation functions calculated between LPLSC and LPUKD for E-W (upper), U-D (middle) and vector components (bottom). Positive time-lags mean that the variational patterns appear in LPLSC transform to LPUKD. Negative time-lags mean that the variational patterns appear in LPUKD transform to LPLSC.

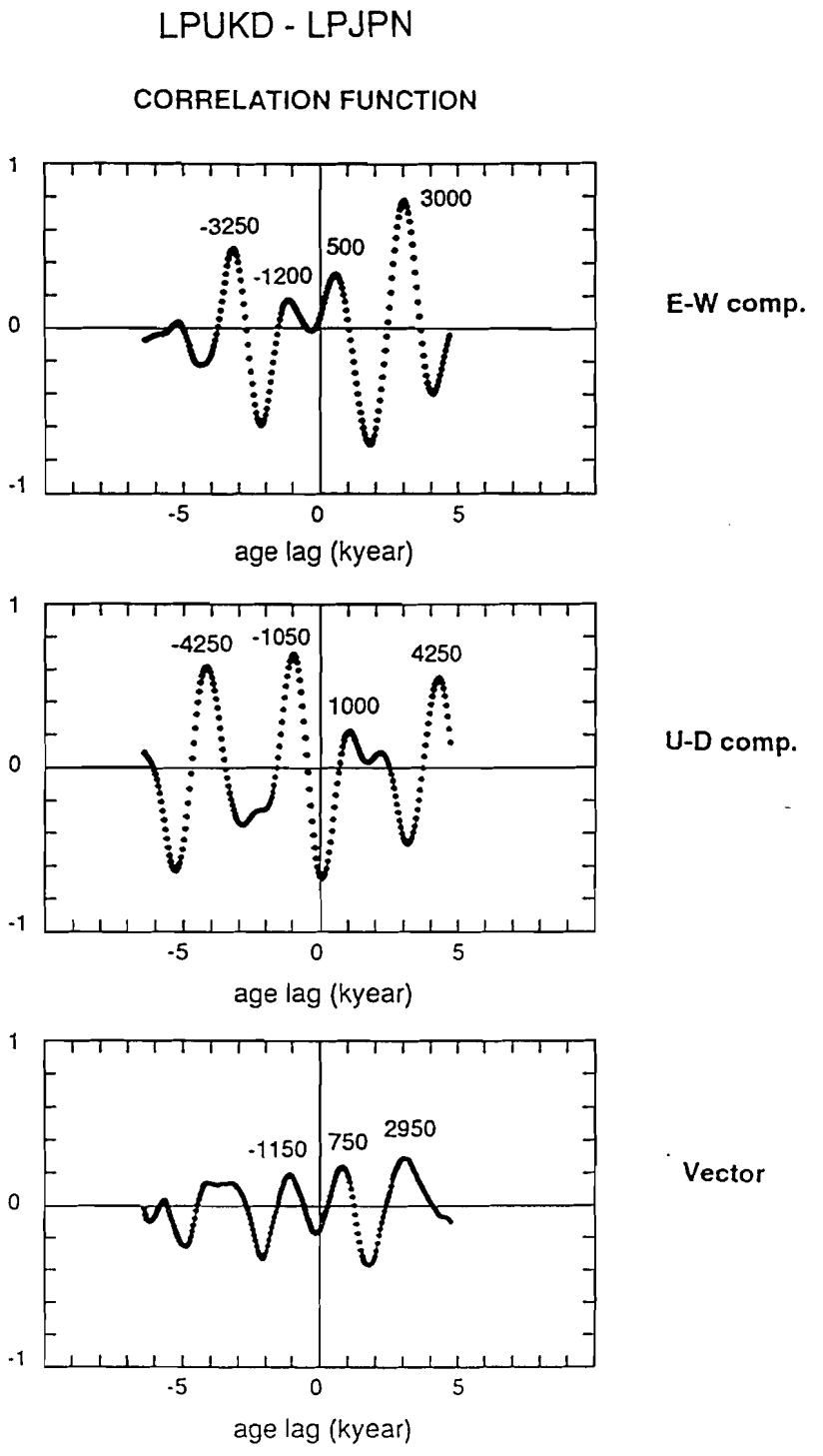


Fig. 2-5-3. (3) Correlation functions calculated between LPUKD and LPJPN for E-W (upper), U-D (middle) and vector components (bottom). Positive time-lags mean that the variational patterns appear in LPUKD transform to LPJPN. Negative time-lags mean that the variational patterns appear in LPJPN transform to LPUKD.

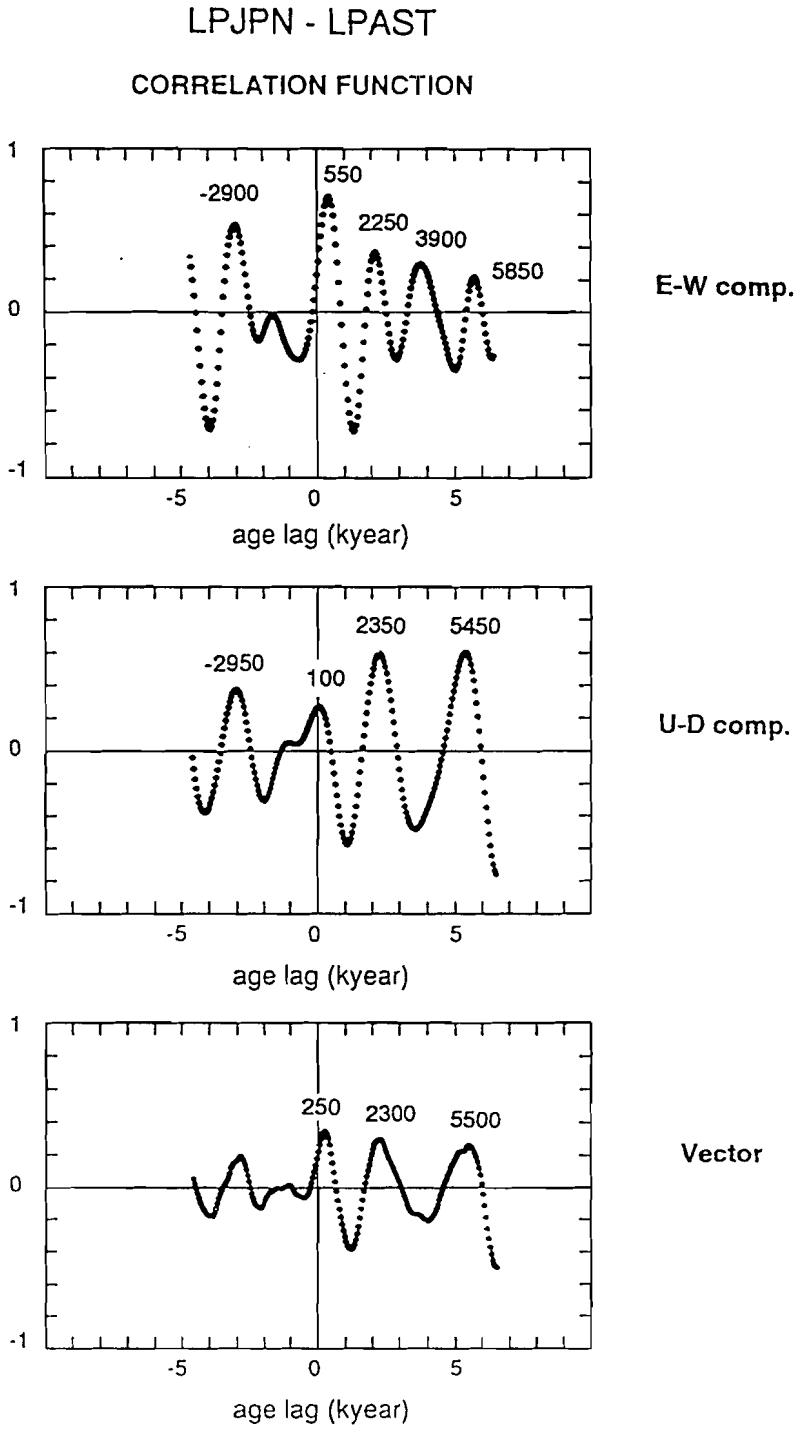


Fig. 2-5-3. (4) Correlation functions calculated between LPJPN and LPAST for E-W (upper), U-D (middle) and vector components (bottom). Positive time-lags mean that the variational patterns appear in LPJPN transform to LPAST. Negative time-lags mean that the variational patterns appear in LPAST transform to LPJPN.

## 2-6. GLOBAL GEOMAGNETIC FIELD VARIATIONS

Dominance of The Westward Drift

The secular variation components of longer period band from U.K., North America, Australia and Japan are characterized by dominance of clockwise sense of vector motion (Fig. 2-6-1). Especially, in North America and Japan, field vectors draw smooth clockwise loops (Figs. 1-3-7 and 2-3-8), suggesting a steady westward drifting field.

The westward drifting rate was estimated 0.16°/year ~ 0.13°/year from the correlation functions. A westward drifting rate has also been estimated by phase lags of inclination maxima and minima between U.K. and North America (Creer, 1981). The estimated rate was 0.16°/year ~ 0.14°/year before 2500 years B.P..

After 2500 years B.P., clear maxima and minima appeared in the inclination changes from U.K. and North America (Figs. 2-2-2 and 2-3-2) suggests an increase of apparent drifting rate up to 0.5°/year (Creer, 1981). However this interpretation is doubtful because of non-uniform data-point-intervals in the North American data set; narrow intervals in younger part and wide in older part (Fig. 2-3-2). Another reason is in the data from U.K.. The U-D component of SPUKD clearly shows the increase of amplitude after 1500 years B.P., and the sense of field motion is counter-clockwise (Figs. 2-3-8, and 2-6-2). It is similar to the features of the accidental counter-clockwise motion appeared in the SV components of LPLSC (after 2000 years B.P.) and LPJPN (during 8000 to 6500 years B.P.). The motion in SPUKD after 1500 years B.P. should be attributed to other sources than to a westward drifting field.

In U.K., looping feature of a field vector is not clearly observed. The high latitude (54°N) of the U.K. site may cause it. The size of looping depends on a distance from source field. If a source field drifts in a low latitude area near Japan, the smallest loop will be observed at U.K. among the four sites. The field may have

drifted near equator or in the Southern Hemisphere, so that clear looping of field vector does not appear in U.K.. This interpretation is consistent with the results from historical geomagnetic records, that is, drifting fields derived from observed field variation are concentrated in the Southern Hemisphere (Yukutake and Tachinaka, 1968a; Bloxham and Gubbins, 1985). Such configuration of non-dipole fields may have been a nature of geomagnetic field for the last about 10000 years.

The secular variation components of periodicity band about 1200 years per cycle were isolated from three sites, U.K., North America, and Australia. During the interval from 4200 years B.P. to 1700 years B.P., the components represent clockwise rotations of field vectors on YZ-plane (Fig. 2-6-2) at the three sites. The amplitudes of variations are relatively large during this intervals (Figs 2-2-8, 2-3-9, and 2-4-7). The persistence of clockwise rotation during this interval is also seen in the SV component of LPJPN, the SV of band of periods 1200 - 3500 years (Fig. 2-6-2). During the interval, the secular variation component of the periodicity about 1200 years per cycle is dominated globally by the westward drifting field.

Almost all looping features are observed in the intervals of clockwise sense over the four records (Figs. 2-6-1 and 2-6-2). The intervals predominated by the motion of clockwise sense are tend to be longer than the intervals of counter-clockwise sense. They may suggest the predominance of the westward drifting components in the geomagnetic field variations.

Characteristic Time of The Standing Fields

Sudden occurrence of standing fields was observed in the SV records from North America and Japan. The linear field motion in the SV component of longer period band in North America suggests that a field source is close to the observation site. The North American anomaly of non-dipole field (Yukutake and Tachinaka, 1968a) can be regarded as a source. This anomaly may have persisted through the past

2000 years, oscillating its intensity. Similarly in Japan, the linear field motion in the SV component of longer period band during the interval from 8000 to 3500 years B.P. may be regarded as a result of intensity fluctuation of the Mongolian anomaly (Yukutake and Tachinaka, 1968a). Hence, it is inferred that standing fields fluctuate their intensities during certain time intervals, and consequently they stop fluctuating.

For the SV component of LPUKD, the elongation directions of linear fluctuation on the YZ-plane are constant during the intervals of 9800 - 6000 years B.P., 5000 - 2000 years B.P., and 1000 - 300 years B.P.. Such persistence of linear fluctuations is also seen in the SV component of SPJPN, whose periodicity is about 700 years, at intervals of 11500 - 7500 years B.P., 6500 - 3500 years B.P., and 2250 - 400 years B.P.. If the shift of fluctuation direction is caused by the change of the source field, then each interval corresponds to the time when a standing field is active. During the last 10000 years, the first interval is 3800 years long for LPUKD , and 4000 years long for SPJPN. The second intervals are 3000 years long for both. The intensity fluctuation duration of a standing field suggested by the SV component of LPJPN is 3500 years long. The time lengths of 3000 - 4000 years may be characteristic for standing fields active at least during the last 10000 years.

The secular variation of periodicity about 700 years was suggested from the SVs of Southeast Australia, North America, and Japan by MEM spectral analyses. Unfortunately, we cannot discuss this component more in detail. Amplitudes of this component from Southeast Australia and North America are too small to be discussed about variational pattern. It may be caused by the filtering effect of post depositional magnetization process, and/or by the smoothing due to stacking.

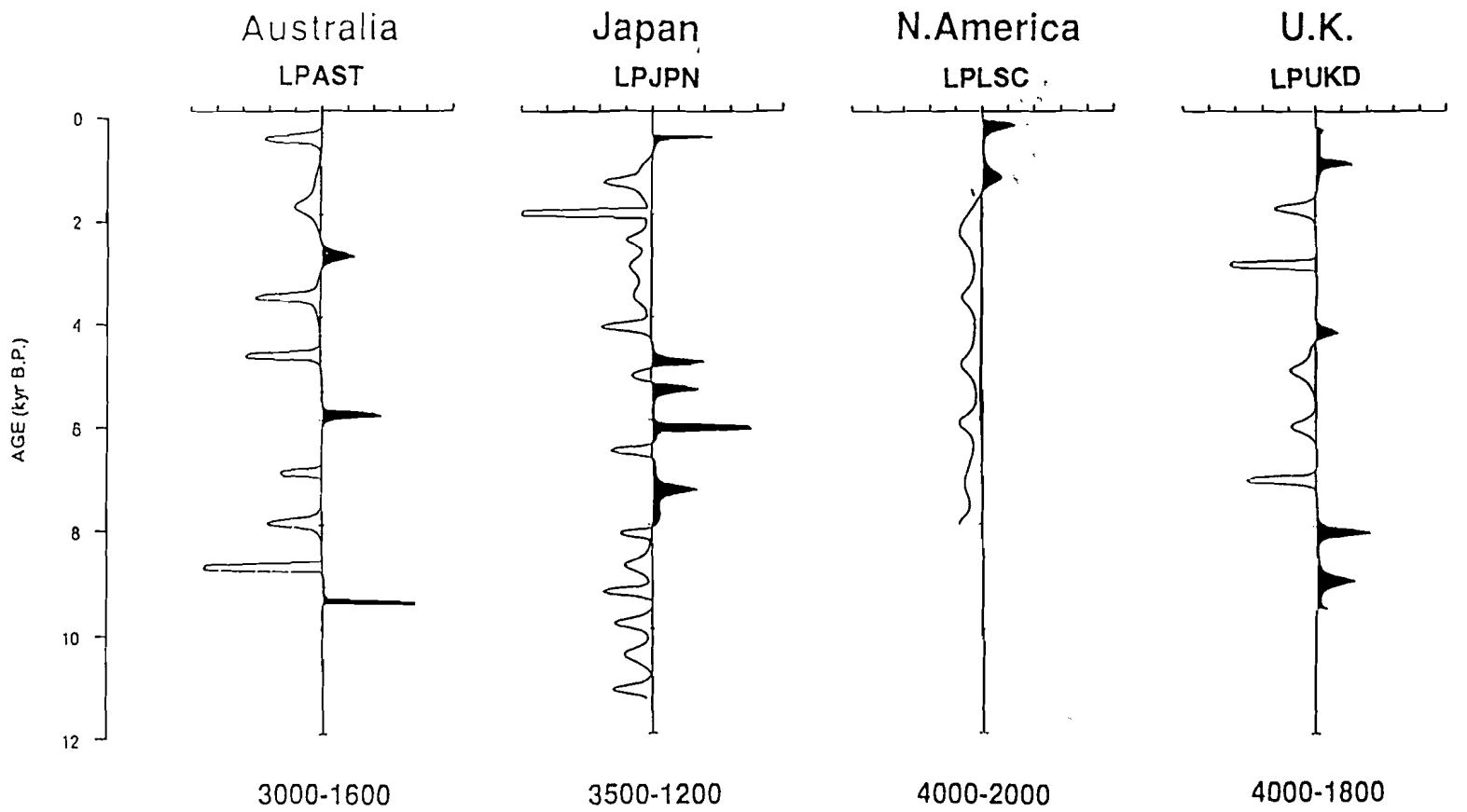


Fig. 2-6-1. Plots of curvature of field direction paths for the SV components of periodicity about 3000 years from four sites.

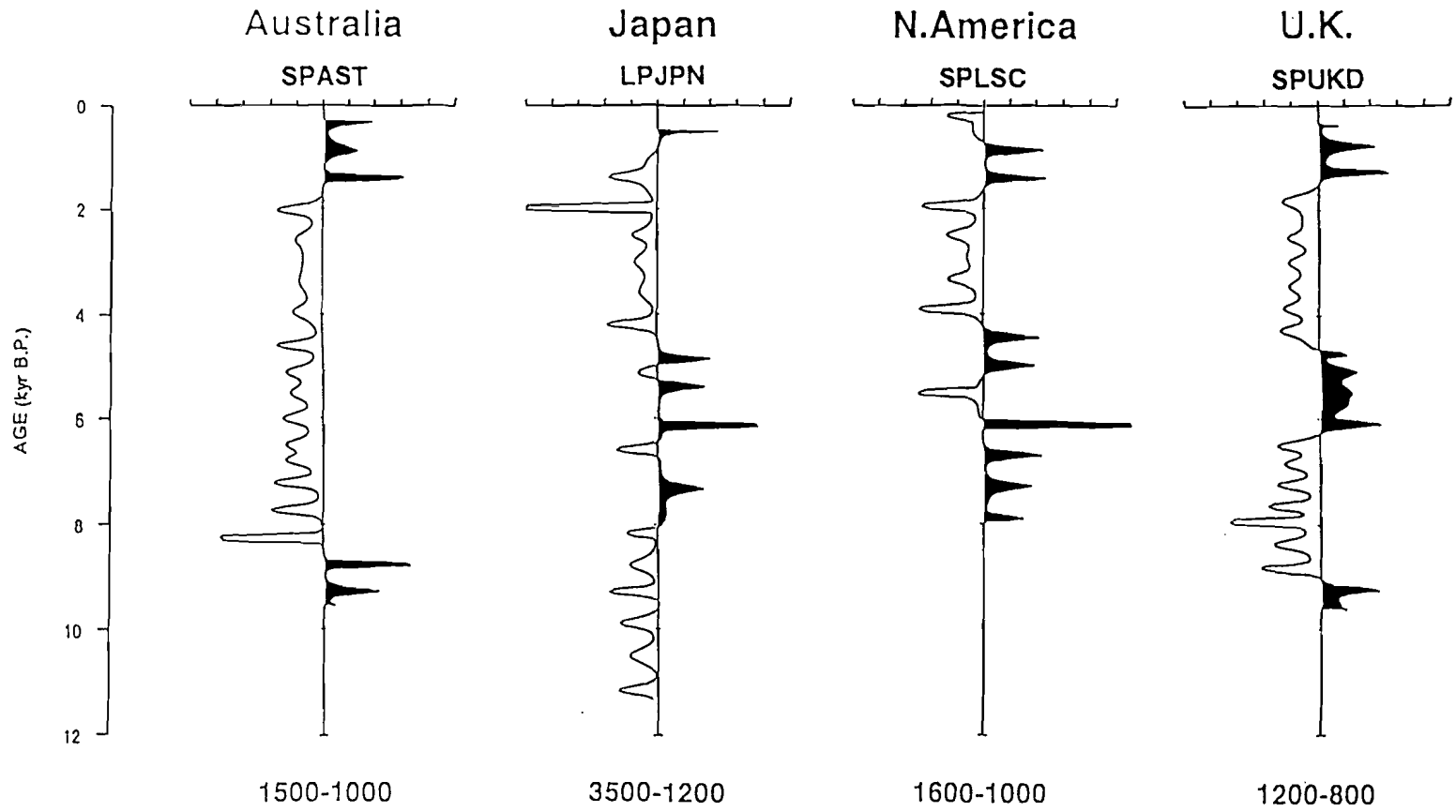


Fig. 2-6-2. Plots of curvature of field direction paths for the SV components of periodicity about 1200 years from four sites.

## 2-7. CONCLUSIONS

A method to analyze a paleomagnetic secular variation by separation into its spectral components was proposed. The method was applied to the secular variation records from U.K., North America, Japan, and southeast Australia. From all sites a spectral component including periodicity of 3000 - 2000 years per cycle was isolated. The component from North America is dominated by clockwise looping of field vectors suggesting a steady westward drifting field. The component of U.K. shows linear motions implying existence of oscillating standing fields. The correlation functions calculated between the records of U.K, North America, and Japan show consistent results that there exist westward drifting fields, and that the drifting velocity is estimated 0.16°/year - 0.13°/year. The absence of clockwise looping in the field motion of U.K. may be due to disturbance by other sources, or the high latitude of the site. The correlation function of U-D components in the low frequency SV components between Australia and Japan shows that there is no time-lag of SV features. This does not deny the result obtained from the three SV records in the Northern Hemisphere that westward drifting is a dominant feature in the low frequency SV components. Continuous clockwise rotations of field vector were commonly seen at the interval from 4200 years B.P. to 1700 years B.P. in the SV component of shorter period bands including periodicities of 1200 - 1000 years per cycle at all the sites except Japan/ In Japan, the same things were seen in the SV component of period band 3500 -1200 years per cycle. The durations dominated by the motion of clockwise sense are generally longer than those of counter-clockwise sense. The amplitudes of clockwise vector motions are larger than those of counter-clockwise ones. Hence, the present analyses conclude that the predominance of westward drifting field components should be a nature of the geomagnetic field variations during the last 10000 years.

Sudden breaks of smooth clockwise loops were observed at 2000 years B.P. in the low frequency SV component from North America, and at 8000 years B.P. in the

low frequency SV component from Japan. Standing non-dipole fields may have fluctuated their intensities during a certain time interval, and consequently their activity may have stopped. The change of field oscillation direction in a polar projection show that one standing field persists for 3000 - 4000 years long. The duration for break of smooth clockwise looping in the low frequency SV in Japan is 3500 years, which suggest that a standing field actively fluctuates for 3500 years long. The time length of 3000 - 4000 years may be a characteristic of activity for standing fields during the last 10000 years.

## REFERENCES


Akaike, H., Fitting autoregressive models for prediction, Ann. Inst. Statist. Math., 21, 243-247, 1969a.

Akaike, H., Power spectrum estimation through autoregressive model fitting, Ann. Inst. Statist. Math., 21, 407-419, 1969b.

Akaike, H., Statistical prediction identification, Ann. Inst. Statist. Math., 22, 203-217, 1970.

Arai, F., T. Oba, H. Kitazato, Y. Horibe and H. Machida, Late Quaternary tephrochronology and paleo-oceanography of the Japan Sea, The Quaternary Res., Tokyo, 20, 209-230, 1981 (in Japanese).

Barton, C. E., Spectral analysis, in *Geomagnetism of Baked Clays and Recent Sediments*, edited by K. M. Creer, P. Tucholka and C. E. Barton, Elsevier, Amsterdam, 262-265, 1983.

Barton, C. E. and M. E. McElhinny, A 10000 yr geomagnetic secular variation record from three Australian maars, Geophys. J. R. astr. Soc., 67, 465-485, 1981.

Barton, C. E. and M. E. McElhinny, Time series analysis of the 10000 yr geomagnetic secular variation record from SE Australia, Geophys. J. R. astr. Soc., 68, 709-724, 1982.

Barton, C. E., Bowler, J. M. and H. A. Polach, Magnetic stratigraphy, sedimentology and $^{14}C$ ages of three Australian maars, unpublished manuscript.

Bauer, L. A., On the secular motion of a free magnetic needle, II, Phys. Rev., 3, 34-48, 1896.

Bloxham, J. and D. Gubbins, The secular variation of Earth's magnetic field, Nature, 317, 777-781, 1985.

Bloxham, J. and D. Gubbins, Thermal core-mantle interactions, Nature, 325, 511-513, 1987.

Bullard, E. C., C. Freedman, H. Gellman, and J. Nixon, The westward drift of the earth's magnetic field, Philos. Trans. R. Soc. Lond, Ser. A, 243, 67-92, 1950.

Burg, J. P., Maximum entropy spectral analysis, 37th Ann. Int. Meeting Soc. Explor. Geophys., Oklahoma City, 1967.

Clark, M., A calibration curve for radiocarbon dates, Antiquity, 49, 251-266, 1975.

Creer, K. M., Long-period geomagnetic secular variations since 12,000 yr BP, Nature, 292, 208-212, 1981.

Creer, K. M. and P. Tucholka, On the current state of lake sediment paleomagnetic research, Geophys. J. R. astr. Soc., 74, 223-238, 1983a.

Creer, K. M. and P. Tucholka, Epilogue, in *Geomagnetism of baked clays and recent sediments*, edited by T. M. Creer, P. Tucholka and C. E. Barton, Elsevier, Amsterdam, 273-305, 1983b.

Creer, K. M., G. Smith, P. Tucholka, E. Bonifay, N. Thouveny and E Truze, A preliminary palaeomagnetic study of the Holocene and late Würmian sediments of Lac du Bouchet (Haute-Loire, France), Geophys. J. R. astr. Soc., 86, 943-964, 1986.

Denham, C. R., Spectral analysis of paleomagnetic time series, J. Geophys. Res., 80, 1897-1901, 1975.

Denham, C. R., Numerical Correlation of recent paleomagnetic records in two Lake Tahoe cores, Earth Planet. Sci. Lett., 54, 48-52, 1981.

Doell, R. R. and A. Cox, Pacific geomagnetic secular variation, Science, 171, 248-254, 1971

Furutani, M., Studies on the forest history in the Osaka area since Wurm glacial age in Japan, The Quaternary Res., Tokyo, 18,121-141, 1979 (in Japanese).

Gibbins, D, Core-mantle interactions, Tectonophys., 187, 385-391, 1991.

Hide, R., On the role of rotation in the generation of magnetic fields by fluid motions, Phil. Trans. R. Soc. Lond. A 306, 223-234, 1982.

Hirooka, K., Archeomagnetic study for the past 2000 years in southwest Japan, Mem. Fac. Sci. Kyoto Univ., 38, 167-207, 1971.

Hirooka, K., Archeomagnetism of baked clays, Results from Japan, in *Geomagnetism of baked clays and recent sediments*, edited by K. M. Creer, P. Tucholka and C. E. Barton, Elsevier, Amsterdam, 150-157, 1983.

Hoffman, K. A., A method for the display and analysis of transitional paleomagnetic data, J. Geophys. Res., 89, 6284-6292, 1984.

Horie, S., K. Yaskawa, A. Yamamoto, T. Yokoyama and M. Hyodo, Paleolimnology of lake Kizaki, Arch. Hydrobiol., 89, 407-415, 1980.

Hyodo, M., Possibility of reconstruction of the past geomagnetic field from homogeneous sediments, J. Geomag. Geoelectr., 36, 45-62, 1984.

Hyodo, M. A fundamental study of magnetizing process in homogeneous sediments by theoretical and observational approach, Ph.D. Thesis, Kobe Univ., Kobe, Japan, 1985.

Hyodo, M., Spatial and temporal distribution of Pacific dipole window, Chikyu Extra, 2, 50-52, 1989 (in Japanese).

Hyodo, M. and K. Yaskawa, Geomagnetic secular variation recorded in the stable remanence of the young sediments collected from Osaka Bay, J. Geomag. Geoelectr., 32, 581-584, 1980.

Hyodo, M. and K. Yaskawa, Geomagnetic secular variation recorded in silty sediments from the Inland Sea, Japan (Seto Naikai), J. Geomag. Geoelectr., 38, 11-26, 1986a.

Hyodo, M. and K. Yaskawa, Palaeomagnetism of a core sediments from the Inland Sea, Japan (Seto Naikai), Geophys. J. R. astr. Soc., 41-56, 1986b.

Hyodo, M., and C. Itota and K. Yaskawa, Geomagnetic field variations reconstructed by deconvolution method from magnetizations of wide-diameter cores of Holocene sediments in Japan, (submitted to J. Geomag. Geoelectr.).

Hyodo, M., H. Morinaga, H. Nishimura, H. Inokuchi and K. Yaskawa, Paleomagnetism of a core from Osaka Bay, J. Geomag. Geoelectr., 37, 29-737, 1985.

Itota, C., M. Hyodo and K. Yaskawa, Separation of paleosecular variation components: A method and its application to a records from Japan (submitted to J. Geomag. Geoelectr.).

Kawai, N. and K. Hirooka, Wobbing motion of the geomagnetic dipole field in historical time during these 2000 years, J. Geomag. Geoelectr., 19, 217-227, 1967.

Klein, J., J. C. Lerman, P. E. Damon and E. K. Ralph, Calibration of radiocarbon dates : Tables based on the consensus data of the workshop on calibrating the radiocarbon time scale, Radiocarbon, 24, 103-150, 1982.

Lund, S. P. and S. K. Banerjee, Late Quaternary secular variation from two Minnesota lakes, J. Geophys. Res., 90, 803-825, 1985.

Lund, S. P. and P. Olsen, Historic and paleomagnetic secular variation and the earth's core dynamo process, Rev. Geophys., 25, 917-928, 1987.

Maeda, Y., Palynological study of the forest history in the coastal area of Osaka Bay since 14000 BP, J. Geosci. Osaka City Univ., 20, 59-93, 1976.

Maeda, Y., Y. Matsushima, H. Sato and S. Kumano, Determination of the upper limit of marine facies, The Quaternary Research, Tokyo, 21, 195-201, 1982.

Matsushima, M and Y, Honkura, Fluctuation of the standing and drifting part of the Earth's magnetic field, Geophys. J., 94, 35-50, 1988.

Merrill, R. T. and M. W. McElhinny, in *The earth's magnetic field - Its history, origin, and planetary perspective*, Academic press, London, 401pp., 1983.

Runcorn, S. K., On the theory of the geomagnetic secular variation, Ann. Geophys., 15, 87-92, 1959.

Saito, M., An automatic design algorithm for band selective recursive digital filters, Butsuri Tanko (Geophysical Exploration), 240-263, 1978 (in Japanese).

Shove, D. J., Dating and related problem, Tree-rings and varves, in *Geomagnetism of baked clays and recent sediments*, edited by K. M. Creer, P. Tucholka and C. E. Barton, Elsevier, Amsterdam, 45-56, 1983.

Skiles, D. D., A method of inferring the direction of drift of the geomagnetic field from paleomagnetic data, Geophys. J. R. astr. Soc., 22, 441-462, 1970.

Smith, G. and K. M. Creer, Analysis of geomagnetic secular variations 10000 to 30000 years bp, Lac du Bouchet, France, Phys. Earth Planet. Int., 44, 1-14, 1986.

Stuiver, M., A high-precision calibration of the AD radiocarbon time scale, Radiocarbon, 24, 1-26, 1982.

Tojo, T., Past climate around Osaka Bay inferred from the pollen analysis of a core sediment, Kobe Univ. Thesis, Kobe, Japan, 1976 (in Japanese).

Turner, G. M. and R. Thompson, Lake sediment record of the geomagnetic secular variation in Britain during Holocene times, Geophys. J. R., astr. Soc., 65, 703-825, 1981.

Turner, G. M. and R. Thompson, Detransformation of the British geomagnetic secular variation record for Holocene times, Geophys. J. R. astr. Soc., 70, 789-792, 1982.

Ulrych, T. J. and T. N. Bishop, Maximum entropy spectral analysis and autoregressive decomposition, Rev. Geophys. Space Phys., 13, 183-200, 1975.

Ulrych, T. J. and R. W. Clayton, Time series modeling and maximum entropy, Phys. Earth Planet. Inter., 12, 188-200, 1976.

Watson, G. S. and R. J. Beran, Testing a sequence of unit vectors for serial correlation, J. Geophys. Res., 22, 5655-5659, 1967.

Watman, K., The relationship between the secular change and the non-dipole fields, Can. J. Phys., 36, 1372-1396, 1958.

Yukutake, T., The westward drift of the magnetic field of the earth, Bull. Earthq. Res. Inst., Univ. Tokyo, 40, 1-65, 1962.

Yukutake, T., The drift velocity of the geomagnetic secular variation, J. Geomag. Geoelectr., 20, 403-413, 1968.

Yukutake, T., On the drifting and standing fields in the geomagnetic field, Heinrich-Herz Int. Rep., 21, 7-20, 1987.

Yukutake, T., and H. Tachinaka, The non-dipole part of the earth's magnetic field, Bull. Earthq. Res. Inst., Univ. Tokyo, 46, 1027-1074, 1968a.

Yukutake, T. and H. Tachinaka, The westward drift of the geomagnetic secular variation, Bull. Earthq. Res. Inst., Univ. Tokyo, 46, 1075-1102, 1968b.

Yukutake, T. and H. Tachinaka, Separation of the earth's magnetic field into the drifting and standing parts, Bull. Earthq. Res. Inst., Univ. Tokyo, 47, 65-97, 1969.